

1 Dear Dr. Maenhaut,

2

3 We kindly thank you for taking our manuscript into consideration. We have prepared
4 a new version of the manuscript and supplement to address the concerns raised by
5 the reviewers. For clarity, a point-by-point response to the reviewers and versions of
6 the manuscript and supplement in which our modifications are visible, are enclosed
7 below.

8

9 In addition to the changes discussed in our responses to the reviewers, two
10 additional revisions have been performed:

- 11 1. Element concentrations have been recalculated to incorporate an improved
12 correction for the spectrum continuum. All reported values and figures have
13 been updated. These improved values differ from those in the original
14 manuscript by $\pm 10\%$ and do not affect any of the major conclusions.
- 15 2. Several changes made to streamline the manuscript were discussed in
16 response to Reviewer #2 – Comment #6 and Reviewer #3 – Comment #6. In
17 addition, we have shortened the description of SR-XRF analysis by only
18 briefly summarizing the changes made to the existing technique. The detailed
19 description on p. 15904-15905 of the ACPD manuscript has been moved to
20 the supplement.

21

22 Kind regards,

23 Suzanne Visser and co-authors

24

Response to Reviewer #2:

We kindly thank the referee for taking our manuscript into consideration and we value the comments raised to improve the manuscript. A point-to-point response to the issues raised is enclosed below.

The manuscript contains results obtained in an extensive study at urban and rural areas in London, UK. The analysis is focused (but no limited) to elemental contents in several fractions of atmospheric particulate matter. Although the general quality of the paper is good, it is necessary to discuss and improve several aspects, which I explain below.

Comment #1:

1. I am concerned about the agreement of the measurements using RDI and PM10 filters, in particular for some elements. The question here is: what are the truly accurate values to be considered in the paper? This problem would not exist if certified reference materials had also been analyzed. Please, do not confuse this accuracy determination with the calibration process, which is thoroughly described in section 2.2.1. The main drawback is that the forthcoming discussions in the manuscript may not have a strong basis.

Response:

The referee refers to the disagreement between measurement techniques in Sect. 3 (Data intercomparison) and specifically Fig. 2, and suggests that this calls into question the experimental results. However, much of this disagreement is expected, resulting from known differences in the measurement techniques (e.g. different size ranges) and thus does not reflect data quality. In addition, we note that this section should be interpreted as a method intercomparison rather than RDI-SR-XRF validation, and that the extent of the agreement is similar to other intercomparison studies of trace element measurement techniques. We have clarified these points by significantly condensing the intercomparison section of the manuscript, with Fig. 2 and the accompanying detailed discussion moved to the Supplement. An overview of the main points is provided below (please note that Cr has been removed from the intercomparison as this element was rejected from the filter analysis during the final quality assurance checks):

1. Most elements (i.e. all except those discussed below) show good agreement between RDI and PM₁₀ filters within $\pm 50\%$ with good Pearson's R of > 0.78 .
2. Quantitative agreement between RDI and PM₁₀ filters should not be obtained for elements with significant mass below the RDI small-size cut off of 300 nm. This includes S, K, Sn and Pb. For S, further investigation is possible by adding the mass from the backup filter to the PM_{1.0-0.3} mass measured by the RDI. Quantitative agreement with the AMS SO₄²⁻ data is then achieved, suggesting the RDI provides accurate PM_{1.0-0.3} values for all these elements.
3. V, Ni and Mo are well-constrained in the RDI-SR-XRF analysis and are well above detection limits, but have low or unknown extraction efficiencies in the PM₁₀ filter-ICP-MS analysis, increasing the uncertainty of the PM₁₀ filter analyses. Further, the RDI measurements of these elements are internally consistent (strong correlations with co-emitted elements). This suggests that the RDI measurements are correct, and the disagreement does not reflect RDI data quality issues.

4. RDI and filter measurements of Na and Mg are strongly correlated but disagree on the absolute magnitude. The RDI relative calibration of these elements is somewhat uncertain (around 13 %), while the filters have unknown extraction efficiency for Na (Mg is well extracted with 90 % efficiency). However, both techniques provide internally consistent results (e.g. correct Na-to-Mg ratios and sensible time series). We also note that Mg lies in an area of the XRF spectrum that is free of overlapping lines, resulting in low fitting errors. Thus, while the absolute concentrations (i.e. the accuracy) differ by a factor of 2.5, relative changes (i.e. the precision) are considered to be robust.

In conclusion, the intercomparison analysis suggests that the RDI provides robust measurements of nearly all trace elements within the PM_{10-0.3} size range. The issues that do exist apply to absolute magnitudes, not relative changes. The analysis in this paper (e.g. urban/kerb increments and diurnal/weekly patterns) relies predominantly on these relative changes (precision), and thus neither the analysis nor the main conclusions are undermined by method reliability.

We agree that the use of certified reference materials would, in theory, be helpful (please note that the filter measurements are calibrated with NIST standards). However, these materials are typically available only in concentrations that are orders of magnitude higher than those attained with ambient sampling, as well as being mounted on a different foil or filter substrate. Both issues can significantly perturb XRF measurements, rendering these materials unsuitable for use. Meanwhile, after this manuscript went to press, we were able, for the first time, to obtain a set of certified single element standards in concentrations relevant to the ambient atmosphere on the same 6 µm PP foil used for RDI sampling. XRF measurements were performed in a recent beamtime and are not directly transferable to beamtimes in which the current data samples were analysed (i.e. different geometry and irradiation conditions). Preliminary results indicate agreement within 25 % with no positive or negative bias between RDI results using the multi- and single-element standards for the elements Na, Ca, Fe, Co, Sr and Ba in the area concentration range 3-5 µg cm⁻² on the PP foil. The use of these single-element standards will not influence the current comparison between SR-XRF and PM₁₀ filters since the deviations of XRF to PM₁₀ filters and to single-element standards go in opposite directions from a 1-to-1 ratio.

Comment #2:

2. Some of the elements affected by the above situation are very important for studies related to elemental concentrations in aerosols. For example, S and K, which are valuable for tracing human activities and/or biomass burning, in page 15907, present doubtful values. Regarding those of Na and Mg, it is not clear to me which values should be taken as more accurate (XRF or ICP).

Response:

We agree with the referee that the precise measurement of S and K is of great help in understanding the distribution of these elements across larger geographical regions. As stated in the response to Comment #1 the quantitative disagreement between RDI and PM₁₀ filters for S, K, Sn and Pb is expected based on differences in measured size ranges. The size distributions of S and K make it therefore

unsurprising (and not alarming) that previous XRF studies (Bukowiecki et al., 2005 and Richard et al., 2010), to which the referee refers at p. 15907, did not achieve good agreement with PM₁₀ filter techniques.

To clarify these points in the text we intend to make the following changes.

1. We will change the last sentence of the RDI description in Sect. 2.2.1 beginning at p. 15902 into:

“This results in sampling of a smaller fraction of PM_{1.0} particles than previously expected and influences those elements that occur predominantly in this size range, notably S, K and Pb.”

2. We include the following sentence in Sect. 4.1 towards the end of the first paragraph to repeat the explanation of the mass underestimation in the results section:

“According to Supplement A and B, elements with considerable mass in the PM_{1.0} fraction (S, Pb, potentially K, Zn, Br, Sn) may be significantly underestimated due to a higher than expected small-end cut point, relative to analysis methods with a smaller cut point towards 0 nm (290-410 nm, rather than the previously estimated value of 100 nm, Bukowiecki et al., 2009c; Richard et al., 2010).”

The referee also points to the disagreement of Na and Mg between both analyses methods, which differ by a factor of 2.5. This is well outside the estimated uncertainty (~25 %) of the RDI-SR-XRF analysis for these elements (see Comment #7), and the reason for the discrepancy is not clear (see Comment #1). In the absence of additional independent measurements of Na and Mg, it is indeed difficult to determine which method provides accurate absolute values. However, we note that both methods provide internally consistent measurements of these elements as evidenced by Na-to-Mg ratios and sensible time series. The critical criterion for the analysis herein is therefore met, providing precise relative changes for each element.

Comment #3:

3. Although the authors made the evaluation of the concentrations using the DE data as a reference, there may be other procedures that provide information about the origin of the elements. A simple method is the use of the Enrichment Factor (EF). Using the figures given in Table 2, I calculated the EF for the elements Fe and K, usually associated to particles with a geological (soil) origin, using Si as reference element and average Earth crust composition. It is possible to find that in the three sites, the EF for Fe in the coarse fraction is very high (of the order of 10), which may agree with the hypothesis given by the authors relating Fe to brake wear. Moreover, I would expect the contribution of brake wear in the rural site to be very low, approximating EF to unity and suggest a soil origin. Instead, the EF is higher at the DE site than the urban one. The authors should try to explain this. EF for Fe in the finest fraction is closer to 1, associating it to a crustal origin. As for K, for the coarse fractions the EF is almost equal to 1. However, for the finest fraction in the three sites it is higher than unity, in particular for DE, where the value is almost 20, showing it has a different origin than soil. I am including a table with the EF (with the last three columns giving the average EF for each site). It may be advisable to calculate the EF for the other elements, not necessarily to include in the manuscript, but as a guide to better understand the origin of each element.

Response:

We greatly appreciate this extended comment on the Enrichment Factor (EF) and the efforts that went into creating the table in the supplement to this comment. We will incorporate EF analysis into the paper by introducing it in Sect. 4.2.1 'Urban increment'. We will compare EF values of several elements that are grouped together in traffic-related and mineral dust groups based on both urban and kerb increment results.

We stress that urban/kerb increment calculations specifically relate concentrations of multiple sites to each other per element, which we believe is very valuable in exploring differences in human exposure at these sites. With EF, each element is related to Si as an indication for anthropogenic or soil origins. A comparison of the EF per element at multiple sites is probably as robust as the current increment calculations, but thus provides different information. The absolute magnitudes of EF are less meaningful since individual element concentrations are biased by the RDI small-size cut off of 300 nm and differences in uncertainties regarding absolute and relative calibrations.

Although we are not able to reproduce the exact EF values as given by the referee, we have calculated the EF for our data based on the upper continental crust composition as given by Wedepohl (1995).

For Fe we obtain EF of close to 40 for the kerbside, 20 for the urban background and 12 for the rural site, independent of size fraction. These results clearly indicate anthropogenic influences of Fe to all sites. The size independency can be understood when realizing that both Si and Fe are reduced by the same factor from the coarse to the fine mode, resulting in the same EF for each size range. The EF of 12 at the rural site is indeed high, but the concentration of Fe has decreased by a factor of 16 compared to 6 for Si between the kerbside and rural site. This strong decrease in Fe relative to Si is in line with an expected strongly reduced anthropogenic influence of mainly traffic at the rural site, and thus a larger soil fraction of Fe.

The EF of K is indeed highest in the fine fraction with values of 14, 26 and 28 at the kerbside, urban background and rural site, respectively, and indicates anthropogenic influence. We group fine fraction K as regionally influenced. The increased EF towards the rural site likely indicates stronger influences of biomass burning relative to the city sites.

Incorporating EF analysis will lead to the following paragraph on p. 15915 of Sect. 4.2.1:

"We group elements together based on similar urban increment values as an indication for co-emission. Mn, Fe, Cu, Zn, Zr, Mo, Sn, Sb and Ba show urban increments on average of 3.5 in the coarse, 3.1 in the intermediate and 2.0 in the fine fraction (Fig. 4). These have been identified as traffic-related elements by e.g. Amato et al., 2011; Bukowiecki et al., 2010; Minguillón et al., 2014; Richard et al., 2011 and Viana et al., 2008. Zr can also have a mineral dust origin (Moreno et al., 2013) as can be seen by the use of Enrichment Factors (EF). EF is a measure of the enrichment of elements relative to the upper continental crust (UCC) and is defined as ppm metal in sample / ppm metal in UCC with Si as reference material (UCC from Wedepohl, 1995). Zr is the only element in this traffic group that is depleted in the atmosphere relative to their UCC concentrations, but with concentrations at NK higher than at DE. Most other elements clearly indicate anthropogenic origin with EF

> 10. The urban increments are similar to that of NO_x, where concentrations at NK were on average a factor 4.9 higher than at DE (mean concentration at NK was 68 ppb, at DE 14 ppb). Black carbon (BC), a marker for both traffic and wood burning emissions, had an urban increment of only 1.1 (concentration at NK 757 ng m⁻³, at DE 633 ng m⁻³), likely due to local wood burning emissions around DE (Mohr et al., 2013). Al, Si, Ca, Ti and Sr as markers for mineral dust (e.g. Amato et al., 2009; Lin et al., 2005; Lucarelli et al., 2000) show a factor 2.0 higher concentrations at NK relative to DE in the coarse, 1.9 in the intermediate and 1.6 in the fine fraction (EF < 10). These results indicate that moving from rural to urban backgrounds yield a larger relative increase in traffic than in mineral dust elements. Surprisingly, sea salt elements (Na, Mg, Cl) show higher concentrations at NK than at DE of up to a factor of 2 for the coarse mode, despite the expected dominance of regional over local sources. This highlights the potential importance of sea or road salt resuspension by traffic. Similar urban increment values for traffic-related, resuspension and sea salt elements have been observed by Lee et al. (1994) for particles below a few µm. Theodosi et al. (2011) also found higher increments (> 2) for trace elements in PM₁₀ aerosol from local anthropogenic sources like fossil fuel combustion (V, Ni, Cd) and traffic (Cu), relative to long range transported Saharan dust (Fe, Mn) with increments close to 1. However, our study suggests that the non-size-resolved increment values reported in the cited studies do not fully capture the urban/rural differences.”

Comments #4 and #5:

4. In the conclusions, Fe is initially associated to traffic, then it is excluded from the list of brake wear related elements. In the text, however, it was suggested to be produced by brake wear and even a reference is given. Please clarify this point.

5. In several cases, the association among the elements does not look strongly justified. For example, why V and Ni are related to traffic? In many studies they are related to industrial sources (fuel oil burning and they are strongly correlated to S). Also, Zr is often linked to soil-derived particles in other papers.

Response:

There might be some misunderstanding about the grouping of elements we use in the paper. We note that we empirically group elements according to their similarities in urban/kerb increments and diurnal/weekly cycles, rather than that we associate them to specific emission sources. With other analysis methods, such as the Enrichment Factor (EF) as proposed in Comment #3, it might be possible to find another distinction between groups of elements related to specific emission sources.

We agree that the group of elements labelled as traffic-related in the kerb increment analysis contains also elements potentially emitted by other sources, such as V and Ni mainly from industrial sources and heavy-oil combustion. We realize that this label is confusing and will change it into anthropogenically-influenced (ANTH). This label is introduced, together with a source justification of all elements in this group, in Sect. 4.2.2 ‘Kerb increment’ in the 2nd paragraph on p. 15919:

“The second group consists of V, Cr, Mn, Fe, Ni, Zn and Pb with increments of 5.7-8.2 (PM_{10-2.5}) in the SW sector (2.6-3.0 for NE) (Fig. 6). V and Ni are typically assigned to industrial sources and heavy-oil combustion (e.g. Mazzei et al., 2007; Viana et al., 2008), Zn is usually associated with tire wear (e.g. Harrison et al., 2012b; Lin et al., 2005), and the other elements are commonly associated with traffic-related emissions (e.g. Amato et al., 2013; Bukowiecki et al., 2009a; Richard et al., 2011). We empirically label this group as anthropogenically-influenced (ANTH). The

EF of V and Ni are much lower than those of the other elements in this group (2 vs. > 10), indicating at least to some extent different source origins. These kerb increments are similar to the ones for NO_x of 8.5 for SW and 2.4 for NE, confirming the anthropogenic influence (traffic and other sources) on these elements. The high braking frequency at MR due to congested traffic probably resulted in increased kerb increments of brake wear relative to ANTH elements that are also influenced by local traffic and other sources around NK. Increments of these ANTH elements are higher than previously reported values of 1.8-4.5 for studies with low time resolution and non-size segregated particles (Boogaard et al., 2011; Janssen et al., 1997). The high increments presented here might be caused by street canyon effects, trapping pollutants emitted at street level and preventing dilution to the urban background. The enhanced kerb increments for brake wear relative to ANTH elements are apparent in all three size fractions, although increments become more similar towards smaller sizes with a factor 1.7 between both element groups in the coarse, 1.5 in the intermediate and 1.4 in the fine mode. Both groups show the additional information gained with size-segregated aerosol, where exposure to trace elements in the street canyon relative to the urban background increases with particle size, either caused by increased traffic-related emissions with particle size or by more efficient transport of submicron particles from street sites to the urban background. Furthermore, the highly time-resolved element measurements presented here enabled us to resolve the systematic, wind direction dependent variability in kerb increments."

The referee points out that Zr is often linked to soil-derived particles, whereas we group it with elements typically related to brake wear based on its urban increment. Both origins have been proposed in previous literature. In line with the response to Comment #3, Zr shows a different EF than the other elements in this group, potentially indicating a different source origin.

In the urban increment analysis no distinction was observed for brake wear and other traffic-related elements, and therefore just formed 1 group. In the analysis of the kerb increment higher values were observed for brake wear (Cu, Zr, Mo, Sn, Sb and Ba) than for other traffic-related (V, Cr, Mn, Fe, Ni, Zn and Pb) elements, and were treated as two different groups. Fe falls in this second category with lower kerb increment values. Some studies (e.g. Harrison et al., 2012b) assign Fe to brake wear, but we assign Fe to the traffic-related group purely based on its lower kerb increment value.

Following the discussion above, we believe the label of the traffic-related group is confusing and this group of elements will be relabelled as anthropogenically-influenced (ANTH). The paper will be changed accordingly.

We will rephrase the 2nd paragraph of the Conclusions at p. 15927-15928 according to the new labelling of the groups:

"Urban and kerb increments were defined as the concentration ratios of urban background to rural, and kerbside to urban background, respectively, and the kerb increments were further explored as a function of wind direction. The group with the largest kerb increments consisted of elements typically associated with brake wear (Cu, Zr, Mo, Sn, Sb, Ba). The second largest increments were formed by anthropogenically-influenced elements typically assigned to non-brake wear traffic emissions (Cr, Mn, Fe, Zn, Pb) but also by elements like V and Ni. This could indicate either a traffic source for these elements or a similar kerbside-to-urban emission gradient. Kerb increments were larger for the brake wear group and under

SW winds due to local street canyon effects, with coarse fraction increments between 10.4 and 16.6 for SW winds (3.3-6.9 for NE winds) against increments for the anthropogenically-influenced group between 5.7 and 8.2 for SW winds (2.6-3.0 for NE winds). The kerb increments for all these elements in the $PM_{10-2.5}$ size fraction are roughly 2 times that of the $PM_{1.0-0.3}$ fraction. Urban increments (no distinction between both groups) were around 3.0. In addition to direct emissions, traffic-related processes influence the concentrations of other elements by resuspension, with mineral dust (Al, Si, Ca, Ti, Sr) increments of 1.3-3.3.”

Comment #6:

6. The paper is very long, and maybe some parts may be reduced, as the comparison with other techniques.

Response:

We appreciate the referee's suggestion and have taken the following steps to condense the manuscript:

1. As suggested by the referee, the method intercomparison will be significantly shortened. We will move Fig. 2 and most of the associated discussion to the Supplement. Only a brief summary will remain in the main text.
2. Furthermore, the discussion about the local wind direction influence at kerbside, urban background and rural sites will be condensed. We are convinced that this analysis is interesting and important in understanding wind direction effects on pollution levels at different micro-environments. However, less detail is possible in this part of the paper and some repetition from the urban increment discussion regarding element grouping can be removed.
3. We will condense the discussion about the kerb increment by removing repetition regarding grouping of elements, already discussed in the urban increment and local wind direction influence discussions. We also condense the comparison of increment values to previous studies in this section.
4. We will condense the discussion about the three case studies regarding regional influences by rephrasing this section.
5. Finally, we will condense the discussion regarding daily/weekly cycles, specifically by removing repetition concerning reasons for enhanced element concentrations during rush hour due to increased braking processes.
6. We also note that the Introduction was condensed at the “technical corrections” stage prior to publication in ACPD by reducing the detail in which trace element measurements across Europe are discussed, and by shortening the introduction of the concept of urban micro-environments.

We feel that the remainder of the paper presents our results with an appropriate level of detail and explanation regarding the discussion of concentration levels of 25 elements in 3 size fractions at 3 sites as a function of increments, wind direction and time.

Comment #7:

7. Finally, a major problem in the entire manuscript is that there is no mention to experimental uncertainties, except for a few elements (Na, Mg or Mo), but there is not a careful explanation on how they were estimated. It is mandatory to present uncertainties in every experimental/laboratory work.

Response:

We agree that presenting uncertainties of this type of work is essential. During the “technical corrections” stage we added a paragraph at the end of Section 4.1 ‘Trace element concentrations’ giving an overview of the main sources of uncertainty in our study. We will extend this in the revised manuscript and add a table to the Supplement reporting element-specific detection limits and size-dependent element uncertainties.

The following text summarizes the major sources of experimental uncertainty:

“The RDI-SR-XRF technique is subject to various sources of uncertainty, which change in importance depending on whether the data are described in terms of absolute/fractional concentrations (as above) or in terms of relative changes/ratios (as in the remainder of the manuscript). A brief overview is presented here:

1. RDI sampling: the fluctuations in the flow rate are negligible within 5 % (Richard et al., 2010) and the uncertainties in the size cut off are discussed in Supplement A.

2. SR-XRF accuracy: uncertainties in the absolute and relative calibrations affect absolute/fractional concentrations, but cancel out for relative changes/ratios, because all samples were measured under the same calibration conditions.

3. Issues such as imperfect flatness of the sample foils and detector dead time corrections (Richard et al., 2010) reduce measurement precision but affect all elements with the same scaling factor.

4. SR-XRF measurement precision is affected by sample inhomogeneity and spectral analysis uncertainties. Sample inhomogeneity was assessed by Bukowiecki et al. (2009c) and found to contribute ± 20 % uncertainty.

For most elements, except Mn, sample inhomogeneity is the largest source of uncertainty. Mn is affected by spectral analysis uncertainties due to peak overlap with Fe, present in much higher concentrations. Therefore, a small change in the energy calibration as function of detector channel leads to a large change in the peak area of Mn. All data points lie well above their element detection limits, resulting in negligible uncertainties from the signal strength. Table S3 in Supplement B provides an estimate of the total uncertainty per size fraction and detection limits for each element. In addition, RDI-SR-XRF measurements (both absolute/fractional and relative/ratio) are affected by atmospheric variability. This variability is likely the predominant source of the data spread evident in Table 2 and the following analyses.”

The following table (in the Supplement) lists estimated total uncertainties per size fraction and detection limits for each element. Note that the sample inhomogeneity dominates the uncertainties for most elements.

Table S3. Estimated total uncertainty (% of measured value) of the calculated element concentrations per size fraction, and detection limits for each element (ng m^{-3}).

| Element | PM _{10-2.5} (%) ^a | PM _{2.5-1.0} (%) ^a | PM _{1.0-0.3} (%) ^a | DL (ng m^{-3}) ^b |
|-----------------|--|---|---|---|
| Na ^c | 25 | 25 | 25 | 2.552 |
| Mg | 24 | 24 | 24 | 0.962 |
| Al | 24 | 25 | 25 | 1.709 |
| Si | 24 | 24 | 24 | 0.420 |
| P | 25 | 25 | 25 | 0.118 |
| S | 24 | 24 | 24 | 0.503 |
| Cl | 24 | 24 | 24 | 0.158 |
| K | 24 | 24 | 24 | 0.031 |

| | | | | |
|----|----|----|----|-------|
| Ca | 21 | 21 | 21 | 0.267 |
| Ti | 24 | 26 | 27 | 0.024 |
| V | 30 | 30 | 24 | 0.008 |
| Cr | 27 | 27 | 26 | 0.015 |
| Mn | 83 | 69 | 46 | 0.042 |
| Fe | 21 | 21 | 21 | 0.033 |
| Ni | 22 | 22 | 21 | 0.005 |
| Cu | 21 | 21 | 21 | 0.028 |
| Zn | 21 | 21 | 21 | 0.058 |
| Br | 21 | 21 | 21 | 0.117 |
| Sr | 21 | 21 | 21 | 0.036 |
| Zr | 21 | 21 | 21 | 0.036 |
| Mo | 21 | 21 | 21 | 0.037 |
| Sn | 21 | 21 | 21 | 0.061 |
| Sb | 21 | 21 | 21 | 0.052 |
| Ba | 21 | 21 | 21 | 0.254 |
| Pb | 21 | 21 | 21 | 0.137 |

^a Combination of uncertainties regarding sample inhomogeneity (20 %), RDI flow rate (5 %), absolute and relative calibration (Na-K 13 %, Ca-Pb 2 %) and spectral analysis specific per element and size fraction (median uncertainties for all data points).

^b As 3x the standard deviation of the spectra signals used for continuum corrections.

^c Na uncertainties might be underestimated due to the overlap with the L lines of Ni, Cu and Zn. In the current analysis the ratio of the L α to K α lines are determined empirically, and quantification of the associated uncertainties is under investigation.

In the Supplement regarding the data intercomparison the first paragraph will introduce the intercomparison and this table, together with a more detailed explanation of the sources of uncertainty in this study. The table will serve as a guide to interpret the comparison between RDI and PM₁₀ filter data, as described in the rest of this Supplement.

References

- Amato, F., Pandolfi, M., Escrig, A., Querol, X., Alastuey, A., Pey, J., Perez, N., and Hopke, P. K.: Quantifying road dust resuspension in urban environment by Multilinear Engine: A comparison with PMF2, *Atmos. Env.*, 43, 2770-2780, 2009.
- Amato, F., Viana, M., Richard, A., Furger, M., Prevot, A. S. H., Nava, S., Lucarelli, F., Bukowiecki, N., Alastuey, A., Reche, C., Moreno, T., Pandolfi, M., Pey, J., and Querol, X.: Size and time-resolved roadside enrichment of atmospheric particulate pollutants, *Atmos. Chem. Phys.*, 11, 2917-2931, 2011.
- Bukowiecki, N., Hill, M., Gehrig, R., Zwicky, C. N., Lienemann, P., Hegedus, F., Falkenberg, G., Weingartner, E., and Baltensperger, U.: Trace metals in ambient air: Hourly size-segregated mass concentrations determined by synchrotron-XRF, *Environ. Sci. Technol.*, 39, 5754-5762, 2005.
- Bukowiecki, N., Richard, A., Furger, M., Weingartner, E., Aguirre, M., Huthwelker, T., Lienemann, P., Gehrig, R., and Baltensperger, U.: Deposition uniformity and particle size distribution of ambient aerosol collected with a rotating drum impactor, *Aerosol Sci. Technol.*, 43, 891-901, 2009c.
- Bukowiecki, N., Lienemann, P., Hill, M., Furger, M., Richard, A., Amato, F., Prevot, A. S. H., Baltensperger, U., Buchmann, B., and Gehrig, R.: PM10 emission factors for non-exhaust particles generated by road traffic in an urban street canyon and along a freeway in Switzerland, *Atmos. Env.*, 44, 2330-2340, 2010.
- Lee, D. S., Garland, J. A., and Fox, A. A.: Atmospheric concentrations of trace elements in urban areas of the United Kingdom, *Atmos. Env.*, 28, 2691-2713, 1994.
- Lin, C. C., Chen, S. J., Huang, K. L., Hwang, W. I., Chang-Chien, G. P., and Lin, W. Y.: Characteristics of metals in nano/ultrafine/fine/coarse particles collected beside a heavily trafficked road, *Environ. Sci. Technol.*, 39, 8113-8122, 2005.

- 1 Lucarelli, F., Mando, P. A., Nava, S., Valerio, M., Prati, P., and Zucchiatti, A.: Elemental
2 composition of urban aerosol collected in Florence, Italy, *Environ. Monit. Assess.*, 65, 165-
3 173, 2000.
- 4 Minguillón, M. C., Cirach, M., Hoek, G., Brunekreef, B., Tsai, M., de Hoogh, K., Jedynska, A.,
5 Kooter, I. M., Nieuwenhuijsen, M., and Querol, X.: Spatial variability of trace elements and
6 sources for improved exposure assessment in Barcelona, *Atmos. Env.*, 89, 268-281, 2014.
- 7 Mohr, C., Lopez-Hilfiker, F. D., Zotter, P., Prévôt, A. S. H., Xu, L., Ng, N. L., Herndon, S. C.,
8 Williams, L. R., Franklin, J. P., Zahniser, M. S., Worsnop, D. R., Knighton, W. B., Aiken, A. C.,
9 Gorkowski, K. J., Dubey, M. K., Allan, J. D., and Thornton, J. A.: Contribution of nitrated
10 phenols to wood burning brown carbon light absorption in Detling, United Kingdom during
11 winter time, *Environ. Sci. Technol.*, 47, 6316-6324, doi:10.1021/es400683v, 2013.
- 12 Moreno, T., Karanasiou, A., Amato, F., Lucarelli, F., Nava, S., Calzolari, G., Chiari, M., Coz,
13 E., Artinano, B., Lumberras, J., Borge, R., Boldo, E., Linares, C., Alastuey, A., Querol, X., and
14 Gibbons, W.: Daily and hourly sourcing of metallic and mineral dust in urban air contaminated
15 by traffic and coal-burning emissions, *Atmos. Env.*, 68, 33-44,
16 doi:10.1016/j.atmosenv.2012.11.037, 2013.
- 17 Richard, A., Bukowiecki, N., Lienemann, P., Furger, M., Fierz, M., Minguillon, M. C., Weideli,
18 B., Figi, R., Flechsig, U., Appel, K., Prevot, A. S. H., and Baltensperger, U.: Quantitative
19 sampling and analysis of trace elements in atmospheric aerosols: impactor characterization
20 and synchrotron-XRF mass calibration, *Atmos. Meas. Tech.*, 3, 1473-1485, 2010.
- 21 Richard, A., Gianini, M. F. D., Mohr, C., Furger, M., Bukowiecki, N., Minguillon, M. C.,
22 Lienemann, P., Flechsig, U., Appel, K., DeCarlo, P. F., Heringa, M. F., Chirico, R.,
23 Baltensperger, U., and Prevot, A. S. H.: Source apportionment of size and time resolved trace
24 elements and organic aerosols from an urban courtyard site in Switzerland, *Atmos. Chem.*
25 *Phys.*, 11, 8945-8963, 2011.
- 26 Theodosi, C., Grivas, G., Zampas, P., Chaloulakou, A., and Mihalopoulos, N.: Mass and
27 chemical composition of size-segregated aerosols (PM1, PM2.5, PM10) over Athens, Greece:
28 local versus regional sources, *Atmos. Chem. Phys.*, 11, 11895-11911, doi:10.5194/acp-11-
29 11895-2011, 2011.
- 30 Viana, M., Kuhlbusch, T. A. J., Querol, X., Alastuey, A., Harrison, R. M., Hopke, P. K.,
31 Winiwarter, W., Vallius, A., Szidat, S., Prevot, A. S. H., Hueglin, C., Bloemen, H., Wahlin, P.,
32 Vecchi, R., Miranda, A. I., Kasper-Giebl, A., Maenhaut, W., and Hittenberger, R.: Source
33 apportionment of particulate matter in Europe: A review of methods and results, *J. Aerosol*
34 *Sci.*, 39, 827-849, doi:10.1016/j.jaerosci.2008.05.007, 2008.
- 35 Wedepohl, K.: The composition of the continental crust, *Geochim. Cosmochim. Acta*, 59,
36 1217-1232, doi:10.1016/0016-7037(95)00038-2, 1995.

37

Response to Reviewer #3:

We kindly thank the referee for taking our manuscript into consideration and we appreciate the comments raised on the manuscript. The referee's main concerns regard the reliability of the measurement technique and the novelty of the results, which we address in detail below.

The manuscript reports on a study on the aerosol composition in three sites in the London area by DRUM impactor & SXRF analysis. The text is extremely long and full of details, however I have major and basics concerns so that I cannot recommend it for publication.

The manuscript can be divided roughly in two parts: 1) technologies and methods, 2) results and discussion

Comment #1:

Part 1: this is potentially the more interesting part of the paper and actually it could/should re-arranged in a separate technical note (or similar...it is now 10-page long) since most of the details now given are likely not necessary in regular article focused on the experimental results (I mean: the joint use of DRUM & SXRF has been already introduced in previous papers).

Response:

We appreciate the referee's suggestion and we agree that some of the technical aspects in this paper are not directly needed to understand the results sections. We have considered submitting a separate technical note including the technical advancements regarding SR-XRF analysis (Sect. 2.2.1, points 1-4 on p. 15904-15906) and the data intercomparison between RDI and PM₁₀ filters (Sect. 3, p. 15907-15910). However, as the referee points out, the current analysis is built on previous papers following a similar methodology (Bukowiecki et al., 2005, 2008, 2009c and Richard et al., 2010). Therefore, we believe that the advancements described in this paper represent an incremental improvement on an existing technique, rather than a reinvention of the method, and are thus best treated within the current paper. However, as noted in the response to Comment #2, the Methods section has been significantly shortened by moving the detailed discussion of the method intercomparison to the Supplement.

Comment #2:

On the other hand, this long discussion fails, in my opinion, in demonstrating the reliability of the adopted methodology and poses the discussion of the experimental results on a "icy ground" (the comparison vs. other techniques show a quite poor agreement).

Response:

The referee refers to the disagreement between measurement techniques in Section 3 (Data intercomparison) and specifically Fig. 2, and suggests that this calls into question the experimental results. However, much of this disagreement is expected, resulting from known differences in the measurement techniques (e.g. different size ranges) and thus does not reflect data quality. In addition, we note that this section

1 should be interpreted as a method intercomparison rather than RDI-SR-XRF
2 validation, and that the extent of the agreement is similar to other intercomparison
3 studies of trace element measurement techniques. We have clarified these points by
4 significantly condensing the intercomparison section of the manuscript, with Fig. 2
5 and the accompanying detailed discussion moved to the Supplement. An overview of
6 the main points is provided below (please note that Cr has been removed from the
7 intercomparison as this element was rejected from the filter analysis during the final
8 quality assurance checks):

- 9 1. Most elements (i.e. all except those discussed below) show good agreement
10 between RDI and PM₁₀ filters within ± 50 % with good Pearson's R of > 0.78 .
- 11 2. Quantitative agreement between RDI and PM₁₀ filters should not be obtained
12 for elements with significant mass below the RDI small-size cut off of 300 nm.
13 This includes S, K, Sn and Pb. For S, further investigation is possible by
14 adding the mass from the backup filter to the PM_{1.0-0.3} mass measured by the
15 RDI. Quantitative agreement with the AMS SO₄²⁻ data is then achieved,
16 suggesting the RDI provides accurate PM_{1.0-0.3} values for all these elements.
- 17 3. V, Ni and Mo are well-constrained in the RDI-SR-XRF analysis and are well
18 above detection limits, but have low or unknown extraction efficiencies in the
19 PM₁₀ filter-ICP-MS analysis, increasing the uncertainty of the PM₁₀ filters.
20 Further, the RDI measurements of these elements are internally consistent
21 (strong correlations with co-emitted elements). This suggests that the RDI
22 measurements are correct, and the disagreement does not reflect RDI data
23 quality issues.
- 24 4. RDI and filter measurements of Na and Mg are strongly correlated but
25 disagree on the absolute magnitude. The RDI relative calibration of these
26 elements is somewhat uncertain (around 13 %), while the filters have
27 unknown extraction efficiency for Na (Mg is well extracted with 90 %
28 efficiency). However, both techniques provide internally consistent results
29 (e.g. correct Na-to-Mg ratios and sensible time series). Thus, while the
30 absolute concentrations can be questioned, relative changes should be
31 considered robust.

32
33 In conclusion, the intercomparison analysis suggests that the RDI provides robust
34 measurements of nearly all trace elements within the PM_{10-0.3} size range. The issues
35 that do exist apply to absolute magnitudes, not relative changes. The analysis in this
36 paper (e.g. urban/kerb increments and diurnal/weekly patterns) relies predominantly
37 on these relative changes, and thus neither the analysis nor the main conclusions are
38 undermined by method reliability.

39
40 **Comment #3:**

41 *I have also to note that, despite of the length, two times the reader is forwarded to*
42 *future papers which should complete the methodological section: this could be*
43 *accepted in a letter but not in this case.*

44
45 **Response:**

46 In addressing the comments #1 and #7 of Referee #2, we have included sufficient
47 information on the analysis method for the reader to grasp the relevant issues. These
48 references are thus no longer needed and have been removed.

Comment #4:

Neglecting the concerns at point 1), the section "results" is a extremely detailed list of "raw" data which are extremely valuable at local level but, in my view, not of general interest since they do not improve our knowledge of atmospheric aerosols.

Response:

We believe that the results sections in this paper are very valuable for the following reasons:

1. The dataset is unique: to our knowledge, no previous study achieves size-resolved measurements of trace elements with fast 2 h time resolution at kerbside, urban background, and rural sites simultaneously. We would in general like to make the remark that there are too few increment studies published for various pollutants. Such combined measurements allow a better assessment which components of the pollution are rather driven by regional, urban or very local pollution.
2. Trace element measurements are directly relevant to human health, both in terms of quantifying exposure to toxic metals and as chemical tracers for exposure to other emission sources. Real-world human exposure depends on the temporal characteristics of size-dependent particle concentrations in specific micro-environments. Accurate exposure assessments therefore require measurements of the unique type performed herein.
3. The present study in London can be conceived as a model study for the assessment of micro-environment (kerbside, urban background, rural) effects on trace element concentrations in cities around the world. This is poorly constrained in most locations, although existing results in Europe suggest important differences can exist depending on the local or regional environment. Such investigations are urgently needed for assessing public health risks and evaluating pollution mitigation strategies.

Comment #5:

A real Source Apportionment study is missing and the added-value of the very demanding DRUM+SXRF analysis remains only partially demonstrated (i.e. the possibility to catch transients and episodes with a high-resolution sampling has been introduced and discussed several times in previous papers on DRUM and other high-resolution samplers/impactors).

Response:

A source apportionment study on this data set is definitely interesting, and will be the subject of a future paper. The source apportionment analysis is complex by itself, as we basically deal with 9 datasets (3 sites and 3 size ranges). The inclusion of the source apportionment would definitely overload the paper. In the current study, we do by far not only demonstrate the possibility to catch transients, but we go much further. The present focus is on exploiting the measurement time resolution to investigate the detailed issues governing local trace element concentrations (e.g. wind direction, street canyons, regional air masses). These are only in a broad sense source-dependent; we feel it is an advantage to investigate these issues without the statistical blurring that inevitably occurs within factor analysis.

Comment #6:

I really don't find "the message" (or better the information) in this 18-page long text, which could and should be considered as a technical report in preparation of an article with a real and full source apportionment exercise.

Response:

In addressing this comment and the comment #6 of Referee #2 we have taken the following steps to condense the manuscript, mainly by rephrasing and repetition removing:

1. In line with the response to comment #2, the method intercomparison will be significantly shortened. We will move Fig. 2 and most of the associated discussion to the Supplement. Only a brief summery will remain in the main text.
2. Furthermore, the discussion about the local wind direction influence at kerbside, urban background and rural sites will be condensed. We are convinced that this analysis is interesting and important in understanding wind direction effects on pollution levels at different micro-environments. However, less detail is possible in this part of the paper and some repetition from the urban increment discussion regarding element grouping can be removed.
3. We will condense the discussion about the kerb increment by removing repetition regarding grouping of elements, already discussed in the urban increment and local wind direction influence discussions. We also condense the comparison of increment values to previous studies in this section.
4. We will condense the discussion about the three case studies regarding regional influences by rephrasing this section.
5. Finally, we will condense the discussion regarding daily/weekly cycles, specifically by removing repetition concerning reasons for enhanced element concentrations during rush hour due to increased braking processes.

We feel that the remainder of the results sections provide a clear overview of urban/kerb increments and diurnal/weekly cycles for the broad range of trace elements, which are needed to understand human exposure levels at multiple micro-environments as a function of size and time. We show strongly enhanced element concentrations at the kerbside, especially for coarse fraction particles up to a factor of 17 relative to urban background levels and being heavily affected by wind direction. All elements influenced by traffic, either by wearing processes or by resuspension exhibit elevated concentrations during rush hours and on weekdays compared to weekends. These occur predominantly at the kerbside but are also clearly observed at the urban background site, indicating largely enhanced health risks during these periods throughout a city.

References

- Bukowiecki, N., Hill, M., Gehrig, R., Zwicky, C. N., Lienemann, P., Hegedus, F., Falkenberg, G., Weingartner, E., and Baltensperger, U.: Trace metals in ambient air: Hourly size-segregated mass concentrations determined by synchrotron-XRF, Environ. Sci. Technol., 39, 5754-5762, 2005.
- Bukowiecki, N., Lienemann, P., Zwicky, C. N., Furger, M., Richard, A., Falkenberg, G., Rickers, K., Grolimund, D., Borca, C., Hill, M., Gehrig, R., and Baltensperger, U.: X-ray fluorescence spectrometry for high throughput analysis of atmospheric aerosol samples: The benefits of synchrotron X-rays, Spectrosc. Acta Pt. B-Atom. Spectr., 63, 929-938, 2008.

- 1 Bukowiecki, N., Richard, A., Furger, M., Weingartner, E., Aguirre, M., Huthwelker, T.,
2 Lienemann, P., Gehrig, R., and Baltensperger, U.: Deposition uniformity and particle size
3 distribution of ambient aerosol collected with a rotating drum impactor, *Aerosol Sci. Technol.*,
4 43, 891-901, 2009c.
- 5 Richard, A., Bukowiecki, N., Lienemann, P., Furger, M., Fierz, M., Minguillon, M. C., Weideli,
6 B., Figi, R., Flechsig, U., Appel, K., Prevot, A. S. H., and Baltensperger, U.: Quantitative
7 sampling and analysis of trace elements in atmospheric aerosols: impactor characterization
8 and synchrotron-XRF mass calibration, *Atmos. Meas. Tech.*, 3, 1473-1485, 2010.
- 9

**Kerb and urban increment of highly time-resolved
trace elements in PM₁₀, PM_{2.5} and PM_{1.0} winter aerosol
in London during ClearfLo 2012**

**S. Visser¹, J.G. Slowik¹, M. Furger¹, P. Zotter¹, N. Bukowiecki¹, R. Dressler², U.
Flechsig³, K. Appel^{4*}, D.C. Green⁵, A.H. Tremper⁵, D.E. Young⁶, P.I. Williams^{6,7},
J.D. Allan^{6,7}, S.C. Herndon⁸, L.R. Williams⁸, C. Mohr⁹, L. Xu¹⁰, N.L. Ng^{10,11}, A.
Detournay¹², J.F. Barlow¹³, C.H. Halios¹³, Z.L. Fleming^{7,14}, U. Baltensperger¹ and
A.S.H. Prévôt¹**

[1] {Laboratory of Atmospheric Chemistry, Paul Scherrer Institute, Villigen,
Switzerland}

[2] {Laboratory of Radiochemistry and Environmental Chemistry, Paul Scherrer
Institute, Villigen, Switzerland}

[3] {Swiss Light Source, Paul Scherrer Institute, Villigen, Switzerland}

[4] {HASYLAB, DESY Photon Science, Hamburg, Germany}

[5] {School of Biomedical and Health Sciences, King's College London, London, UK}

[6] {School of Earth, Atmospheric and Environmental Sciences, University of
Manchester, Manchester, UK}

[7] {National Centre for Atmospheric Science, UK}

[8] {Aerodyne Research, Inc., Billerica, MA, USA}

[9] {Department of Atmospheric Sciences, University of Washington, Seattle, WA,
USA}

[10] {School of Chemical and Biomolecular Engineering, Georgia Institute of
Technology, Atlanta, GA, USA}

[11] {School of Earth and Atmospheric Sciences, Georgia Institute of Technology,
Atlanta, GA, USA}

[12] {Centre for Ecology and Hydrology, Penicuik, Midlothian, Scotland}

[13] {Department of Meteorology, University of Reading, Reading, UK}

[14] {Department of Chemistry, University of Leicester, Leicester, UK}

[*] {now at: European XFEL, Hamburg, Germany}

Correspondence to: M. Furger (markus.furger@psi.ch)

Abstract

Ambient concentrations of trace elements with 2 h time resolution were measured in $PM_{10-2.5}$, $PM_{2.5-1.0}$ and $PM_{1.0-0.3}$ size ranges at kerbside, urban background and rural sites in London during winter 2012. Samples were collected using rotating drum impactors (RDIs) and subsequently analysed with synchrotron radiation-induced X-ray fluorescence spectrometry (SR-XRF). Quantification of kerb and urban increments (defined as kerb-to-urban and urban-to-rural concentration ratios, respectively), and assessment of diurnal and weekly variability provided insight into sources governing urban air quality and the effects of urban micro-environments on human exposure. Traffic-related elements yielded the highest kerb increments, with values in the range of ~~11.6 to 18.5~~10.4 to 16.6 for SW winds (~~3.6 to 9.4~~3.3 to 6.9 for NE) observed for elements influenced by brake wear (e.g. Cu, Sb, Ba) and ~~5.6 to 8.0~~5.7 to 8.2 for SW (~~2.6 to 6.5~~2.6 to 3.0 for NE) for other traffic-related processes (e.g. Cr, Fe, Zn). Kerb increments for these elements were highest in the $PM_{10-2.5}$ mass fraction, roughly 32 times that of the $PM_{1.0-0.3}$ fraction. These elements also showed the highest urban increments (~ 3.0), although no difference was observed between brake wear and other traffic-related elements. All elements influenced by traffic~~Traffic-related elements~~ exhibited higher concentrations during morning and evening rush hour, and on weekdays compared to weekends, with the strongest trends observed at the kerbside site, and additionally enhanced by winds coming directly from the road, consistent with street canyon effects. Elements related to mineral dust (e.g. Al, Si, Ca, Sr) showed significant influences from traffic-induced resuspension, as evidenced by moderate kerb (~~2.0 to 4.1~~3.4 to 5.4 for SW, ~~1.4 to 2.1~~1.7 to 2.3 for NE) and urban (~~1.7 to 2.3~~~ 2) increments and increased concentrations during peak traffic flow. Elements related to regional transport showed no significant enhancement at kerb or urban sites, with the exception of $PM_{10-2.5}$ sea salt (factor of 1.5 to 2.0up to 2), which may be influenced by traffic-induced resuspension of sea and/or road salt. Heavy duty vehicles appeared to have a larger effect than passenger vehicles on the concentrations of all elements influenced by resuspension (including sea salt) and wearing processes. Trace element concentrations in London were influenced by both local and regional sources, with coarse and intermediate fractions dominated by traffic-induced resuspension and wearing processes and fine particles influenced by regional transport.

1 **1 Introduction**

2 Ambient particulate matter (PM) has long been recognized to have a detrimental
3 effect on public health in urban areas (e.g. Dockery and Pope, 1994). Of particular
4 interest are particles with an aerodynamic diameter less than 10 μm (PM_{10}) as these
5 particles can penetrate deeply into the lungs (Franklin et al., 2008; Zhou et al., 2011).
6 Reche et al. (2012) ~~showed-reported~~ even higher toxicity to human cells for the
7 $\text{PM}_{2.5-1.0}$ than for the $\text{PM}_{10-2.5}$ fraction. Particle toxicity is known to vary significantly
8 with PM composition and emission sources (Kelly and Fussell, 2012), with identified
9 toxic constituents including soluble secondary inorganic particles, elemental and
10 organic carbon, and especially metals. Effective mitigation strategies therefore
11 require detailed, size-dependent characterization of particle composition and
12 emission sources.

13 In addition to their direct effects on human health, metals and trace elements are of
14 importance because their high source specificity and atmospheric stability make
15 them effective tracers for source apportionment. In Europe, four main source types in
16 PM_{10} are commonly identified: vehicles (~~with tracers~~ including e.g. Fe, Ba, Zn, Cu),
17 crustal materials (e.g. Al, Si, Ca, Fe), sea salt (mainly Na, Cl, Mg) and mixed
18 industrial/fuel-oil combustion (mainly V, Ni, S) and secondary aerosol (mainly S)
19 (Putaud et al., 2010; Viana et al., 2008). The contribution of mineral dust and sea salt
20 in most urban areas is larger in PM_{10} than in $\text{PM}_{2.5}$ (Harrison et al., 2001; Weijers et
21 al., 2011). Emissions from vehicle exhaust, industry and secondary aerosol are
22 predominantly emitted and formed as $\text{PM}_{1.0}$ or in $\text{PM}_{2.5}$ (Bukowiecki et al., 2010;
23 Harrison et al., 2011; Richard et al., 2011). Several of these sources have been
24 directly linked to adverse health effects. For example, the largest aerosol source of
25 human toxicity in Barcelona was attributed to traffic activities (encompassing vehicle
26 emissions, road dust and secondary nitrate), with fuel oil combustion and industrial
27 emissions also contributing to increased cancer risk (Reche et al., 2012). Turoczi et
28 al. (2012) observed higher toxicity from direct emissions (e.g. from traffic) than from
29 photochemically processed aerosol.

30 The Clean Air for London project (ClearfLo; www.clearflo.ac.uk) is a multinational
31 effort to elucidate the processes driving poor air quality in London, implemented
32 through comprehensive measurements of particle- and gas-phase composition, ~~as~~
33 ~~well as and~~ meteorological parameters (Bohnenstengel et al., 2014). ClearfLo builds
34 upon recent modelling and monitoring studies in London (Arnold et al., 2004;
35 Bohnenstengel et al., 2011; Bohnenstengel et al., 2013b; Harrison et al., 2012a;
36 Mavrogianni et al., 2011). Despite improved air quality, PM_{10} concentrations are not
37 ~~fallingdecreasing~~, resulting in frequent exceedances of the daily PM_{10} limit (Harrison

et al., 2008). Such exceedances are caused by complex interactions of regional and local emission sources, together with meteorological factors such as wind speed, air mass origin, and daily cycles of the atmospheric boundary layer (Charron and Harrison, 2005; Harrison and Jones, 2005; Jones et al., 2010). Currently, emissions by industrial sources and stationary combustion are modest, ~~however while,~~ traffic is thought to contribute up to 80 % of the total PM₁₀ in London, compared to less than 20 % for the entire UK, according to emission inventories between 1970 and 2001 (Dore et al., 2003).

The spatial density of emission sources found in typical urban environments leads to elevated particle concentrations compared to nearby rural locations. As an example, ~~bBuildings, e.g.,~~ buildings may influence local meteorology by restricting air circulation (street canyon effect), producing human exposures that are orders of magnitude higher than those predicted by regional dispersion models (Zhou and Levy, 2008). This provides both acute exposure risk and increased long-term exposure for those passing through regularly, thereby producing a non-negligible impact on public health. To assess the impact of such micro-environments, we here investigate London trace element concentrations in terms of increments, defined as the concentration ratios between an environment of interest and a reference site (e.g. Charron et al., 2007).

Only a few studies have investigated trace elements through simultaneous measurements at ~~urban background and rural or kerbside~~ multiple sites. Harrison et al. (2012b) reported increments of kerbside to urban background sites in London for non-size segregated aerosol with a time resolution of 1 to 4 days ~~in London~~. Theodosi et al. (2011) found that at urban and suburban sites in Athens and a regional site in Finokalia, Greece crustal elements dominate ~~the coarse mode~~ coarse particles (PM_{10-2.5}), whereas anthropogenic sources such as fossil fuel combustion were confined ~~in the fine mode to fine particles~~ (V, Ni and Pb have > 70 % of their mass in PM_{1.0}). Bukowiecki et al. (2009a) and Bukowiecki et al. (2010) examined trace elements in PM_{10-2.5}, PM_{2.5-1.0} and PM_{1.0-0.1} aerosol at street canyon and urban background sites in Zürich, Switzerland, and showed increasing increments (note: 1 means no increment) with particle size from about 1.2 (fine mode) to 2.4 (coarse mode) (averaged over all elements). All these studies report increments close to 1 for elements originating from regional sources such as sea salt and Saharan dust, while local, especially traffic-related sources yield increments around 2 for resuspension-related elements and between 3 and 5 for traffic-related elements. Additionally, the 1 h time resolution used by Bukowiecki et al. (2009a) and Bukowiecki et al. (2010) enabled identification of enhanced increments for resuspension and wearing related elements like Si and Sb during peak traffic flows.

1 There is a need for more high time-resolved size segregated increment analyses to
2 assess the exposure to trace elements from emission sources within urban areas
3 under varying meteorological conditions. Here we present size segregated (~~PM_{40-2.57}~~
4 ~~PM_{2.5-1.0} and PM_{1-0.3}~~) measurements of aerosol trace elements with 2 h time
5 resolution performed simultaneously at kerbside and urban background sites in
6 London, and ~~at a rural site outside London during the winter intensive field campaign~~
7 ~~of ClearfLo~~. We assess the effects of urban micro-environments on human exposure
8 to particulate pollutants through the quantification of urban and kerb increments.
9 These exposures are further investigated in terms of contributing emission sources,
10 diurnal and weekly variability, local wind patterns, and regional transport effects.

12 2 Methods

13 2.1 Measurement campaigns

14 The ClearfLo project was a measurement program in and around London lasting two
15 years (2011-2012) and including two month-long Intensive Observation Periods
16 (IOPs) in 2012 (~~Bohnenstengel et al., 2013a~~ Bohnenstengel et al., 2014). This paper
17 focuses on the winter IOP lasting from 6 January to 11 February 2012.
18 Measurements took place at three sampling sites located at or near permanent air
19 quality measurement stations in the Automatic Urban and Rural Network (AURN): a
20 kerbside site close to a very busy road, an urban background site in a residential
21 area, and a rural background site away from direct emission sources (see Fig. 1).

22 The urban background sampling site was at the grounds of the Sion Manning
23 Secondary School in North Kensington (NK, lat 51°31'21"N, lon 0°12'49"W). NK is
24 situated within a highly trafficked suburban area of London (Bigi and Harrison, 2010;
25 Harrison et al., 2012a). During the ClearfLo IOPs this site served as the main
26 measurement site and was upgraded with a full suite of particle- and gas-phase
27 instruments, ~~as well as and~~ instruments to measure meteorological parameters
28 (Bohnenstengel et al., 2013a). The kerbside site was located at Marylebone Road
29 (MR, lat 51°31'21"N, lon 0°09'17"W) about 4.1 km to the east of NK (Charron and
30 Harrison, 2005; Harrison et al., 2011). This site is located at the southern side of a
31 street canyon, with an axis running approximately 260° to 80°. Measurements took
32 place at 1 m from a busy six-lane road with a traffic flow of approximately 73 000
33 vehicles per day of which 15 % consists of heavy duty vehicles ~~(trucks and buses)~~.
34 Braking and stationary vehicle queues are frequent at the site due to a heavily used
35 pedestrian light-controlled crossing (65 m west of MR) and a signal-controlled

junction (200 m west of MR). The rural site at the Kent Showgrounds at Detling (DE, lat 51°18'07"N, lon 0°35'22"E) ~~is was situated~~ approximately 45 km to the southeast of London downtown on a plateau at 200 m a.s.l. surrounded by fields and villages, and ~~is was~~ close to the permanent measurement station of Kent and Medway Air Quality Monitoring Network. The site provides excellent opportunities to compare the urban and kerbside air pollution with the rural background pollution levels (~~Bohnenstengel et al., 2013a;~~ Bohnenstengel et al., 2014; Mohr et al., 2013). A busy road with ~ 160 000 vehicles per day ~~(traffic fleet composition unknown) is located~~ runs approximately 150 m south of DE. Meteorological parameters were measured at DE and at the British Telecom (BT) Tower (lat 51°31'17"N, lon 0°08'20"W), ~ 0.5 km east of MR (Harrison et al., 2012a).

2.2 Instrumentation

2.2.1 RDI-SR-XRF

Rotating drum impactors

Rotating drum impactors (RDIs) were deployed at MR, NK and DE with a 2 h time resolution (see Table 1 for details). A detailed description of the RDI can be found in Bukowiecki et al. (2005), Bukowiecki et al. (2009c) and Richard et al. (2010). In short, aerosols are sampled through an inlet that removes all particles with aerodynamic diameter $d > 10 \mu\text{m}$ at a flow rate of $1 \text{ m}^3 \text{ h}^{-1}$. The particles are size segregated in three size ranges based on ~~aerodynamic diameter d~~ ($\text{PM}_{10-2.5}$ (coarse), $\text{PM}_{2.5-1.0}$ (intermediate) and $\text{PM}_{1.0-0.3}$ (fine)) by passing sequentially through three rectangular nozzles of decreasing size ~~(width 1.52, 0.68 and 0.3 mm, length 10 mm)~~. Particle deposition occurs via impaction on ~~a~~ $6 \mu\text{m}$ thick polypropylene (PP) foils mounted on aluminium wheels and coated with Apiezon to minimize particle bouncing effects. After the last impaction stage a backup filter samples all remaining particles before the air passes through a pump. After each 2 h sampling interval the three wheels rotate stepwise to a blank section of the foil before a new sampling interval takes place. The small-size collection limit of the fine fraction was previously estimated at 100 nm (Bukowiecki et al., 2009c; Richard et al., 2010). However, new laboratory measurements of the RDI collection efficiency indicate an instrument-dependent (i.e. based on the machining of the specific nozzle) small-end cut point of approximately 290-410 nm (see Supplement A for details). This results in sampling of a smaller size range ($\text{PM}_{1.0-0.3}$) than the $\text{PM}_{1.0-0.1}$ range reported in previous studies, and influences

~~the measured concentrations of elements with significant mass near this cut point-an underestimation of the total mass of trace elements that occur predominantly in the PM_{4.0} fraction, notably (S, K and Pb).~~

SR-XRF analysis

Trace element analysis on the RDI samples was performed with synchrotron radiation-induced X-ray fluorescence spectrometry (SR-XRF) at the X05DA beamline (Flechsigg et al., 2009) at the Swiss Light Source (SLS) at Paul Scherrer Institute (PSI), Villigen PSI, Switzerland and at Beamline L at Hamburger Synchrotronstrahlungslabor (HASYLAB) at Deutsches Elektronen-Synchrotron (DESY), Hamburg, Germany (beamline dismantled November 2012). The RDI samples with the deposited particles were placed directly into the X-ray beam. Irradiation of the samples took place at a 45° angle for 30 s. The light spot of the incoming beam was ~ 140 by 70 µm at SLS (monochromatic excitation at 10.5 keV, in vacuum) and ~ 80 by 150 µm at HASYLAB (polychromatic excitation, in air). Fluorescence light produced by the elements in the samples was detected by energy-dispersive detectors (silicon drift detector at SLS, nitrogen cooled Si(Li)-detector at HASYLAB) at a 90° angle relative to the incoming beam. At SLS K α lines of the elements with atomic number $Z = 11-30$ (Na-Zn) were measured, and at HASYLAB K α lines of the elements with $Z = 22-56$ (Ti-Ba) and L α lines of $Z = 82$ (Pb).

The fluorescence counts per element were calibrated to the element mass concentration using multi-element standards, where each standard consisted of a set of preselected elements in 5 different concentrations ranging between 0.05 and 0.4 µg cm⁻². The absolute element concentrations in these standards were determined with inductively coupled plasma-optical emission spectroscopy (ICP-OES). The absolute calibration factor for the SR-XRF system was referenced to Fe and determined from the linear relation between the SR-XRF response and the ICP-OES measurements. Because the fluorescence yield increases with atomic number Z , a relative calibration curve was constructed as follows: for each element present in the standards and having a detectable K α_1 line, an absolute calibration factor was determined as for Fe, and a dimensionless relative response factor was calculated as the ratio of this absolute factor to that of Fe. These relative response factors were plotted as a function of line energy and ~~the a polynomial curve was fit by a custom function that smoothly blends exponential (low energy) and sigmoidal (high energy)~~

functions. ~~The response curve was interpolated~~ to obtain response factors by interpolation for elements not present in the standard. In total 25 elements were quantified (Na, Mg, Al, Si, P, S, Cl, K, Ca, Ti, V, Cr, Mn, Fe, Ni, Cu, Zn, Br, Sr, Zr, Mo, Sn, Sb, Ba, Pb). Details of the methodology can be found elsewhere (Bukowiecki et al., 2005; Bukowiecki et al., 2008; Richard et al., 2010), with the following significant changes (see Supplement B for further details):

1. At SLS, we used an e2v SiriusSD detector (SiriusSD-30133LE-IS) and in-house built vacuum chamber to extend the measured range of elements down to Na and Mg.

2. Reference standards for calibration of element fluorescence counts to mass concentrations were produced on the same 6 µm PP substrate as used for RDI sampling allowing the use of identical geometry and irradiation time for RDI samples and reference standards, thereby reducing uncertainties in absolute and relative calibrations.

3. Data were processed with the Spectral Analysis for Multiple Instruments – toolkit for XRF (SAMI-XRF) developed in-house within the IGOR Pro software environment (Wavemetrics, Inc., Portland, OR, USA). SAMI handles spectral fitting, quantification of associated uncertainties, and calculation and application of calibration parameters.

~~1. At SLS, we replaced the silicon drift detector (Roentec Xflash 2001 type 1102, Bruker AXS) with an e2v SiriusSD detector (SiriusSD-30133LE-IS). This detector is equipped with a thin polymer window resulting in a wider energy range down to about 300 eV and a better energy resolution of 133 eV (Mn K α at 5.9 keV). In addition, the setup accepts a higher throughput resulting in negligible dead time effects. We also replaced the helium chamber with an in-house built vacuum chamber (sample exposure system for micro-X-ray fluorescence measurements, SESmiX) which reaches about 10⁻⁶ bar. This extended the measured range of elements down to Na and Mg.~~

~~2. Reference standards for calibration of element fluorescence counts to mass concentrations were produced on the same 6 µm PP substrate as used for RDI sampling, in contrast to the previous standard where a much thicker 25-µm PP foil was used. Two standards suitable for measurements at both SLS and HASYLAB contained elements in equal concentrations, and have a similar mix of elements as the standard previously used. Two additional standards containing only specifically selected light elements were produced. One standard contained Na, Al, P and Ca;~~

the other Mg, Si, S, K and Ca. The concentrations of these elements were increased by a factor 3.8 relative to the other two standards to improve signal-to-noise ratios in the SR-XRF calibration. Co was added to these additional standards, but in the same concentration as in the other two foils and was used as a quality check of the fabrication procedure of the four standards. The concentration difference of the light elements was taken into account before applying the relative calibration of the sample elements. The new reference standards allowed the use of identical geometry and irradiation time for RDI samples and reference standards, meaning that all SR-XRF measurements exhibit the same scattering and secondary fluorescence excitation. This reduced uncertainties in both the absolute and relative calibration of the samples.

3. Previously, spectra were fitted with the WinAxil software package (Canberra Inc; Van Espen et al., 1986). This rather old spectral fitting package allows little flexibility in spectrum continuum correction and peak fitting. PyMCA (Sole et al., 2007) on the other hand, is more flexible, but lacks the possibility to save uncertainty calculations in batch mode. In this study, spectra were fitted with an in-house developed software package called Spectral Analysis for Multiple Instruments — toolkit for XRF (SAMI-XRF) using the IGOR Pro software environment (Wavemetrics, Inc., Portland, OR, USA) to evaluate the data and create custom interfaces to accomplish specialized tasks. SAMI will be described in detail in a future manuscript. Briefly, SAMI sequentially determines (1) energy calibration of the X-ray line as a function of detector channel; (2) spectrum continuum correction; (3) peak width calibration as a function of energy (assuming Gaussian peak shape and a general square root law of the full-width-half-maximum (FWHM) energy relation); and (4) peak fitting of the entire spectrum, at which stage only peak heights are fitted as a free parameter and all other parameters are fixed. Steps (1) and (3) are performed with user-selected reference peaks, and incorporates fitting of complex (multi-Gaussian) peak shapes caused by nearly complete overlapping $K\alpha_1$ and $K\alpha_2$ lines. Step (2) utilizes collected spectra of a blank foil as a reference for the continuum shape, and scales this reference to user-selected element-free regions of the processed spectra. Step (4) allows lines to be fitted freely or fixed to another line, e.g. to the strongest line in a shell. For example, the $K\alpha_2$ and $K\beta$ lines are fixed to the $K\alpha_1$ line according to the relative intensities given by Bearden (1967). In this study, all lines within an electron shell were fitted fixed to the strongest line in that shell. Additionally, Ni, Cu and Zn $L_{\alpha_{1,2}}$ lines were fixed to the $K\alpha_1$ line to reduce the influence of peak overlap with Na. The ratios of $L_{\alpha_{1,2}}$ to $K\alpha_1$ for Ni, Cu and Zn were determined by fitting calibration

~~standards having these elements but low Na. Final fits were then obtained using the acquired relations, thereby reducing uncertainties in the Na concentrations due to peak overlap and improving Na quantification.~~

2.2.2 Other measurements

~~Here a short description is given of Measurements from additional relevant~~ particle- and gas-phase instruments deployed at MR, NK and DE during the winter IOP ~~discussed in this paper are described here.~~ Daily PM₁₀ filter samples (midnight to midnight) were collected at MR and NK using Partisol 2025 samplers (Thermo Scientific, Inc.). The filters were digested in a 1:2 mixture of perchloric and hydrofluoric acid, and subsequently analysed by ~~inductively coupled plasma~~ICP- mass spectrometry (ICP-MS, calibration with NIST standards) for the determination of Na, Al, Ca, Ti, V, ~~Cr~~, Mn, Fe, Ni, Cu, Zn, Sr, Mo, Sb, Ba and Pb. Additionally, Mg, K and Sn were available at NK. High-resolution time-of-flight aerosol mass spectrometers (HR-ToF-AMS, Aerodyne Research, Inc., Billerica, MA, USA) were deployed at MR (-with a 5 min time resolution)-at MR, NK (a 5 min resolution every 30 min-at NK), and DE a 2 min resolution)-at DE to characterise the non-refractory submicron aerosol components (DeCarlo et al., 2006). PM₁₀ mass concentrations were measured at all three sites with FDMS-TEOM (-Filter Dynamics Measurement System Tapered Element Oscillating Microbalances—(FDMS-TEOM; Thermo Scientific, Inc.) with a 1 h time resolution. NO_x measurements at MR and NK were performed with a NO_x chemiluminescent analyser with a single chamber and a single detector (API, A Series, model M200A; 15 min resolution) ~~with a 15-min time resolution.~~ At DE NO was collected-determined with a Thermo Scientific 42i analyser and NO₂ with an Aerodyne CAPS-NO₂ (SN 1002) and an Aerodyne QCL-76-D. These NO and NO₂ measurements were summed together to obtain NO_x with a (1 min time-resolution). Black carbon (BC) was measured with a 2-wavelength Aethalometer ($\lambda = 370$ and 880 nm, model AE22, Magee Scientific) at MR and a 7-wavelength Aethalometer ($\lambda = 370$ -950 nm, model AE31, Magee Scientific) at NK and DE (5 min, all three with a time-resolution-of 5 min), with and a 2.5 μ m cyclone at MR and DE and a 3.5 μ m cyclone at NK. Traffic counts by vehicle group at MR from road sensors (number of vehicles per 15 min) were available as well. Wind direction and wind speed data for MR and NK were taken from the BT Tower (30 min resolution) where anemometers were placed to the top of an open lattice scaffolding tower of 18 m height on top of the main structure (190.8 m a.g.l.; Wood et al., 2010), whereas local data were used at DE (1 min resolution). Air mass origins were

1 analysed with back trajectory simulations using the UK Met Office's Numerical
2 Atmospheric Modelling Environment (NAME) dispersion model (Jones et al., 2007).

3 4 **3 Data intercomparison and uncertainty**

5 Here we compare RDI-SR-XRF data with independent filter data (24 h PM₁₀ trace
6 element data analysed with ICP-MS; roughly 9 % uncertainty at a 95 % confidence
7 interval) for 18 elements collected at MR and NK (no filter data was available at DE).
8 For this comparison, the three size ranges of the RDI were summed up to total PM₁₀
9 and averaged to the filter collection period. Details of the intercomparison results can
10 be found in Supplement C. In short, the majority of the elements (Al, Ca, Ti, Mn, Fe,
11 Cu, Zn, Sr, Sb, Ba) agree within approximately ± 50 % with Pearson's $R > 0.78$. Fit
12 coefficients deviate more for the other elements due to low filter sample extraction
13 efficiencies (V, Ni, Mo), uncertainties in the XRF relative calibration (Na, Mg) and
14 differences in the particle size range sampled by the two (K, Sn, Pb). Thus, for the
15 measured size range, the intercomparison calls into question only the absolute
16 magnitudes of Na and Mg concentrations determined by the XRF. However, these
17 elements are retained in the ensuing analysis as (1) they are well correlated with the
18 filters (Pearson's $R > 0.89$); (2) they yield internally consistent results (e.g.
19 appropriate ratio for sea salt), as described in the following sections; (3) the ensuing
20 analysis relies on relative changes/ratios per element across sites and is therefore
21 not affected by a systematic bias in absolute magnitude.

22 The agreement between XRF and filter measurements in the present study
23 compares favourably with that obtained in previous intercomparisons of trace
24 element measurement techniques. Previously, Comparison of RDI-SR-XRF
25 performance was analysed by Bukowiecki et al. (2005) and Richard et al. (2010).
26 Both studies compared RDI-SR-XRF element concentrations with daily element
27 concentrations from a high volume sampler followed by with subsequent analysis by
28 using laboratory-based wavelength dispersive XRF (Bukowiecki et al., 2005) and by
29 ICP-OES and ICP-MS (Richard et al., 2010). Most elements showed yielded slopes
30 between 0.7 and 1.6, (except for S and K), with Pearson's $R > 0.5$. The
31 spread/biases in these intercomparisons are not necessarily due to SR-XRF issues,
32 as can be seen by from a comparison by Salcedo et al. (2012) of ICP with proton-
33 induced X-ray emission (PIXE) and AMS trace element measurements. Agreement
34 between ICP and PIXE data was in the same range as between either method with
35 and the the AMS data, with slopes ranging between 0.06 and 0.93 with Pearson's R

from about 0.3 to 0.7. ~~These studies show the challenges in the quantification of trace elements with different analysis techniques.~~

Estimated uncertainties (per size fraction) and detection limits for each measured element are given in Supplement Table S3. A brief overview is presented here:

1. RDI sampling: the fluctuations in the flow rate are negligible within 5 % (Richard et al., 2010) and the uncertainties in the size cut off are discussed in Supplement A.

2. SR-XRF accuracy: uncertainties in the absolute and relative calibrations affect absolute/fractional concentrations, but cancel out for relative changes/ratios, because all samples were measured under the same calibration conditions.

3. Issues such as imperfect flatness of the sample foils and detector dead time corrections (Richard et al., 2010) reduce measurement precision but affect all elements with the same scaling factor.

4. SR-XRF measurement precision is affected by sample inhomogeneity and spectral analysis uncertainties. Sample inhomogeneity was assessed by Bukowiecki et al. (2009c) and found to contribute ± 20 % uncertainty.

For most elements, except Mn, sample inhomogeneity is the largest source of uncertainty. Mn is affected by spectral analysis uncertainties due to peak overlap with Fe, present in much higher concentrations. Therefore, a small change in the energy calibration as function of detector channel leads to a large change in the peak area of Mn. All data points lie well above their element detection limits, resulting in negligible uncertainties from the signal strength. In addition, RDI-SR-XRF measurements (both absolute/fractional and relative/ratio) are affected by atmospheric variability. This variability is likely the predominant source of the data spread evident in Table 2 and the following analyses.

~~Here we compare RDI-SR-XRF data with independent filter data (24-hr PM₁₀ trace element data analysed with ICP-MS; roughly 9% uncertainty at a 95% confidence interval) for 19 elements collected at MR and NK (no filter data was available at DE). For this comparison, the three size ranges of the RDI were summed up to total PM₁₀ and averaged to the filter collection period. The intercomparison results are shown in Figure 2, and are divided into four groups to facilitate discussion. Fit coefficients and Pearson's R values for the intercomparison are shown in Table S2. Elements shown in Figure 2a (Al, Ca, Ti, Mn, Fe, Cu, Zn, Sr, Sb, Ba) agree within approximately $\pm 50\%$ with good correlations ($R > 0.74$). In Figure 2b-d, we show elements for which~~

the intercomparison shows significant biases and/or no significant correlation between RDI and filters. Note that the elements exhibiting good agreement in Figure 2a span orders of magnitude difference in concentration (and fluorescence counts), suggesting that there are no global or concentration-dependent biases in the RDI-SR-XRF data. This leaves the element relative calibration (i.e. element fluorescence yield as a function of line energy), spectral peak fitting, and instrument size cut points as issues to address.

Figure 2b shows good correlations for Mo ($R = 0.86$), but the RDI measures a factor 3 higher concentrations than found on the filters. Visual inspection of the spectrum indicates that significant interferences between lines are unlikely, and this is confirmed by peak fitting sensitivity tests investigating the response of the calculated concentrations to uncertainties in line energy calibration (i.e. energy as a function of detector channel), the continuum, and calculated peak width. We estimate a 3% uncertainty in the measurement of Mo due to spectral analysis. Strong correlations between filter and RDI time series also suggest that spectral fitting errors are not the cause of the discrepancy. Mo falls in a well-constrained region of the calibration curve (although is not directly measured on calibration foils), so relative calibration errors would require a systematic bias across this entire region of the calibration curve. While there are not enough jointly measured elements within the intercomparison to evaluate this possibility, good agreement between RDI and filter measurements is obtained through Sr ($K\alpha = 14.1$ keV) and at Sb ($K\alpha = 26.4$ keV) (Mo $K\alpha$ lines fall at 17.5 keV), suggesting such a bias is unlikely. For ICP-OES the extraction efficiency was unknown for Mo, potentially indicating that the filter data might be underestimated. The other elements (V, Cr, Ni) in Figure 2b show no significant correlation between RDI and filters. Similar to the discussion of Mo, we do not expect significant spectral interferences for these elements, and this is confirmed by the uncertainty analysis described above, which yielded around 20% uncertainty for V, Cr and Ni. Unlike Mo, the relative calibration is well-constrained both in terms of elements directly measured on calibration foils and in terms of intercomparison with nearby elements in the XRF calibration curve, where V and Cr fall just above Ca and Ti and just below Mn and Fe, and Ni just above Mn and Fe and just below Cu and Zn. RDI and filter measurements are shown to be in good agreement for these six elements in Figure 2a. However, the ICP-OES had an extraction efficiency for Ni of 66%, whereas for V and Cr this was unknown, leading to increased uncertainties of these elements relative to others. Further, as shown in the following sections, the RDI time series of V, Cr and Ni (including both urban/kerb increments and

diurnal/weekly cycles) are consistent with those of elements expected to be co-emitted by the same sources. We therefore assume the RDI V, Cr and Ni measurements to be valid, even though they are close to the minimum detection limits of SR-XRF.

Figure 2c shows good correlations for Na and Mg ($R > 0.87$), but the RDI concentrations are a factor 2 higher than the filters. The two measurement techniques each provide internally consistent results, with the Mg to Na ratio for the filter data at NK and the RDI data at NK and MR of approximately 0.13, which is close to the theoretical sea salt ratio of 0.12. The XRF relative calibration curve for Na and Mg is difficult to constrain due to the low response of these elements, but only led to an uncertainty of 10%. The extraction efficiency for Mg in ICP-OES was 90%, but was unknown for Na. However, it remains unclear why the results of both methods differ for these elements.

The elements K, Sn and Pb in Figure 2d show reasonable to good correlations between RDI and filter measurements ($R > 0.53$) but the RDI data is only about half the filter data (filter measurements of K and Sn only at NK). Pb has a significant fraction of the mass in the fine fraction (see Figure 3). Underestimation by the RDI is explained by an unexpectedly high small-end cut point of 290-410 nm (compared to 100 nm), as discussed below. K and Sn also have a significant fraction of their mass in the fine fraction, and might be affected by the cut off similarly to Pb.

S is a useful element for evaluation of the small-end cut off, as it is dominant in the fine fraction and measurable by several techniques. Therefore, we compared S data obtained with the RDI to simultaneous S mass calculated from sulphate (SO_4) measured by an AMS at MR, NK, and DE. The results in Supplement A show that the S mass in the RDI is on average about three times lower than that measured by the AMS. This is consistent with the discrepancy between RDI and filter measurements for fine fraction dominated elements. The RDI backup filter, which collects particles too small to impact at the $\text{PM}_{4.0-0.3}$ stage, was analysed for SO_4^{2-} using ion chromatography (Supplement A). Adding the S from this analysis to the S collected at the RDI $\text{PM}_{4.0-0.3}$ stage yielded mass closure with the S from AMS measurements within 20% at all three sites. This suggests that elements with considerable mass in the small end of the $\text{PM}_{4.0}$ size range may be significantly underestimated. This affects S and Pb, and potentially also K, Zn, Br and Sn. To further investigate this underestimation, new RDI collection efficiency measurements for the $\text{PM}_{4.0}$ deposition stage were performed (Supplement A). The actual small-end cut off was determined to be 290-410 nm, rather than the previously measured value of 100 nm

(Bukowiecki et al., 2009c; Richard et al., 2010), and found to be very sensitive to the machining tolerances of the PM_{1.0} nozzle.

Only a small fraction of the measured elements are affected by this cut off issue. Further, because the analysis presented in the following sections depends on site-to-site ratios (for the same element) and relative concentration changes, potential biases are reduced by the similar (though not identical, see Fig. S2) cut offs of the different RDI units. The conclusions presented herein are thus not significantly affected by this artefact.

4 Results and discussion

4.1 Trace element concentrations

During the ClearfLo winter IOP total mass concentrations of the analysed trace elements ranged from less than 0.01 $\mu\text{g m}^{-3}$ to ~44.20 $\mu\text{g m}^{-3}$. Typically, concentrations were highest at MR and lower at NK and DE, and decreased with particle size. Total trace element concentration in the coarse mode ranged on average from 0.8 to 3.7 $\mu\text{g m}^{-3}$. Intermediate mode concentrations ranged from 0.6 to 1.3 $\mu\text{g m}^{-3}$, whereas fine mode values varied between 0.5 and 0.6 $\mu\text{g m}^{-3}$. An overview of the obtained trace element concentrations as a function of size and site is given in Table 2. Note that S is not a trace element, but is commonly reported in trace element studies and is a good tracer for regional transport. Among the analysed trace elements, highest concentrations at MR were found for Na (2637 %), Cl (2319 %) and Fe (187 %), followed by Si (7%), S (6%) and Ca (5%). At NK, this was the case for highest concentrations were found for Na (3547 %), Cl (2619 %) and Fe (97 %), followed by S (8%), Mg (5%) and Si (5%). and At DE highest concentrations were found for Na (3549 %), Cl (2411 %) and S (147 %), followed by Mg (6%), Si (5%) and Fe (4%). Bukowiecki et al., 2009c; Richard et al., 2010. Total analysed mass measured by the RDI-SR-XRF (trace elements + S) contributed on average 4821 % to the total PM₁₀ mass (from FDMS-TEOM) of 32 (5-74) $\mu\text{g m}^{-3}$ at MR (not extrapolated to the corresponding oxides), 4417 % to the mass of 23 (1.4-63) $\mu\text{g m}^{-3}$ at NK and 4214 % to the mass of 17 (0.5-58) $\mu\text{g m}^{-3}$ at DE.

A comparison between the contributions of coarse, intermediate and fine fractions to the total PM₁₀ mass of each trace element is shown in Fig. 2 for MR, NK and DE the three sites. The figure shows that MR trace elements at MR are dominated by the coarse fraction. Analysis in the following sections and previous measurements at this

site (Charron and Harrison, 2005) suggest this is caused by large contributions of resuspension and traffic-related mechanical abrasion processes, which primarily contribute to the coarse fraction. For all elements at this site, except S, Br and Pb, the coarse fraction contributes more than 50 %. Mass fractions of intermediate mode elements to total PM₁₀ are rather constant with contributions ranging from 4413 to 2827 %. The fine fraction contributes up to 50 % of total mass for S, K, Zn, Br and Pb; for other elements fine contributions are less than 4720 %. S, K, Zn, Br and Pb are typically dominated by the fine fraction with known sources including heavy oil combustion (S, K, Zn; Lucarelli et al., 2000), traffic exhaust (Br, Pb; Formenti et al., 1996), industrial processes (Zn, Pb; Moffet et al., 2008), and secondary sulphate and wood combustion (S, K, Pb; Richard et al., 2011).

For most elements, particle mass contributions of the smaller size fractions are more important as one moves from kerbside to urban background to rural sites (Fig. 2). The relatively large fine fraction contribution at DE is probably caused by the absence of local traffic which results in lower contributions of resuspension and traffic-related processes to total element concentrations, ~~as discussed in the following sections~~. A different behaviour is observed for Cr, Ni and Mo with on average 80 % of their mass at DE in the coarse fraction, compared to 7073 % at MR and 5060 % at NK. The time series of these coarse mode species are very spiky, ~~Cr and Mo are very spiky, correlate strongly with Ni, and are slightly enhanced with SW winds neither correlated to wind direction nor to wind speed, nor but are not to~~ collocated with measurements of BC and AMS species, suggesting emissions from a local industrial source, potentially from stainless steel production (Querol et al., 2007; Witt et al., 2010) near DE rather than regional transport.

Comparing the contributions of groups of elements to total trace element concentrations at the sites provides an overview of local and regional sources affecting London; a detailed source apportionment study will be the subject of a future manuscript. Na, Mg and Cl are typical s-Sea salt elements and (Na, Mg, Cl) contribute around 6065 % to the total PM₁₀ trace element mass at all three sites, indicating that the air pollutant levels caused by elements are dominated by natural emission sources being transported to London. ~~Note, however, that the absolute mass concentrations of these elements at MR are approximately 1.5 times higher than at NK and 2-3 times higher than at DE. This indicates the important role of anthropogenic activities (e.g. traffic) in the resuspension of these natural particles, but possibly also the application of road salt in winter (e.g. Lee et al., 1994).~~ Mineral dust elements (Al, Si, Ca, Ti) mainly brought into the air via resuspension contribute

on average 14 % at MR, NK and DE 17% to the total elemental mass at MR, 13% at NK and 12% at DE. For some typical-specific brake wear elements (Cu, Sb, Ba) these contributions are 4.41.1, 0.60.4 and 0.3 % at MR, NK and DE, respectively. Although these metals contribute a small fraction of total PM₁₀ mass concentrations, they induce-have adverse health effects. Xiao et al. (2013) e.g. found that Zn, Fe, Pb and Mn were the major elements responsible for plasmid DNA damage, whereas Kelly and Fussell (2012) found that increases in PM₁₀ as a result of increased Ni, V, Zn and Cu contributions showed highest mortality risks, as opposed to increased Al and Si.

~~The RDI-SR-XRF technique is subject to various sources of uncertainty, which change in importance depending on whether the data are described in terms of absolute/fractional concentrations (as above) or in terms of relative changes/ratios (as in the remainder of the manuscript). A brief overview is presented here:~~

~~1. RDI sampling: the fluctuations in the flow rate are negligible within 5 % (Richard et al., 2010) and the uncertainties in the size cut off are discussed in Section 3;~~

~~2. SR-XRF accuracy: uncertainties in the absolute and relative calibrations affect absolute/fractional concentrations, but cancel out for relative changes/ratios, because all samples were measured under the same calibration conditions.~~

~~3. Issues such as imperfect flatness of the sample foils and detector dead time corrections (-) reduce measurement precision but affect all elements with the same scaling factor.~~

~~4. SR-XRF measurement precision is affected by sample inhomogeneity and spectral analysis uncertainties. Sample inhomogeneity was assessed by Bukowiecki et al. (2009c) and found to contribute ± 20 % uncertainty. A comprehensive assessment of spectral analysis uncertainties is beyond the scope of the current work, but will be discussed in a future manuscript. The results of this analysis were discussed for selected elements in Section 3.~~

~~In addition, RDI-SR-XRF measurements (both absolute/fractional and relative/ratio) are affected by atmospheric variability. This variability is likely the predominant source of the data spread evident in Table 2 and the following analyses.~~

4.2 Urban and kerb increment

4.2.1 Urban increment

The urban increment compares the trace element concentrations ~~per trace element~~ at the urban background site to the concentrations at the rural site, and is calculated here as the ratio of concentrations at NK to DE. Figure 3 shows the mean, median and 25-75th percentile urban increment ratios for the coarse, intermediate and fine fractions per element. Most elements, ~~(except Cl, Ni, and coarse mode Cr and Mo)~~ are enriched at the urban background site by factors between 1.0 and 4.76.5 (median ratios). Increments decrease towards smaller sizes. The coarse and intermediate fractions show highest increment factors, while the fine fraction shows lower increments. Ni and coarse mode Cr show higher concentrations at DE relative to NK, as does the mean value of coarse Mo. Especially at DE Cr and Ni show strong correlations with Pearson's R of 0.85. As discussed in the previous section, enhanced coarse mode Cr, Ni and Mo may indicate ~~a stainless steel production or other an~~ industrial source near the rural siteDE. ~~These elements show strong correlations with Pearson's R of 0.88 at DE vs 0.57 at NK.~~

Coarse mode Zr exhibits low concentrations at DE, where the median value actually falls below detection limit, though discrete events above detection limit also exist. For this reason, the median-based urban increment is not plotted, while the mean ratio is driven by several large concentration peaks at NK, resulting in a large mean ratio of 9.521. In the case of Cl, a large spread in the urban increment values is seen for all three size ranges. Cl is likely depleted relative to other sea salt elements like Na and Mg (throughout the campaign Cl concentrations fall to 0, whereas Na and Mg concentrations remain positive) due to replacement by nitrate, and the extent of such depletion is greater in small particles (Nolte et al., 2008). At DE, Cl depletion seems apparent at all size ranges, whereas at MR depletion ~~only~~ mainly takes place in the PM_{1.0-0.3} fraction. NK shows Cl depletion especially in the PM_{1.0-0.3} fraction, but to some extent also in intermediate mode particles.

For ease of discussion, we empirically group elements based on similar urban increment values. Mn, Fe, Cu, Zn, Zr, Mo, Sn, Sb and Ba show urban increments on average of 3.5 in the coarse, 3.1 in the intermediate and 2.0 in the fine fraction (Fig. 3). These have been identified as Typical traffic-related elements by (Mn, Fe, Cu, Zn, Zr, Mo, Sn, Sb, Ba; see e.g. Amato et al., 2011; Bukowiecki et al., 2010; Minguillón et al., 2014; Richard et al., 2011 and Viana et al., 2008. Zr has also been linked to mineral dust (Moreno et al., 2013). We can understand that from analysing

the Enrichment Factors of these elements (EF). EF is a measure of the enrichment of elements relative to the upper continental crust (UCC) and is defined as $\text{ppm metal in the sample} / \text{ppm metal in UCC}$ with Si as reference material (UCC from Wedepohl, 1995). Zr is the only element in this traffic group that is depleted in the atmosphere relative to their UCC concentrations, but with concentrations at NK higher than at DE. Most other elements clearly indicate anthropogenic origin with $EF > 10$. Dependent on the method, Zr can be either grouped with traffic-related elements or with dust elements. ~~show urban increments on average of 3.0 in the coarse, 3.5 in the intermediate and 2.5 in the fine fraction (Figure 4).~~ These urban increments are similar to that of NO_x , where concentrations at NK were on average a factor 4.9 higher than at DE (~~the~~ mean concentration at NK was 68 ppb, at DE 14 ppb). ~~However, b~~Black carbon (BC), ~~a marker for both traffic and wood burning emissions,~~ had an urban increment of only 1.1 (concentration at NK 757 ng m^{-3} , at DE 633 ng m^{-3}), likely due to local wood burning emissions around DE (Mohr et al., 2013). Al, Si, Ca, Ti and Sr as markers for mineral dust (e.g. Amato et al., 2009; Lin et al., 2005; Lucarelli et al., 2000) show a factor 2.0 higher concentrations at NK relative to DE in the coarse, 1.9 in the intermediate and 1.6 in the fine fraction ($EF < 10$). ~~Mineral dust elements (Al, Si, Ca, Ti, Sr; see) show a factor 2.3 higher concentrations at NK relative to DE in the coarse, 2.2 in the intermediate and 1.7 in the fine fraction.~~ These results indicate that moving from rural to urban backgrounds yields a larger relative increase in traffic than in mineral dust elements. Surprisingly, sea salt elements (Na, Mg, Cl) show higher concentrations at NK than at DE of up to a factor of 2 for the coarse mode, despite the expected dominance of regional over local sources. This highlights the potential importance of sea or road salt resuspension by traffic. Similar urban increment values for traffic-related, resuspension and sea salt elements have been observed by Lee et al. (1994) for particles below a few μm . Theodosi et al. (2011) also found higher increments (> 2) for trace elements in PM_{10} aerosol from local anthropogenic sources like fossil fuel combustion (V, Ni, Cd) and traffic (Cu), relative to long-range transported Saharan dust (Fe, Mn) with increments close to 1. However, our study suggests that the non-size-resolved increment values ~~for increments~~ reported in the cited studies do not fully capture the urban/rural differences.

The influence of regional transport by anthropogenically produced elements in our study (Fig. 3Figure 4) is seen by the low urban increments between 4.21.1 and 2.01.8 for P, S, K, Zn, Br, Sn and Pb in $\text{PM}_{1.0-0.3}$ ($EF > 25$) and of 1.6 for total PM_{10} mass (concentration at NK 23 $\mu\text{g m}^{-3}$, at DE 17 $\mu\text{g m}^{-3}$). The concentrations of the

main components in PM₁₀ (sulphate, nitrate and secondary organic compounds) within an urban area are mostly influenced by regional transport, as found in London during the REPARTEE project (Harrison et al., 2012a) and in Paris during the MEGAPOLI project (Crippa et al., 2013; Freutel et al., 2013), resulting in low increments for total PM₁₀ mass. Similar urban increment values (1.3 to 1.8) for 1 and 24 h total PM_{2.5} mass concentrations were reported across many sites in the UK (Harrison et al., 2012c).

4.2.2 Kerb increment

While the urban increment investigates the effect of diffuse emission sources on particle concentrations, the kerb increment investigates an urban micro-environment, specifically the local effects of roadside emissions and activities. Here, the kerb increment is calculated as the ratio of concentrations at MR to NK. However, observed concentrations at MR strongly depend on wind direction, because the road runs from approximately 260° to 80° and the street canyon with the surrounding buildings and intersections creates a complex wind circulation system (Balogun et al., 2010). Since the measurement station is located at the southern side of the canyon, measurements during time periods with winds from the south are influenced by on-road emissions on top of the urban background pollution. Higher concentrations were observed with SSE winds, i.e. perpendicular to the direction of the road. The influence of wind direction on the air pollutant concentrations in the street canyon at MR was identified by e.g. Balogun et al. (2010), Charron and Harrison (2005) and Harrison et al. (2012b), with higher concentrations corresponding with SSE winds, i.e. perpendicular to the direction of the road. Since the measurement station is located at the southern side of the canyon, measurements during time periods with winds from the south are influenced by on-road emissions on top of the urban background pollution.

In this study we have averaged the 30-min wind direction data collected at the elevated BT Tower to the RDI 2-hr time resolution at MR and NK, and the 1-min wind direction data collected at DE to the RDI 2-hr time resolution at the same site. In this study, the RDI-SR-XRF data was split into four equally spaced wind direction sectors based on wind direction data; N (315 - 45°), E (45 - 135°), S (135 - 225°) and W (225 - 315°). Figure 4~~Figure 5~~ shows size-resolved trace element concentrations per wind sector normalized to the global median concentration for each element at MR. As expected, w~~W~~inds from the south yield the highest concentrations, whereas

1 northern winds yield the lowest, independent of size fraction. West and east winds
2 are parallel to the street canyon and yield intermediate concentrations, ~~consistent~~
3 ~~with e.g. Charron and Harrison (2005) and Harrison and Jones (2005).~~ Similar
4 behaviour is observed for NO_x, and no directional biases for high wind speeds are
5 observed (~~Fig. S6~~~~Figure S5~~).

6 Traffic-related and some other anthropogenically-related elements (V, Cr, Mn, Fe, Ni,
7 Cu, Zn, Zr, Mo, Sn, Sb, Ba) show the strongest wind direction dependency with up to
8 a factor of 2-3 higher concentrations during S relative to N winds for the three size
9 fractions (Fig. 4). A factor of 1.5-2 is obtained for resuspended dust elements.
10 Harrison et al. (2012b) found a ratio of 2 for Fe (as tracer for brake wear) and 1.2 for
11 Al (as tracer for mineral dust) for SW versus NE winds for particles between 2 and 3
12 µm. However, they were limited by their time resolution of several days, resulting in
13 potentially substantial wind direction variations during each measurement, which
14 would blur the different conditions and yield reduced ratios.

15 ~~Figure 5 shows that typical traffic-related elements from exhaust emissions and~~
16 ~~brake and tire wear (V, Cr, Mn, Fe, Ni, Cu, Zn, Zr, Mo, Sn, Sb, Ba) are about a factor~~
17 ~~3 higher during S compared to N winds for the coarse fraction, and a factor of 2 for~~
18 ~~the intermediate and fine fractions. Although some studies have assigned V and Ni to~~
19 ~~industrial sources (Mazzei et al., 2007) and Zr to soil-related particles (Moreno et al.,~~
20 ~~2013), here they are empirically grouped with traffic elements due to their similar kerb~~
21 ~~increments and diurnal/weekly cycles (Section 4.3). This does not rule out effects~~
22 ~~from other sources (e.g. industrial influences on Ni can be observed at the low-traffic~~
23 ~~rural site), but suggest that traffic is the dominant emission source at the kerbside~~
24 ~~site. The attribution of e.g. Zr to traffic is consistent with previous studies (Amato et~~
25 ~~al., 2011; Bukowiecki et al., 2009b; Bukowiecki et al., 2010).-~~

26 ~~Resuspended mineral dust elements (Al, Si, Ca, Ti, Sr) show smaller enrichments~~
27 ~~than elements related to wearing and exhaust emissions, with concentration ratios for~~
28 ~~S to N wind conditions of approximately 2 for the coarse fraction, and 1.5 for~~
29 ~~intermediate and fine fractions. Harrison et al. (2012b) found a ratio of 2 for Fe (as~~
30 ~~tracer for brake wear) and 1.2 for Al (as tracer for mineral dust) for SW versus NE~~
31 ~~winds for particles between 2 and 3 µm. However, they were limited by their time~~
32 ~~resolution of several days, needed to sample enough PM to be quantitative, which~~
33 ~~resulted in potentially substantial wind direction variations during each measurement~~
34 ~~and possibly in reduced ratios.~~

Other elements ~~In the coarse and intermediate mode, Na, Mg, S, Cl, K and Br show~~
only minor correlations with wind direction (~~Fig. 4~~Figure 5), indicating more influence
from regional transport ~~indicating that these elements are influenced more by~~
regional transport, instead of being locally ~~emitted~~ affected by traffic. Only fine
mode~~In the fine mode, Na and Mg also show little wind direction influence, whereas~~
S, K and Br seem to be enriched with winds from the east, potentially related to long-
range transport from the European continent. ~~Cl is highly variable in all four wind~~
~~sectors, and, as discussed previously, is likely depleted throughout the campaign by~~
~~nitrate chemistry.~~

Local wind direction has a greatly reduced effect at urban background and rural sites.
At NK, the element concentrations are only subject to high concentration outliers for
E winds (Supplement Fig. S4), ~~potentially~~ At NK, the element concentrations are
~~less influenced by wind direction (Figure S3), but subject to high concentration~~
~~outliers for E winds. This could be~~ caused by the transport of pollutants from
~~emission sources in~~ downtown London, or by lower wind speeds occurring with E
winds resulting in reduced dilution and increased concentrations of traffic pollutants
(e.g. NO_x) throughout the city (Supplement S6~~Figure S5~~). The rural site hardly also
shows ~~a slight~~ wind direction dependent concentration ~~se~~ (Supplement Fig. S5-6
Figure S4). ~~Interpretation of data from the E sector is unclear due to the low number~~
~~of data points (45 out of 318 data points). Here, winds from N and E sectors result in~~
~~enhanced concentrations relative to S and W sectors, especially in the fine mode.~~
~~Interpretation of data from the E sector is unclear due to the low number of data~~
~~points (45 out of 323 data points). These wind directions were accompanied by low~~
~~wind speeds (Figure S5), reducing dilution and leading to the accumulation of~~
~~pollutants emitted from villages and towns in the surrounding area (Mohr et al.,~~
~~2013).~~ Only ~~d~~Data from the N sector show enhanced concentrations for several
elements correlating with ~~correspond to~~ higher wind speeds and back trajectories
consistent with transport from continental Europe.

To simplify reporting of the kerb increment and facilitate comparison with previous
studies (e.g. Harrison et al., 2012b), we combined the south/west sectors and the
north/east sectors into SW (135-315°) and NE (315-135°) sectors. To eliminate
meteorological and/or regional transport effects, this segregation is performed at both
MR and NK. The kerb increment is then calculated as the ratio of MR to NK and
shown in Fig. 5~~Figure 6~~ (Supplement Fig. S7~~Figure S6~~ shows the increments s for the
4 individual sectors). As with the urban increment, we focus on the ratio of the
medians at MR and NK to reduce the effects of outliers. Two features become

1 directly visible; the kerb increment is much higher for coarse than for intermediate
2 and fine particles, and kerb increments are much higher for SW than for NE wind
3 conditions. ~~Even for NE conditions~~With the latter, kerb increments are on average
4 ~~3.3, 2.7, 1.6 and 1.7~~ for coarse, ~~1.5 for~~ intermediate and ~~1.4 for~~ fine mode particles,
5 ~~respectively~~. This significant enhancement is likely due to recirculation of particles
6 within the street canyon following their resuspension and/or emission by traffic.
7 However, these increments are much smaller than those observed in the SW sector,
8 where enhancements relative to NK of ~~7.2, 6.7, 3.3 and 3.1~~ ~~for (coarse, 3.4 for~~
9 ~~intermediate, and 2.7 for fine) mode elements~~ are observed. These results indicate
10 the existence of micro-environments within the street canyon dependent on wind
11 direction.

12 ~~Several~~As in the previous discussion, we again group elements ~~can be grouped~~
13 ~~according to their similarity in by~~ kerb increments (Fig. 5Figure 6). The first group
14 consists of Cu, Zr, Mo, Sn, Sb and Ba and yields the highest increments in the
15 coarse mode ranging from ~~44.6 to 10.4~~ to ~~48.5 to 16.6~~ in the SW sector (~~3.6 to 9.4~~~~3.3 to 6.9~~ for
16 NE). These elements are typically associated with brake wear (e.g. Bukowiecki et al.,
17 2009b; Harrison et al., 2012b), and are much higher than the increments of 4.1 to 4.4
18 reported by Harrison et al. (2012b) at the same sites for particles < 21 µm. ~~They~~
19 ~~assigned Fe, Cu, Sb and Ba to brake wear, but in the current study Fe has a~~
20 ~~significantly lower kerb increment than other brake wear tracers, suggesting a~~
21 ~~significant alternative source (Fe, Cu, Sb and Ba were assigned to brake wear).~~
22 ~~However, w~~When combining all size fractions and ignoring wind direction influences,
23 increments in this study are about ~~5.4 to 4.9~~, and more similar to previous studies. The
24 discrepancies between the kerb increments obtained using these two calculation
25 strategies highlights the difficulties in characterizing human exposure to locally
26 generated pollutants in urban environments, as the detailed topography and
27 microscale meteorology greatly alter particle concentrations, and the effects are size-
28 dependent. Amato et al. (2011) calculated road side increments in Barcelona for
29 trace elements in PM₁₀ with a 1 h time resolution and found increments for brake
30 wear elements of only 1.7 (based on Fe, Cu, Sb, Cr, Sn ~~as tracers for brake wear~~).
31 These low increments are probably due to the reduced dispersion in Barcelona
32 caused by a complex topography, resulting in high urban background levels.

33 The second group consists of V, Cr, Mn, Fe, Ni, Zn and Pb ~~elements with increments~~
34 ~~of 5.7 to 8.2 (PM_{10-2.5}) in the SW sector (2.6 to 3.0 for NE) that might be affected by other~~
35 ~~traffic-related processes than brake wear (V, Cr, Mn, Fe, Ni, Zn, Pb) with increments~~

of 5.6 to 8.0 in the SW sector (2.6-6.5 for NE) (Fig. 5Figure 6). V and Ni are typically assigned to industrial sources and heavy-oil combustion (e.g. Mazzei et al., 2007; Viana et al., 2008), Zn is usually associated with tire wear (e.g. Harrison et al., 2012b; Lin et al., 2005), and the other elements are commonly associated with traffic-related emissions (e.g. Amato et al., 2013; Bukowiecki et al., 2009a; Richard et al., 2011). ~~We label this group as anthropogenically-influenced (ANTH). The EF of V and Ni are much lower than those of the other elements in this group (2 vs. > 10), indicating at least to some extent different source origins.~~ These ~~kerb~~ increments are similar to the ones for NO_x of 8.5 for SW and 2.4 for NE, ~~confirming the anthropogenic influence (traffic and other sources) of traffic~~ on these elements. The high braking frequency at MR due to congested traffic probably resulted in increased ~~kerb~~ increments of brake wear relative to ~~other traffic-related~~ANTH elements that are also ~~emitted-influenced~~ by local traffic ~~and other sources~~ aroundt NK. ~~Similar to the brake wear elements, combining all size fractions and ignoring wind direction influences yield kerb increments of about 3.1 (4.8, 2.3 and 2.1 for coarse, intermediate and fine mode, respectively), which mask the systematically higher values recorded for specific locations/meteorological conditions in the micro-environment. Increments of these ANTH elements are higher than previously reported values of 1.8-4.5 for studies with low time resolution and non-size segregated particles. These averaged values are however similar to the 2.8 for PM₁₀ trace elements (time resolution of 42 hrs per week) reported in the Netherlands (Boogaard et al., 2011; Janssen et al., 1997), and to the 4.5 and 3.2 for Fe in PM₁₀ and PM_{2.5}, respectively (daily measurements) also found in the Netherlands (Janssen et al., 1997). However, reported increments for V, Mn and Zn are below 1.8 and much smaller than found at MR relative to NK.~~ The high increments presented here might be caused by street canyon effects, trapping pollutants emitted at street level and preventing dilution to the urban background. ~~In more open street sites pollutants are diluted more easily, resulting in reduced concentration differences between street and urban background sites.~~ The enhanced ~~kerb~~ increments for brake wear relative to ~~other traffic-related~~ANTH elements ~~is~~are apparent in all three size fractions, although increments become more similar towards smaller sizes with a factor ~~4.9~~1.7 between both element groups in the coarse, 1.5 in the intermediate and ~~1.2~~1.4 in the fine mode. Both ~~traffic-related~~ groups show the additional information gained with size-segregated aerosol, where exposure to trace elements in the street canyon relative to the urban background increases with particle size, either caused by increased traffic-related emissions with particle size or by more efficient transport of submicron particles from street sites to the urban background. Furthermore, the

highly time-resolved element measurements presented here enabled us to resolve the systematic, wind direction dependent variability in ~~the~~ kerb increments.

The third group is associated with mineral dust (Al, Si, Ca, Ti, Sr) ~~and with~~ coarse mode ~~kerb~~ increments ~~of 3.4-5.4 for the SW sector yield winds 3.3 to 5.24 (1.7-2.31.8-2.4 for NE) (Fig. 5Figure 6)~~. These elements are brought into the air both by traffic-induced resuspension and transport from other locations. This second process increases both urban background and kerbside concentrations, and thus reduces kerb increments relative to direct traffic-related elements. Lower kerb increments for mineral dust than traffic-related elements are generally observed in ~~kerb~~ increment studies (Amato et al., 2011; Boogaard et al., 2011; Bukowiecki et al., 2009b; Harrison et al., 2012b), although the dust increments found in this study are larger than most reported increments (typically ~~1-2between 1 and 2~~). As in the traffic-related groups, increments increase with particle size, indicating ~~that enhanced~~ human exposure at the street side ~~is enhanced for of~~ particles above 1 μm .

~~Na, Mg and Cl S~~(sea salt ~~(Na, Mg, Cl)~~ forms the fourth group and yields ~~s~~ kerb increments of 1.0 to ~~2.02.7~~, independent of size fraction but with slightly enhanced ratios with SW compared to NE winds (~~Fig. 5Figure 6~~). Similar increments were observed for total PM_{10} mass. As discussed for urban increments, even though these elements have regional sources, they are influenced by resuspension processes within the urban area which are enhanced at kerbside sites.

The remaining elements (P, S, K, Br) can be grouped together. In the coarse mode, these elements yield increments similar to the mineral dust group, indicating that this group is influenced by resuspension processes in the street canyon (~~Fig. 5Figure 6~~). However, especially in the fine mode increments around 1 were found, consistent with regional transport dominating over local emission sources.

4.3 Temporal trends in trace element concentrations

In contrast to traditional trace element measurements, the RDI-SR-XRF enables measurement of element concentrations with high time resolution (2 h in this work). This enables investigation of diurnal cycles, which are useful both for source discrimination and in determining the processes contributing to elevated PM levels. We also discuss weekly cycles, which can be useful in distinguishing emissions from heavy duty and passenger vehicles (~~HDV and LDV~~); ~~HDVheavy duty vehicle~~ numbers typically diminish during the weekend. Back trajectory analysis aids source

discrimination by understanding regional transport influences by different air mass origin. Here we discuss the temporal trends of trace elements in five groups based on expected sources and the increment analyses in Sect. 4.2, in order of increasing local influence: regional background, sea salt, mineral dust, traffic-related and brake wear.

[Figures 6 and 7](#)~~Figure 7 and Figure 8~~ show size-segregated median diurnal and weekly cycles, respectively, for 5 elements representative of the classes mentioned above: Na (sea salt), Si (mineral dust), S (regional background), Fe (traffic-related) and Sb (brake wear) at [the three sites MR, NK and DE](#). Because of the wind direction effect evident at MR, diurnal cycles at all three sites are shown for SW and NE winds. Wind direction analyses are not incorporated into the weekly cycles because the month-long campaign provided insufficient data points for meaningful division. This also means that weekly cycles are subject to influences by mesoscale events. For example, sea salt shows no clear weekly cycle, except for a peak on Fridays in intermediate and fine fractions coinciding with westerly winds, which coincidentally occurred more frequently on Fridays than on other days. Except for such events, regionally dominated elements tend to display flat, featureless diurnal/weekly cycles, while elements dominated by recurring local processes (e.g. traffic patterns) show interpretable features. Diurnal and weekly cycles of all other elements can be found in [Supplement Fig. S8-9](#)~~Figure S7 and Figure S8~~. For comparison, diurnal and weekly cycles of NO_x and total PM₁₀ mass at all sites, and of traffic flow at MR are shown in [Fig. 8](#)~~Figure 9~~. The time series of these species were averaged to the RDI collection times before obtaining the cycles. BC diurnal and weekly cycles (not shown) are very similar to those of NO_x.

4.3.1 Regional influences

Elements dominated by regional sources (P, S, K, Br) occur mainly in the fine fraction and are similar to total PM₁₀ mass in showing no obvious diurnal and weekly patterns. This interpretation is consistent with the urban/kerb increment analysis discussed in Sect. 4.2. Weekly patterns suggest fine Zn and Pb are also dominated by regional transport ([Supplement Fig. S9](#)~~Figure S8~~). P, S and K have been identified as tracers for mixed wood combustion and secondary sulphate (Amato et al., 2011; Richard et al., 2011), whereas Hammond et al. (2008) have identified S, K and Pb from mixed secondary sulphate and coal combustion. Br is usually associated with sea salt (Lee et al., 1994; Mazzei et al., 2007) or traffic emissions (Gotschi et al.,

2005; Lee et al., 1994), but Maenhaut (1996) has also found Br, together with S, K, Pb and other elements in biomass burning. In this study, the diurnal cycle of fine Br is different from the Na, Mg and Cl cycles, ~~and is but~~ more similar to K. Br is thus ~~more~~ likely ~~more~~ associated with wood burning than with other sources.

The time series of ~~this group of elements~~ (fine S, K, Zn, Pb) at NK (~~very similar at MR and DE~~) ~~is are~~ explored in relation to total PM₁₀ mass, wind direction ~~at the BT Tower~~ and air mass origin, and compared to representative elements from the other emission groups (coarse Na, Si, S, Sb; ~~Fig. 9 Figure 10~~). Air mass origin was studied with back trajectories simulated for three case study periods (marine, European mainland and locally influenced) using the NAME model (Jones et al., 2007). Particles are released into the model atmosphere from the measurement location and their origin is tracked using meteorological fields from the Unified Model, a numerical weather prediction model. Each particle carries mass of one or more pollutant species and evolves by various physical and chemical processes during 24 h preceding arrival at NK. Potential emission source regions can be highlighted along the pathway to the measurement site at 0-100 m above ground. ~~The time series of these fine mode elements at MR and DE (not shown) are very similar to NK, consistent with the absence of an increment and thus the predominance of regional sources for these elements.~~

Under marine air mass origin (case A, 18-24 January, Fig. 9) with strong W winds the concentrations of the fine mode elements are fairly low, whereas sea salt concentrations are enhanced (see Na in Fig. 9). Although the air mass has also passed over Ireland and the Midlands, the influence of these rather sparsely populated regions on pollution levels seems small. This is confirmed by low total PM₁₀ mass and NO_x concentrations. Enhanced fine fraction and total PM₁₀ mass concentrations (latter not shown) occur during north easterlies with high wind speeds from the European mainland (case B) bringing in pollutants through regional transport.

~~Case A in Figure 10 is at the end of a period with predominantly westerly winds (18-24 Jan) and a marine air mass origin associated with high wind speeds (air has travelled a long distance in 24 hrs). Although the air mass has also passed over Ireland and the Midlands, the influence of these rather sparsely populated regions on pollution levels is small. Under these conditions concentrations of fine S, K, Zn and Pb are fairly low. In comparison, sea salt elements (see coarse Na in Figure 10) are enhanced during this period. Total PM₁₀ mass and NO_x (not shown) concentrations are low as well, showing that with strong westerlies pollution levels at NK are low and~~

not strongly influenced by traffic. In case B (right in the middle of a 3-day episode), north easterlies (with high wind speeds) from the European continent bring in pollutants through regional transport leading to a large regional pollution episode characterised by elevated concentrations of fine S, K, Zn and Pb. Total PM₁₀ mass showed strongly enhanced concentrations as well. During this episode, both the urban background and rural site observed the highest concentrations for these trace elements of the entire campaign. Traffic influenced species were not enhanced during this pollution episode. However, mineral dust and traffic-related elements, as well as NO_x, were not enhanced at the urban background in case B. Elevated concentrations of all trace elements, NO_x and PM₁₀ mass occurred only during a local pollution episode of roughly 3 days caused by local air mass stagnation over London and the south eastern UK (case C). Wind direction in case C is variable, but the NAME footprint shows local air mass stagnation over London and the southeast of the UK accompanied by low wind speeds. This local pollution episode of roughly 3 days resulted in elevated concentrations of all trace elements, NO_x and total PM₁₀ mass (NK no data, MR and DE elevated concentrations), independent of emission source. The very high concentrations observed in case B through regional transport from the European mainland were identified as the main reason for PM₁₀ limit exceedances at urban background sites in London by Charron et al. (2007), while exceedances were much less frequent under marine influenced air as represented by case A in this study.

4.3.2 Sea salt

The sea salt group (Na, Mg, Cl) yields comparable, rather flat diurnal cycles for fine and intermediate mode Na, Mg and Cl, and coarse mode Na and Cl (Na in Fig. 6Figure 7; others in Supplement Fig. S8Figure S7), and no obvious weekly patterns (Na in Fig. 7Figure 8; others in Supplement Fig. S9Figure S8). This indicates that the regional transport of sea salt is probably the main source of Na, Mg and Cl, as seen in case A in Fig. 9Figure 10.

Interestingly, although coarse mode sea salt exhibits no obvious temporal trend, the urban and kerb increments indicates additional source contributions besides regional transported sea salt. The urban increment might be caused by the natural sea salt gradient observed in the UK, with reducing concentrations from west to east (Fowler and Smith, 2000), while the kerb increment could be the result of road salt resuspension in addition to sea salt resuspension. The effects of road salt are

supported by enhanced kerb increments (~ 2.0) with respect to the ClearfLo summer IOP (~ 1.4 ; not published). Coarse mode Mg originates probably both from mineral dust and sea salt, because at MR with SW winds Mg correlates with Al and Si temporal trends, while with NE winds Mg correlates better with Na and Cl.

4.3.3 Mineral dust and traffic

Both mineral dust and traffic-related elements are strongly influenced by traffic patterns at MR, which are shown in [Fig. 8](#) as the number of vehicles per 2 h split in light (passenger) LDV and heavy-duty HDV vehicles (shorter/longer than 5.2 m). Heavy-duty vehicle HDV numbers peak in the morning, whereas LDV passenger vehicle numbers peak in the evening when the flow of traffic leaves the urban area, consistent with Harrison et al. (2012b). A single peak during midday in the weekend compared to a double peak at weekdays is observed for LDV light-duty vehicles. HDV Heavy-duty vehicle numbers show a similar pattern during weekdays (morning maximum), but with a reduced maximum on Saturday and a small maximum that is shifted towards midday on Sunday. Charron and Harrison (2005) reported similar traffic patterns during two years of traffic counts, and stated very small week-to-week variability, except during holidays.

The element diurnal ([Fig. 6](#) for Si, Fe and Sb; [Figure-Supplement Fig. S8](#) for others) and weekly ([Fig. 7](#) for Si, Fe and Sb; [Figure-Supplement Fig. S9](#) for others) cycles yield highest concentrations at MR and lower concentrations at NK and DE, consistent with observed urban and kerb increments. More importantly, and only retrievable with high time-resolved data, concentrations are higher during the day than at night, with night time concentrations at MR and NK similar to median urban background and rural concentrations, respectively, demonstrating the effects of local traffic and enhanced human exposure during daytime. Weekdays yield stronger increments than weekends and closely follow NO_x and HDV heavy-duty vehicle traffic patterns ([Fig. 8](#)), indicating the strong influence of these vehicles on element concentrations. This is consistent with observations by Charron et al. (2007), who observed-stated that PM_{10} limit exceedances at MR are more likely to occur on weekdays, in combination with large regional contributions from the European mainland with easterly winds. Similarly, Barmpadimos et al. (2011) found strong weekly cycles for $\text{PM}_{10-2.5}$ and $\text{PM}_{2.5}$ mass concentrations in Switzerland over a 7-12 year period, with higher concentrations on weekdays and lowest on Sundays.

At MR in the street canyon with SW winds, all coarse mode elements (including dust elements) except Na and Cl exhibit a double peak in the diurnal cycles, closely following the flow of traffic and confirming that traffic-related processes such as braking and resuspension dominate the concentration of most elements. ~~that element concentrations in the street canyon are mainly driven by traffic instead of mesoscale meteorological processes (see Charron et al., 2007). Especially during rush hour, most braking and stationary queues occur due to the heavily used pedestrian traffic light-controlled crossing and the signal-controlled junction in close proximity to the measurement site, leading to enhanced concentrations of brake wear elements and possibly also to increased resuspension, especially induced by heavy duty vehicles (Bukowiecki et al., 2009a).~~ With NE winds, source discrimination based on diurnal patterns is possible between mineral dust (e.g. Si in Fig. 6 Figure 7) and traffic-related elements (e.g. Fe and Sb in Fig. 6 Figure 7). Mineral dust yields a strong maximum between 8:00 and 14:00 LT, and continued high concentrations throughout the day, while the traffic-related group yields a reduced double peak relative to SW winds. The increase in mineral dust concentrations coincides with the start of traffic flows at 6:00 LT resulting in resuspension of particles within the street canyon. However, concentrations decrease before traffic flows reduce, possibly as a result of increased mixing and dilution during the day with growth of the mixing boundary layer growth. At NK diurnal and weekly patterns ~~for of the dust and traffic groups mineral dust and traffic-related elements~~ yield similar variability but reduced concentrations relative to MR, which suggests increased human exposure during day time and weekdays and confirms that traffic dominates urban background element concentrations in London (see Dore et al., 2003). At DE, freshly emitted pollutants from London and other cities in the south eastern UK have been diluted and mixed with other pollutants during their transport to the rural background, resulting in no obvious diurnal and weekly patterns independent of size range.

The kerb increments at MR under SW winds were divided into two traffic-related groups: brake wear (Cu, Zr, Mo, Sn, Sb, Ba) and other traffic-related (V, Cr, Mn, Fe, Ni, Zn, Pb) elements. However, the diurnal and weekly cycles of all these elements correlate well and no obvious split into two groups is seen. Apparently, both groups are co-emitted as a single group under comparable vehicle fleet and/or set of driving conditions, at least on a 2 h time scale, but in different ratios at MR and NK. The ratio of these two element classes for SW to NE wind sectors at MR is about almost 2.5, with the lack of difference between these classes supporting co-emission. In a future manuscript we will further explore the diurnal variability of emission sources at both

1 | sites with statistical analyses based on the ~~m~~Multilinear Engine (Canonaco et al.,
2 | 2013; Paatero, 1999).

4 | 5 Conclusions

5 | Aerosol trace element composition was measured at kerbside, urban background
6 | and rural sites in the European megacity of London during winter 2012. Sampling
7 | with rotating drum impactors (RDI) and subsequent measurements with synchrotron
8 | radiation-induced X-ray fluorescence spectrometry (SR-XRF) yielded trace element
9 | mass concentrations in $PM_{10-2.5}$, $PM_{2.5-1.0}$ and $PM_{1.0-0.3}$ aerosol with a 2 h time
10 | resolution. Total median element mass concentrations of $4.65.4 \mu g m^{-3}$, $2.42.9 \mu g m^{-3}$
11 | ³ and $4.01.1 \mu g m^{-3}$ were found at kerbside, urban background and rural sites,
12 | respectively, which constitutes 1214 to 1821 % to total PM_{10} mass (highest at
13 | kerbside; lowest at rural site), neglecting the corresponding oxides. The contribution
14 | of emission sources to coarse fraction elements was on average largest at kerbside
15 | (63 %) and reduced for urban background (4750 %) and rural sites (4447 %).

16 | Urban and kerb increments were defined as the concentration ratios of urban
17 | background to rural, and kerbside to urban background, respectively, and the kerb
18 | increments were further explored as a function of wind direction. The group with the
19 | largest kerb increments consisted of elements typically associated with brake wear
20 | (Cu, Zr, Mo, Sn, Sb, Ba). The second largest kerb increments were observed for
21 | anthropogenically-influenced elements typically assigned to non-brake wear traffic
22 | emissions (Cr, Mn, Fe, Zn, Pb) but also V and Ni. This could indicate either a traffic
23 | source for these elements or a similar kerbside-to-urban emission gradient. Kerb
24 | increments were larger for the brake wear group and under SW winds due to local
25 | street canyon effects, with coarse fraction increments between 10.4 and 16.6 for SW
26 | winds (3.3-6.9 for NE winds) against increments for the anthropogenically-influenced
27 | group between 5.7 and 8.2 for SW winds (2.6-3.0 for NE winds). ~~Traffic-related~~
28 | ~~elements (Mn, Fe, Cu, Zn, Zr, Mo, Sn, Sb, Ba) yielded largest kerb and urban~~
29 | ~~increments, with kerb increment values ranging between 5.8 and 18.5 for SW winds~~
30 | ~~(2.6-9.4 for NE winds) and urban increments of around 3.0. Traffic-related kerb~~
31 | ~~increments could be further divided into elements from brake wear and other traffic-~~
32 | ~~related processes. Brake wear elements (Cu, Zr, Mo, Sn, Sb, Ba) showed a factor 2~~
33 | ~~larger increments than other traffic-related elements (11.6-18.5 vs. 5.6-8.0 in coarse~~
34 | ~~mode with SW winds).~~ The k ~~K~~ kerb increments for ~~these traffic-related~~ all these
35 | elements in the $PM_{10-2.5}$ size fraction are roughly 3-timestwice that of the $PM_{1.0-0.3}$

fraction, ~~and are also highest for SW winds due to local street canyon effects.~~ Urban increments (no distinction between both groups) were around 3.0. In addition to direct emissions, traffic-related processes influence the concentrations of other elements by resuspension, with mineral dust ~~increments~~ (Al, Si, Ca, Ti, Sr) increments of 4.7-4.1-3.3.

The highly time-resolved data enabled studying diurnal patterns. ~~Diurnal cycles of~~ The cycles of mineral dust elements and coarse Na, Mg and Cl both indicate major concentration enhancements during periods of heavy traffic, whereas regionally-influenced elements (~~PM_{4.0-0.3}~~ fine P, S, K, Zn, Br, Pb) showed no enhancements. All traffic-related elements at the kerbside site yielded temporal patterns similar to variations in heavy duty vehicle numbers as opposed to total vehicle numbers, and resulted in enhanced exposure to elements during day time and weekdays. Traffic-related processes therefore exhibit a dominant influence on air quality at the kerbside and urban background sites, and should be the main focus of health effect studies and mitigation strategies. With technological improvements for the reduction of traffic exhaust emissions, the traffic contribution to coarse PM is becoming more important as shown by decreasing PM_{2.5} mass trends with no significant changes of coarse PM (Barmpadimos et al., 2012).

Trace element and total PM₁₀ mass concentrations are also affected by mesoscale meteorology, increasing with the transport of air masses from the European mainland. Under these conditions, coarse and intermediate fraction trace elements are hardly affected, but fine fraction elements (~~P, S, K, Zn, Br, Pb~~) showed elevated concentrations. Trace element concentrations in London are therefore influenced by both local and regional sources, with coarse and intermediate fractions dominated by anthropogenic activities (particularly traffic-induced resuspension and wearing processes), whereas fine fractions are significantly influenced by regional processes.

These observations highlight both the strong influence of regional factors on overall air quality, as well as the need for detailed characterization of urban micro-environments for accurate assessment of human exposure to airborne particulates and the associated health risks.

Acknowledgements

This research, which was conducted in the context of the ClearfLo project, is mainly financed by the Swiss National Science Foundation (SNFSSNSF grant 200021_132467/1), the ClearfLo project (NERC grant NE/H00324X/1) and the

European Community's Seventh Framework Programme (FP/2007-2013, grant number 312284). The Detling site was supported by the US Department of Energy Atmospheric Systems Research Program (DOE Award No. DE-SC0006002). J.G. Slowik acknowledges support from the SNSF through the Ambizione program (grant PX00P2 _31673). [Filter digestions were carried out by the wet geochemistry laboratory at Royal Holloway, University of London.](#) EMPA loaned us a RDI during the ClearfLo project. Parts of the work were carried out at the Swiss Light Source, Paul Scherrer Institute, Villigen, Switzerland. We thank Andreas Jaggi for technical support at the beamline X05DA. Parts were performed at the light source facility DORIS III at HASYLAB/DESY. DESY is a member of the Helmholtz Association (HGF). We thank Christophe Frieß for excellent support in acquiring and testing the detector, and we thank Peter Lienemann and Sylvia Köchli for valuable input for the production of calibration standards.

References

- Amato, F., Pandolfi, M., Escrig, A., Querol, X., Alastuey, A., Pey, J., Perez, N., and Hopke, P. K.: Quantifying road dust resuspension in urban environment by Multilinear Engine: A comparison with PMF2, *Atmos. Env.*, 43, 2770-2780, 2009.
- Amato, F., Viana, M., Richard, A., Furger, M., Prevot, A. S. H., Nava, S., Lucarelli, F., Bukowiecki, N., Alastuey, A., Reche, C., Moreno, T., Pandolfi, M., Pey, J., and Querol, X.: Size and time-resolved roadside enrichment of atmospheric particulate pollutants, *Atmos. Chem. Phys.*, 11, 2917-2931, 2011.
- Amato, F., Schaap, M., Denier van der Gon, H. A. C., Pandolfi, M., Alastuey, A., Keuken, M., and Querol, X.: Short-term variability of mineral dust, metals and carbon emission from road dust resuspension, *Atmos. Env.*, 74, 134-140, 2013.
- Arnold, S. J., ApSimon, H., Barlow, J., Belcher, S., Bell, M., Boddy, J. W., Britter, R., Cheng, H., Clark, R., Colville, R. N., Dimitroulopoulou, S., Dobre, A., Grealley, B., Kaur, S., Knights, A., Lawton, T., Makepeace, A., Martin, D., Neophytou, M., Neville, S., Nieuwenhuijsen, M., Nickless, G., Price, C., Robins, A., Shallcross, D., Simmonds, P., Smalley, R. J., Tate, J., Tomlin, A. S., Wang, H., and Walsh, P.: Introduction to the DAPPLE Air Pollution Project, *Sci. Total Environ.*, 332, 139-153, 2004.
- Balogun, A. A., Tomlin, A. S., Wood, C. R., Barlow, J. F., Belcher, S. E., Smalley, R. J., Lingard, J. J. N., Arnold, S. J., Dobre, A., Robins, A. G., Martin, D., and Shallcross, D. E.: In-street wind direction variability in the vicinity of a busy intersection in central London, *Bound.-Layer Meteor.*, 136, 489-513, 10.1007/s10546-010-9515-y, 2010.
- Barmapadimos, I., Nufer, M., Oderbolz, D. C., Keller, J., Aksoyoglu, S., Hueglin, C., Baltensperger, U., and Prévôt, A. S. H.: The weekly cycle of ambient concentrations and traffic emissions of coarse (PM₁₀–PM_{2.5}) atmospheric particles, *Atmos. Env.*, 45, 4580-4590, 2011.
- Barmapadimos, I., Keller, J., Oderbolz, D., Hueglin, C., and Prévôt, A. S. H.: One decade of parallel fine (PM_{2.5}) and coarse (PM₁₀–PM_{2.5}) particulate matter

1 measurements in Europe: trends and variability, *Atmos. Chem. Phys.*, 12, 3189-
2 3203, 10.5194/acp-12-3189-2012, 2012.

3 Bearden, J. A.: X-ray wavelengths, *Rev. Mod. Phys.*, 39, 78-124,
4 10.1103/RevModPhys.39.78, 1967.

5 Bigi, A., and Harrison, R. M.: Analysis of the air pollution climate at a central urban
6 background site, *Atmos. Env.*, 44, 2004-2012, 2010.

7 Bohnenstengel, S. I., Evans, S., Clark, P. A., and Belcher, S. E.: Simulations of the
8 London urban heat island, *Quart. J. Roy. Meteorol. Soc.*, 137, 1625-1640,
9 10.1002/qj.855, 2011.

10 Bohnenstengel, S. I., Belcher, S. E., Allan, J. D., Allen, G., Bacak, A., Bannan, T. J.,
11 Barlow, J. F., Beddows, D. C. S., Bloss, W. J., Booth, A. M., Chemel, C., Coceal, O.,
12 Di Marco, C. F., Faloon, K. H., Fleming, Z., Furger, M., Geitl, J. K., Graves, R. R.,
13 Green, D. C., Grimmond, C. S. B., Halios, C., Hamilton, J. F., Harrison, R. M., Heal,
14 M. R., Heard, D. E., Helfter, C., Herndon, S. C., Holmes, R. E., Hopkins, J. R., Jones,
15 A. M., Kelly, F. J., Kotthaus, S., Langford, B., Lee, J. D., Leigh, R. J., Lewis, A. C.,
16 Lidster, R. T., Lopez-Hilfiker, F. D., McQuaid, J. B., Mohr, C., Monks, P. S., Nemitz,
17 E., Ng, N. L., Percival, C. J., Prévôt, A. S. H., Ricketts, H. M. A., Sokhi, R., Stone, D.,
18 Thornton, J. A., Tremper, A. H., Valach, A. C., Visser, S., Whalley, L. K., Williams, L.
19 R., Xu, L., Young, D. E., and Zotter, P.: Meteorology, air quality and health in
20 London: The ClearLo project, *Bull. Am. Meteor. Soc.*, (under review), 2013a.

21 Bohnenstengel, S. I., Hamilton, I., Davies, M., and Belcher, S. E.: Impact of
22 anthropogenic heat emissions on London's temperatures, *Quart. J. Roy. Meteorol.*
23 *Soc.*, 10.1002/qj.2144, 2013b.

24 Bohnenstengel, S. I., Belcher, S. E., Aiken, A., Allan, J. D., Allen, G., Bacak, A.,
25 Bannan, T. J., Barlow, J. F., Beddows, D. C. S., Bloss, W. J., Booth, A. M., Chemel,
26 C., Coceal, O., Di Marco, C. F., Dubey, M. K., Faloon, K. H., Fleming, Z. L., Furger,
27 M., Gietl, J. K., Graves, R. R., Green, D. C., Grimmond, C. S. B., Halios, C. H.,
28 Hamilton, J. F., Harrison, R. M., Heal, M. R., Heard, D. E., Helfter, C., Herndon, S.
29 C., Holmes, R. E., Hopkins, J. R., Jones, A. M., Kelly, F. J., Kotthaus, S., Langford,
30 B., Lee, J. D., Leigh, R. J., Lewis, A. C., Lidster, R. T., Lopez-Hilfiker, F. D.,
31 McQuaid, J. B., Mohr, C., Monks, P. S., Nemitz, E., Ng, N. L., Percival, C. J., Prévôt,
32 A. S. H., Ricketts, H. M. A., Sokhi, R., Stone, D., Thornton, J. A., Tremper, A. H.,
33 Valach, A. C., Visser, S., Whalley, L. K., Williams, L. R., Xu, L., Young, D. E., and
34 Zotter, P.: Meteorology, air quality, and health in London: The ClearLo project, *Bull.*
35 *Am. Meteor. Soc.*, 10.1175/BAMS-D-12-00245.1, 2014.

36 Boogaard, H., Kos, G. P. A., Weijers, E. P., Janssen, N. A. H., Fischer, P. H., van der
37 Zee, S. C., de Hartog, J. J., and Hoek, G.: Contrast in air pollution components
38 between major streets and background locations: Particulate matter mass, black
39 carbon, elemental composition, nitrogen oxide and ultrafine particle number, *Atmos.*
40 *Env.*, 45, 650-658, 2011.

41 Bukowiecki, N., Hill, M., Gehrig, R., Zwicky, C. N., Lienemann, P., Hegedus, F.,
42 Falkenberg, G., Weingartner, E., and Baltensperger, U.: Trace metals in ambient air:
43 Hourly size-segregated mass concentrations determined by synchrotron-XRF,
44 *Environ. Sci. Technol.*, 39, 5754-5762, 2005.

45 Bukowiecki, N., Lienemann, P., Zwicky, C. N., Furger, M., Richard, A., Falkenberg,
46 G., Rickers, K., Grolimund, D., Borca, C., Hill, M., Gehrig, R., and Baltensperger, U.:
47 X-ray fluorescence spectrometry for high throughput analysis of atmospheric aerosol
48 samples: The benefits of synchrotron X-rays, *Spectrosc. Acta Pt. B-Atom. Spectr.*, 63,
49 929-938, 2008.

1 Bukowiecki, N., Gehrig, R., Lienemann, P., Hill, M., Figi, R., Buchmann, B., Furger,
2 M., Richard, A., Mohr, C., Weimer, S., Prevot, A. S. H., and Baltensperger, U.: PM10
3 emission factors of abrasion particles from road traffic, Schweizerische
4 Eidgenossenschaft, 2009a.

5 Bukowiecki, N., Lienemann, P., Hill, M., Figi, R., Richard, A., Furger, M., Rickers, K.,
6 Falkenberg, G., Zhao, Y. J., Cliff, S. S., Prevot, A. S. H., Baltensperger, U.,
7 Buchmann, B., and Gehrig, R.: Real-world emission factors for antimony and other
8 brake wear related trace elements: Size-segregated values for light and heavy duty
9 vehicles, *Environ. Sci. Technol.*, 43, 8072-8078, 2009b.

10 Bukowiecki, N., Richard, A., Furger, M., Weingartner, E., Aguirre, M., Huthwelker, T.,
11 Lienemann, P., Gehrig, R., and Baltensperger, U.: Deposition uniformity and particle
12 size distribution of ambient aerosol collected with a rotating drum impactor, *Aerosol*
13 *Sci. Technol.*, 43, 891-901, 2009c.

14 Bukowiecki, N., Lienemann, P., Hill, M., Furger, M., Richard, A., Amato, F., Prevot, A.
15 S. H., Baltensperger, U., Buchmann, B., and Gehrig, R.: PM10 emission factors for
16 non-exhaust particles generated by road traffic in an urban street canyon and along a
17 freeway in Switzerland, *Atmos. Env.*, 44, 2330-2340, 2010.

18 Canonaco, F., Crippa, M., Slowik, J. G., Baltensperger, U., and Prevot, A. S. H.:
19 SoFi, an IGOR-based interface for the efficient use of the generalized multilinear
20 engine (ME-2) for the source apportionment: ME-2 application to aerosol mass
21 spectrometer data, *Atmos. Meas. Tech.*, 6, 3649-3661, 10.5194/amt-6-3649-2013,
22 2013.

23 Charron, A., and Harrison, R. M.: Fine (PM_{2.5}) and coarse (PM_{2.5-10}) particulate
24 matter on a heavily trafficked London highway: Sources and processes, *Environ. Sci.*
25 *Technol.*, 39, 7768-7776, 10.1021/es050462i, 2005.

26 Charron, A., Harrison, R. M., and Quincey, P.: What are the sources and conditions
27 responsible for exceedences of the 24 h PM10 limit value (50 µg m⁻³) at a heavily
28 trafficked London site?, *Atmos. Env.*, 41, 1960-1975, 2007.

29 Crippa, M., DeCarlo, P. F., Slowik, J. G., Mohr, C., Heringa, M. F., Chirico, R.,
30 Poulain, L., Freutel, F., Sciare, J., Cozic, J., Di Marco, C. F., Elsasser, M., Nicolas, J.
31 B., Marchand, N., Abidi, E., Wiedensohler, A., Drewnick, F., Schneider, J., Borrmann,
32 S., Nemitz, E., Zimmermann, R., Jaffrezo, J. L., Prévôt, A. S. H., and Baltensperger,
33 U.: Wintertime aerosol chemical composition and source apportionment of the
34 organic fraction in the metropolitan area of Paris, *Atmos. Chem. Phys.*, 13, 961-981,
35 10.5194/acp-13-961-2013, 2013.

36 DeCarlo, P. F., Kimmel, J. R., Trimborn, A., Northway, M. J., Jayne, J. T., Aiken, A.
37 C., Gonin, M., Fuhrer, K., Horvath, T., Docherty, K. S., Worsnop, D. R., and Jimenez,
38 J. L.: Field-deployable, high-resolution, time-of-flight aerosol mass spectrometer,
39 *Anal. Chem.*, 78, 8281-8289, 10.1021/ac061249n, 2006.

40 Dockery, D. W., and Pope, C. A., III: Acute respiratory effects of particulate air
41 pollution, in: *Annual Review of Public Health*, edited by: Omenn, G. S., *Annual*
42 *Review of Public Health*, Annual Reviews Inc., P.O. Box 10139, 4139 El Camino
43 Way, Palo Alto, California 94306, USA, 107-132, 1994.

44 Dore, C. J., Goodwin, J. W. L., Watterson, J. D., Murrels, T. P., Passant, N. R.,
45 Hobson, M. M., Haigh, K. E., Baggott, S. L., Pye, S. T., Coleman, P. J., and King, K.
46 R.: UK Emissions of Air Pollutants 1970 to 2001, National Atmospheric Emissions
47 Inventory, 2003.

- 1 Flechsig, U., Jaggi, A., Spielmann, S., Padmore, H. A., and MacDowell, A. A.: The
2 optics beamline at the Swiss Light Source, Nucl. Instrum. Methods Phys. Res. Sect.
3 A-Accel. Spectrom. Dect. Assoc. Equip., 609, 281-285, 2009.
- 4 Formenti, P., Prati, P., Zucchiatti, A., Lucarelli, F., and Mando, P. A.: Aerosol study in
5 the town of Genova with a PIXE analysis, Nucl. Instrum. Methods Phys. Res. Sect.
6 B-Beam Interact. Mater. Atoms, 113, 359-362, 1996.
- 7 Fowler, D., and Smith, R.: Spatial and temporal variability in the deposition of
8 acidifying species in the UK between 1986 and 1997, Department of Environment,
9 Food and Rural Affairs, 2000.
- 10 Franklin, M., Koutrakis, P., and Schwartz, J.: The role of particle composition on the
11 association between PM_{2.5} and mortality, Epidemiology, 19, 680-689,
12 10.1097/EDE.0b013e3181812bb7, 2008.
- 13 Freutel, F., Schneider, J., Drewnick, F., von der Weiden-Reinmüller, S. L., Crippa,
14 M., Prévôt, A. S. H., Baltensperger, U., Poulain, L., Wiedensohler, A., Sciare, J.,
15 Sarda-Estève, R., Burkhardt, J. F., Eckhardt, S., Stohl, A., Gros, V., Colomb, A.,
16 Michoud, V., Doussin, J. F., Borbon, A., Haeffelin, M., Morille, Y., Beekmann, M., and
17 Borrmann, S.: Aerosol particle measurements at three stationary sites in the
18 megacity of Paris during summer 2009: meteorology and air mass origin dominate
19 aerosol particle composition and size distribution, Atmos. Chem. Phys., 13, 933-959,
20 10.5194/acp-13-933-2013, 2013.
- 21 Gotschi, T., Hazenkamp-Von Arxb, M. E., Heinrich, J., Bono, R., Burney, P.,
22 Forsberg, B., Jarvis, D., Maldonado, J., Norback, D., Stern, W. B., Sunyer, J., Toren,
23 K., Verlato, G., Villani, S., and Kunzli, N.: Elemental composition and reflectance of
24 ambient fine particles at 21 European locations, Atmos. Env., 39, 5947-5958, 2005.
- 25 Hammond, D. M., Dvonch, J. T., Keeler, G. J., Parker, E. A., Kamal, A. S., Barres, J.
26 A., Yip, F. Y., and Brakefield-Caldwell, W.: Sources of ambient fine particulate matter
27 at two community sites in Detroit, Michigan, Atmos. Env., 42, 720-732, 2008.
- 28 Harrison, R. M., Yin, J., Mark, D., Stedman, J., Appleby, R. S., Booker, J., and
29 Moorcroft, S.: Studies of the coarse particle (2.5–10 µm) component in UK urban
30 atmospheres, Atmos. Env., 35, 3667-3679, 2001.
- 31 Harrison, R. M., and Jones, A. M.: Multisite study of particle number concentrations
32 in urban air, Environ. Sci. Technol., 39, 6063-6070, 10.1021/es040541e, 2005.
- 33 Harrison, R. M., Stedman, J., and Derwent, D.: New Directions: Why are PM₁₀
34 concentrations in Europe not falling?, Atmos. Env., 42, 603-606, 2008.
- 35 Harrison, R. M., Beddows, D. C. S., and Dall'Osto, M.: PMF analysis of wide-range
36 particle size spectra collected on a major highway, Environ. Sci. Technol., 45, 5522-
37 5528, 2011.
- 38 Harrison, R. M., Dall'Osto, M., Beddows, D. C. S., Thorpe, A. J., Bloss, W. J., Allan,
39 J. D., Coe, H., Dorsey, J. R., Gallagher, M., Martin, C., Whitehead, J., Williams, P. I.,
40 Jones, R. L., Langridge, J. M., Benton, A. K., Ball, S. M., Langford, B., Hewitt, C. N.,
41 Davison, B., Martin, D., Petersson, K. F., Henshaw, S. J., White, I. R., Shallcross, D.
42 E., Barlow, J. F., Dunbar, T., Davies, F., Nemitz, E., Phillips, G. J., Helfter, C., Di
43 Marco, C. F., and Smith, S.: Atmospheric chemistry and physics in the atmosphere of
44 a developed megacity (London): an overview of the REPARTEE experiment and its
45 conclusions, Atmos. Chem. Phys., 12, 3065-3114, 2012a.
- 46 Harrison, R. M., Jones, A. M., Gietl, J., Yin, J., and Green, D. C.: Estimation of the
47 contributions of brake dust, tire wear, and resuspension to nonexhaust traffic
48 particles derived from atmospheric measurements, Environ. Sci. Technol., 46, 6523-
49 6529, 10.1021/es300894r, 2012b.

- 1 Harrison, R. M., Laxen, D., Moorcroft, S., and Laxen, K.: Processes affecting
2 concentrations of fine particulate matter (PM_{2.5}) in the UK atmosphere, *Atmos. Env.*,
3 46, 115-124, 2012c.
- 4 Janssen, N. A. H., Van Mansom, D. F. M., Van Der Jagt, K., Harssema, H., and
5 Hoek, G.: Mass concentration and elemental composition of airborne particulate
6 matter at street and background locations, *Atmos. Env.*, 31, 1185-1193, 1997.
- 7 Jones, A. M., Harrison, R. M., and Baker, J.: The wind speed dependence of the
8 concentrations of airborne particulate matter and NO_x, *Atmos. Env.*, 44, 1682-1690,
9 2010.
- 10 Jones, A. R., Thomson, D. J., Hort, M., and Devenish, B.: The UK Met Office's next-
11 generation atmospheric dispersion model, NAME III, *Air Pollution Modeling and its*
12 *Application XVII*, edited by: Borrego, C., and Norman, A.-L., Springer, 2007.
- 13 Kelly, F. J., and Fussell, J. C.: Size, source and chemical composition as
14 determinants of toxicity attributable to ambient particulate matter, *Atmos. Env.*, 60,
15 504-526, 2012.
- 16 Lee, D. S., Garland, J. A., and Fox, A. A.: Atmospheric concentrations of trace
17 elements in urban areas of the United Kingdom, *Atmos. Env.*, 28, 2691-2713, 1994.
- 18 Lin, C. C., Chen, S. J., Huang, K. L., Hwang, W. I., Chang-Chien, G. P., and Lin, W.
19 Y.: Characteristics of metals in nano/ultrafine/fine/coarse particles collected beside a
20 heavily trafficked road, *Environ. Sci. Technol.*, 39, 8113-8122, 2005.
- 21 Lucarelli, F., Mando, P. A., Nava, S., Valerio, M., Prati, P., and Zucchiatti, A.:
22 Elemental composition of urban aerosol collected in Florence, Italy, *Environ. Monit.*
23 *Assess.*, 65, 165-173, 2000.
- 24 Maenhaut, W.: "Global Change" related and other atmospheric aerosol research at
25 the University of Gent, and the role of PIXE therein, *Nucl. Instrum. Methods Phys.*
26 *Res. Sect. B-Beam Interact. Mater. Atoms*, 109, 419-428, 1996.
- 27 Mavrogianni, A., Davies, M., Batty, M., Belcher, S. E., Bohnenstengel, S. I.,
28 Carruthers, D., Chalabi, Z., Croxford, B., Demanuele, C., Evans, S., Giridharan, R.,
29 Hacker, J. N., Hamilton, I., Hogg, C., Hunt, J., Kolokotroni, M., Martin, C., Milner, J.,
30 Rajapaksha, I., Ridley, I., Steadman, J. P., Stocker, J., Wilkinson, P., and Ye, Z.: The
31 comfort, energy and health implications of London's urban heat island, *Build Serv.*
32 *Eng. Res. Technol.*, 32, 35-52, 10.1177/0143624410394530, 2011.
- 33 Mazzei, F., Lucarelli, F., Nava, S., Prati, P., Valli, G., and Vecchi, R.: A new
34 methodological approach: The combined use of two-stage streaker samplers and
35 optical particle counters for the characterization of airborne particulate matter, *Atmos.*
36 *Env.*, 41, 5525-5535, 2007.
- 37 Minguillón, M. C., Cirach, M., Hoek, G., Brunekreef, B., Tsai, M., de Hoogh, K.,
38 Jedynska, A., Kooter, I. M., Nieuwenhuijsen, M., and Querol, X.: Spatial variability of
39 trace elements and sources for improved exposure assessment in Barcelona, *Atmos.*
40 *Env.*, 89, 268-281, 2014.
- 41 Moffet, R. C., Desyaterik, Y., Hopkins, R. J., Tivanski, A. V., Gilles, M. K., Wang, Y.,
42 Shutthanandan, V., Molina, L. T., Abraham, R. G., Johnson, K. S., Mugica, V.,
43 Molina, M. J., Laskin, A., and Prather, K. A.: Characterization of aerosols containing
44 Zn, Pb, and Cl from an industrial region of Mexico City, *Environ. Sci. Technol.*, 42,
45 7091-7097, 2008.
- 46 Mohr, C., Lopez-Hilfiker, F. D., Zotter, P., Prévôt, A. S. H., Xu, L., Ng, N. L., Herndon,
47 S. C., Williams, L. R., Franklin, J. P., Zahniser, M. S., Worsnop, D. R., Knighton, W.
48 B., Aiken, A. C., Gorkowski, K. J., Dubey, M. K., Allan, J. D., and Thornton, J. A.:
49 Contribution of nitrated phenols to wood burning brown carbon light absorption in

1 Detling, United Kingdom during winter time, *Environ. Sci. Technol.*, 47, 6316-6324,
2 10.1021/es400683v, 2013.

3 Moreno, T., Karanasiou, A., Amato, F., Lucarelli, F., Nava, S., Calzolari, G., Chiari,
4 M., Coz, E., Artinano, B., Lumberras, J., Borge, R., Boldo, E., Linares, C., Alastuey,
5 A., Querol, X., and Gibbons, W.: Daily and hourly sourcing of metallic and mineral
6 dust in urban air contaminated by traffic and coal-burning emissions, *Atmos. Env.*,
7 68, 33-44, 10.1016/j.atmosenv.2012.11.037, 2013.

8 Nolte, C. G., Bhawe, P. V., Arnold, J. R., Dennis, R. L., Zhang, K. M., and Wexler, A.
9 S.: Modeling urban and regional aerosols—Application of the CMAQ-UCD Aerosol
10 Model to Tampa, a coastal urban site, *Atmos. Env.*, 42, 3179-3191, 2008.

11 Paatero, P.: The multilinear engine—A table-driven, least squares program for
12 solving multilinear problems, including the n-way parallel factor analysis model,
13 *Journal of Computational and Graphical Statistics*, 8, 854-888,
14 10.1080/10618600.1999.10474853, 1999.

15 Putaud, J. P., Van Dingenen, R., Alastuey, A., Bauer, H., Birmili, W., Cyrys, J.,
16 Flentje, H., Fuzzi, S., Gehrig, R., Hansson, H. C., Harrison, R. M., Herrmann, H.,
17 Hittenberger, R., Hüglin, C., Jones, A. M., Kasper-Giebl, A., Kiss, G., Kousa, A.,
18 Kuhlbusch, T. A. J., Löschau, G., Maenhaut, W., Molnar, A., Moreno, T., Pekkanen,
19 J., Perrino, C., Pitz, M., Puxbaum, H., Querol, X., Rodriguez, S., Salma, I., Schwarz,
20 J., Smolik, J., Schneider, J., Spindler, G., ten Brink, H., Tursic, J., Viana, M.,
21 Wiedensohler, A., and Raes, F.: A European aerosol phenomenology – 3: Physical
22 and chemical characteristics of particulate matter from 60 rural, urban, and kerbside
23 sites across Europe, *Atmos. Env.*, 44, 1308-1320, 2010.

24 Querol, X., Viana, M., Alastuey, A., Amato, F., Moreno, T., Castillo, S., Pey, J., de la
25 Rosa, J., Sánchez de la Campa, A., Artíñano, B., Salvador, P., García Dos Santos,
26 S., Fernández-Patier, R., Moreno-Grau, S., Negral, L., Minguillón, M. C., Monfort, E.,
27 Gil, J. I., Inza, A., Ortega, L. A., Santamaría, J. M., and Zabalza, J.: Source origin of
28 trace elements in PM from regional background, urban and industrial sites of Spain,
29 *Atmos. Env.*, 41, 7219-7231, 2007.

30 Reche, C., Moreno, T., Amato, F., Viana, M., van Drooge, B. L., Chuang, H.-C.,
31 Bérubé, K., Jones, T., Alastuey, A., and Querol, X.: A multidisciplinary approach to
32 characterise exposure risk and toxicological effects of PM10 and PM2.5 samples in
33 urban environments, *Ecotoxicology and Environmental Safety*, 78, 327-335, 2012.

34 Richard, A., Bukowiecki, N., Lienemann, P., Furger, M., Fierz, M., Minguillon, M. C.,
35 Weideli, B., Figi, R., Flechsig, U., Appel, K., Prevot, A. S. H., and Baltensperger, U.:
36 Quantitative sampling and analysis of trace elements in atmospheric aerosols:
37 impactor characterization and synchrotron-XRF mass calibration, *Atmos. Meas.*
38 *Tech.*, 3, 1473-1485, 2010.

39 Richard, A., Gianini, M. F. D., Mohr, C., Furger, M., Bukowiecki, N., Minguillon, M. C.,
40 Lienemann, P., Flechsig, U., Appel, K., DeCarlo, P. F., Heringa, M. F., Chirico, R.,
41 Baltensperger, U., and Prevot, A. S. H.: Source apportionment of size and time
42 resolved trace elements and organic aerosols from an urban courtyard site in
43 Switzerland, *Atmos. Chem. Phys.*, 11, 8945-8963, 2011.

44 Salcedo, D., Laskin, A., Shutthanandan, V., and Jimenez, J. L.: Feasibility of the
45 detection of trace elements in particulate matter using online high-resolution aerosol
46 mass spectrometry, *Aerosol Sci. Technol.*, 46, 1187-1200,
47 10.1080/02786826.2012.701354, 2012.

48 Sole, V. A., Papillon, E., Cotte, M., Walter, P., and Susini, J.: A multiplatform code for
49 the analysis of energy-dispersive X-ray fluorescence spectra, *Spectrosc. Acta Pt. B-
50 Atom. Spectr.*, 62, 63-68, 2007.

- 1 Theodosi, C., Grivas, G., Zarnmpas, P., Chaloulakou, A., and Mihalopoulos, N.: Mass
2 and chemical composition of size-segregated aerosols (PM₁, PM_{2.5}, PM₁₀) over
3 Athens, Greece: local versus regional sources, *Atmos. Chem. Phys.*, 11, 11895-
4 11911, 10.5194/acp-11-11895-2011, 2011.
- 5 Turoczi, B., Hoffer, A., Toth, A., Kovats, N., Acs, A., Ferincz, A., Kovacs, A., and
6 Gelencser, A.: Comparative assessment of ecotoxicity of urban aerosol, *Atmos.*
7 *Chem. Phys.*, 12, 7365-7370, 10.5194/acp-12-7365-2012, 2012.
- 8 Van Espen, P., Janssens, K., and Nobels, J.: AXIL-PC, software for the analysis of
9 complex X-ray spectra, *Chemometrics Intell. Lab. Syst.*, 1, 109-114, 1986.
- 10 Viana, M., Kuhlbusch, T. A. J., Querol, X., Alastuey, A., Harrison, R. M., Hopke, P.
11 K., Winiwarter, W., Vallius, A., Szidat, S., Prevot, A. S. H., Hueglin, C., Bloemen, H.,
12 Wahlin, P., Vecchi, R., Miranda, A. I., Kasper-Giebl, A., Maenhaut, W., and
13 Hitzengerger, R.: Source apportionment of particulate matter in Europe: A review of
14 methods and results, *J. Aerosol Sci.*, 39, 827-849, 10.1016/j.jaerosci.2008.05.007,
15 2008.
- 16 Wedepohl, K.: The composition of the continental crust, *Geochim. Cosmochim. Acta*,
17 59, 1217-1232, [http://dx.doi.org/10.1016/0016-7037\(95\)00038-2](http://dx.doi.org/10.1016/0016-7037(95)00038-2), 1995.
- 18 Weijers, E. P., Schaap, M., Nguyen, L., Matthijsen, J., van der Gon, H., ten Brink, H.
19 M., and Hoogerbrugge, R.: Anthropogenic and natural constituents in particulate
20 matter in the Netherlands, *Atmos. Chem. Phys.*, 11, 2281-2294, 10.5194/acp-11-
21 2281-2011, 2011.
- 22 Witt, M. L. I., Meheran, N., Mather, T. A., de Hoog, J. C. M., and Pyle, D. M.: Aerosol
23 trace metals, particle morphology and total gaseous mercury in the atmosphere of
24 Oxford, UK, *Atmos. Env.*, 44, 1524-1538, 10.1016/j.atmosenv.2010.01.008, 2010.
- 25 Wood, C. R., Lacser, A., Barlow, J. F., Padhra, A., Belcher, S. E., Nemitz, E., Helfter,
26 C., Famulari, D., and Grimmond, C. S. B.: Turbulent flow at 190 m height above
27 London during 2006-2008: A climatology and the applicability of similarity theory,
28 *Bound.-Layer Meteor.*, 137, 77-96, 10.1007/s10546-010-9516-x, 2010.
- 29 Xiao, Z. H., Shao, L. Y., Zhang, N., Wang, J., and Wang, J. Y.: Heavy metal
30 compositions and bioreactivity of airborne PM₁₀ in a valley-shaped city in
31 northwestern China, *Aerosol Air Qual. Res.*, 13, 1116-1125,
32 10.4209/aaqr.2012.10.0287, 2013.
- 33 Zhou, J. A., Ito, K., Lall, R., Lippmann, M., and Thurston, G.: Time-series analysis of
34 mortality effects of fine particulate matter components in Detroit and Seattle, *Environ.*
35 *Health Perspect.*, 119, 461-466, 10.1289/ehp.1002613, 2011.
- 36 Zhou, Y., and Levy, J. I.: The impact of urban street canyons on population exposure
37 to traffic-related primary pollutants, *Atmos. Env.*, 42, 3087-3098, 2008.

38

1 **Tables**

2

3 **Table 1.** Measurement campaign details.

| Site | Start/End date | Site type | Sampling time | Inlet height | Sampling platform |
|------|----------------------|------------------|---------------|--------------|----------------------------|
| MR | 11 Jan – 14 Feb 2012 | kerbside | 2 h | 4 m | container at 1 m from road |
| NK | 11 Jan – 9 Feb 2012 | urban background | 2 h | 4 m | container |
| DE | 17 Jan – 13 Feb 2012 | rural | 2 h | 1.5 m | grass field |

4

5

6

1 **Table 2.** Mean, median and 25-75th percentile trace element concentrations (ng m⁻³)
2 for PM_{10-2.5}, PM_{2.5-1.0} and PM_{1.0-0.3} at MR, NK and DE.

| Marylebone Road | | | | | | | | | | | | |
|-----------------|----------------------|--------|-----------|-----------|-----------------------|--------|-----------|-----------|-----------------------|--------|-----------|-----------|
| Element | PM _{10-2.5} | | | | PM _{2.5-1.0} | | | | PM _{1.0-0.3} | | | |
| | mean | median | 25th perc | 75th perc | mean | median | 25th perc | 75th perc | mean | median | 25th perc | 75th perc |
| Na | 1760.6 | 1645.8 | 862.9 | 2507.8 | 402.5 | 282.2 | 177.5 | 527.0 | 122.7 | 70.8 | 47.8 | 124.9 |
| Mg | 189.7 | 173.5 | 119.1 | 245.7 | 66.1 | 51.3 | 35.2 | 89.4 | 26.2 | 21.9 | 15.5 | 30.1 |
| Al | 134.8 | 108.8 | 73.4 | 168.1 | 48.1 | 43.0 | 32.0 | 58.9 | 13.6 | 12.6 | 8.4 | 16.9 |
| Si | 295.1 | 228.2 | 139.5 | 379.3 | 99.8 | 79.5 | 46.1 | 128.8 | 29.4 | 24.3 | 14.6 | 37.4 |
| P | 16.3 | 14.5 | 9.9 | 20.8 | 6.7 | 6.0 | 3.9 | 8.9 | 4.8 | 3.7 | 2.5 | 6.5 |
| S | 125.1 | 110.9 | 78.8 | 154.4 | 64.3 | 53.7 | 38.4 | 81.2 | 196.1 | 83.0 | 37.6 | 285.9 |
| Cl | 989.5 | 862.8 | 366.4 | 1457.3 | 296.2 | 149.9 | 41.7 | 448.3 | 115.0 | 35.7 | 7.2 | 146.5 |
| K | 42.9 | 38.4 | 27.4 | 52.1 | 16.3 | 14.0 | 9.4 | 21.5 | 17.8 | 11.9 | 8.0 | 23.2 |
| Ca | 233.4 | 176.2 | 108.2 | 307.0 | 74.2 | 52.5 | 31.9 | 94.9 | 20.3 | 15.0 | 9.0 | 25.1 |
| Ti | 7.5 | 5.9 | 3.4 | 10.0 | 2.6 | 2.0 | 1.2 | 3.6 | 0.8 | 0.7 | 0.4 | 1.1 |
| V | 2.2 | 1.9 | 1.1 | 2.9 | 0.9 | 0.8 | 0.4 | 1.1 | 0.4 | 0.4 | 0.2 | 0.6 |
| Cr | 6.3 | 3.6 | 2.0 | 6.0 | 1.7 | 1.4 | 0.9 | 2.4 | 0.6 | 0.4 | 0.3 | 0.7 |
| Mn | 9.4 | 7.7 | 4.6 | 12.2 | 3.4 | 2.9 | 2.0 | 4.4 | 1.4 | 1.0 | 0.6 | 1.7 |
| Fe | 693.1 | 601.7 | 347.0 | 929.9 | 259.9 | 226.8 | 136.4 | 348.6 | 90.4 | 75.8 | 43.6 | 122.3 |
| Ni | 2.1 | 0.6 | 0.4 | 1.0 | 0.3 | 0.2 | 0.1 | 0.4 | 0.2 | 0.1 | 0.1 | 0.2 |
| Cu | 26.0 | 22.9 | 12.6 | 33.3 | 9.5 | 8.2 | 4.6 | 12.5 | 3.3 | 2.6 | 1.4 | 4.5 |
| Zn | 10.9 | 8.9 | 5.2 | 14.1 | 4.3 | 3.6 | 2.0 | 5.6 | 4.6 | 3.0 | 1.6 | 6.5 |
| Br | 2.3 | 1.8 | 1.0 | 3.0 | 0.8 | 0.6 | 0.4 | 1.0 | 1.7 | 1.1 | 0.6 | 2.3 |
| Sr | 1.1 | 0.9 | 0.7 | 1.4 | 0.4 | 0.4 | 0.2 | 0.6 | 0.2 | 0.1 | 0.1 | 0.2 |
| Zr | 2.5 | 1.8 | 0.9 | 3.3 | 1.1 | 0.8 | 0.4 | 1.4 | 0.4 | 0.2 | 0.1 | 0.5 |
| Mo | 3.1 | 2.2 | 1.1 | 3.9 | 1.3 | 1.0 | 0.6 | 1.6 | 0.5 | 0.4 | 0.2 | 0.6 |
| Sn | 4.1 | 3.3 | 1.9 | 5.5 | 1.7 | 1.5 | 0.8 | 2.3 | 0.7 | 0.6 | 0.3 | 1.0 |
| Sb | 3.3 | 2.5 | 1.3 | 4.4 | 1.3 | 1.0 | 0.6 | 1.8 | 0.5 | 0.4 | 0.3 | 0.7 |
| Ba | 18.3 | 14.5 | 8.3 | 24.7 | 7.6 | 6.5 | 3.9 | 10.3 | 2.7 | 2.1 | 1.2 | 3.7 |
| Pb | 1.6 | 0.9 | 0.6 | 1.7 | 0.7 | 0.5 | 0.3 | 0.9 | 1.6 | 0.8 | 0.4 | 2.1 |

| North Kensington | | | | | | | | | | | | |
|------------------|----------------------|--------|-----------|-----------|-----------------------|--------|-----------|-----------|-----------------------|--------|-----------|-----------|
| Element | PM _{10-2.5} | | | | PM _{2.5-1.0} | | | | PM _{1.0-0.3} | | | |
| | mean | median | 25th perc | 75th perc | mean | median | 25th perc | 75th perc | mean | median | 25th perc | 75th perc |
| Na | 1146.7 | 985.7 | 519.5 | 1730.1 | 408.9 | 288.4 | 186.8 | 542.0 | 127.9 | 63.3 | 43.9 | 141.5 |
| Mg | 103.8 | 90.6 | 54.9 | 152.2 | 60.1 | 46.8 | 33.1 | 80.5 | 22.3 | 16.4 | 9.7 | 27.8 |
| Al | 50.4 | 42.5 | 26.6 | 66.8 | 35.6 | 32.3 | 21.3 | 43.0 | 10.3 | 8.9 | 6.4 | 12.6 |
| Si | 97.9 | 79.5 | 39.8 | 122.1 | 60.3 | 48.2 | 26.8 | 82.0 | 16.3 | 11.6 | 6.9 | 20.1 |

| | | | | | | | | | | | | |
|----|-------|-------|-------|-------|-------|-------|------|-------|-------|------|------|-------|
| P | 6.5 | 5.6 | 3.3 | 9.0 | 4.2 | 3.7 | 2.3 | 5.3 | 3.3 | 2.3 | 1.4 | 4.1 |
| S | 63.5 | 56.4 | 38.2 | 85.6 | 53.9 | 43.0 | 30.3 | 65.9 | 174.8 | 82.0 | 37.9 | 211.5 |
| Cl | 545.2 | 429.4 | 138.4 | 879.0 | 271.3 | 107.8 | 24.8 | 394.8 | 90.2 | 14.0 | 3.5 | 94.3 |
| K | 22.3 | 19.8 | 12.8 | 30.7 | 14.2 | 12.2 | 8.3 | 19.9 | 15.4 | 10.2 | 6.2 | 18.7 |
| Ca | 92.4 | 70.2 | 40.5 | 114.5 | 49.9 | 37.2 | 21.0 | 59.9 | 11.8 | 8.6 | 4.9 | 14.1 |
| Ti | 2.7 | 1.7 | 0.9 | 3.2 | 1.6 | 1.2 | 0.5 | 2.3 | 0.4 | 0.3 | 0.1 | 0.5 |
| V | 0.6 | 0.4 | 0.2 | 0.7 | 0.4 | 0.3 | 0.1 | 0.5 | 0.2 | 0.2 | 0.1 | 0.3 |
| Cr | 1.2 | 0.8 | 0.4 | 1.5 | 0.6 | 0.5 | 0.3 | 0.8 | 0.2 | 0.1 | 0.0 | 0.2 |
| Mn | 2.4 | 1.7 | 1.0 | 3.0 | 1.7 | 1.5 | 0.8 | 2.2 | 0.8 | 0.5 | 0.1 | 0.9 |
| Fe | 163.8 | 120.8 | 69.9 | 202.6 | 98.8 | 72.7 | 39.0 | 126.0 | 30.1 | 18.5 | 9.6 | 34.8 |
| Ni | 0.4 | 0.2 | 0.1 | 0.4 | 0.1 | 0.1 | 0.0 | 0.2 | 0.1 | 0.1 | 0.0 | 0.1 |
| Cu | 4.9 | 3.6 | 1.8 | 6.4 | 3.7 | 2.5 | 1.4 | 4.6 | 1.2 | 0.6 | 0.4 | 1.4 |
| Zn | 2.9 | 1.9 | 1.0 | 3.4 | 2.1 | 1.5 | 0.8 | 2.8 | 3.2 | 1.9 | 0.8 | 4.3 |
| Br | 1.3 | 1.0 | 0.4 | 1.8 | 0.7 | 0.5 | 0.3 | 1.0 | 1.6 | 1.1 | 0.5 | 1.9 |
| Sr | 0.5 | 0.4 | 0.2 | 0.6 | 0.3 | 0.2 | 0.2 | 0.4 | 0.1 | 0.1 | 0.0 | 0.1 |
| Zr | 0.5 | 0.2 | 0.1 | 0.4 | 0.3 | 0.2 | 0.1 | 0.4 | 0.1 | 0.1 | 0.0 | 0.1 |
| Mo | 0.8 | 0.3 | 0.2 | 0.7 | 0.5 | 0.3 | 0.1 | 0.6 | 0.2 | 0.1 | 0.1 | 0.2 |
| Sn | 0.7 | 0.5 | 0.2 | 0.9 | 0.5 | 0.4 | 0.2 | 0.7 | 0.3 | 0.2 | 0.1 | 0.3 |
| Sb | 0.5 | 0.3 | 0.2 | 0.6 | 0.4 | 0.2 | 0.1 | 0.5 | 0.2 | 0.2 | 0.1 | 0.3 |
| Ba | 4.3 | 2.1 | 1.2 | 4.5 | 2.7 | 1.8 | 0.9 | 3.5 | 1.0 | 0.6 | 0.3 | 1.2 |
| Pb | 0.4 | 0.2 | 0.1 | 0.4 | 0.4 | 0.2 | 0.1 | 0.6 | 1.4 | 0.7 | 0.3 | 1.8 |

| Detling Element | PM _{10-2.5} | | | | PM _{2.5-1.0} | | | | PM _{1.0-0.3} | | | |
|--------------------|----------------------|--------|--------------|--------------|-----------------------|--------|--------------|--------------|-----------------------|--------|--------------|--------------|
| | mean | median | 25th perc | 75th perc | mean | median | 25th perc | 75th perc | mean | median | 25th perc | 75th perc |
| Na | 523.9 | 375.2 | 33.1 | 842.0 | 219.1 | 123.3 | 43.0 | 272.0 | 95.0 | 50.9 | 22.5 | 126.5 |
| Mg | 49.9 | 37.8 | 9.4 | 72.4 | 32.4 | 23.0 | 7.1 | 44.6 | 19.4 | 14.0 | 5.1 | 24.3 |
| Al | 25.6 | 23.6 | 12.1 | 35.1 | 27.8 | 26.8 | 13.9 | 38.2 | 7.6 | 7.3 | 3.6 | 11.0 |
| Si | 50.4 | 40.8 | 21.4 | 64.5 | 31.6 | 24.9 | 11.1 | 46.1 | 10.9 | 8.4 | 4.8 | 15.5 |
| P | 3.1 | 2.5 | 1.1 | 4.2 | 2.0 | 1.6 | 0.8 | 2.7 | 3.2 | 1.6 | 0.9 | 4.1 |
| S | 36.2 | 31.7 | 6.8 | 48.0 | 33.3 | 30.5 | 13.1 | 47.9 | 224.1 | 59.8 | 27.8 | 242.8 |
| Cl | 237.3 | 50.8 | 3.6 | 380.1 | 135.0 | 9.2 | 2.6 | 148.4 | 64.3 | 10.3 | 3.4 | 57.2 |
| K | 13.8 | 11.8 | 3.5 | 17.7 | 8.2 | 7.5 | 2.6 | 12.5 | 19.9 | 8.2 | 3.6 | 19.8 |
| Ca | 37.5 | 28.8 | 11.1 | 46.6 | 20.0 | 14.7 | 5.9 | 25.1 | 8.2 | 4.9 | 2.7 | 8.3 |
| Ti | 1.0 | 0.6 | 0.3 | 1.3 | 0.7 | 0.4 | 0.2 | 1.0 | 0.2 | 0.2 | 0.1 | 0.3 |
| V | 0.2 | 0.1 | 0.1 | 0.2 | 0.1 | 0.1 | 0.1 | 0.2 | 0.2 | 0.1 | 0.0 | 0.3 |
| Cr | 4.0 | 0.9 | 0.3 | 2.9 | 0.8 | 0.3 | 0.2 | 0.6 | 0.1 | 0.1 | 0.0 | 0.2 |
| Mn | 1.8 | 0.6 | 0.3 | 1.3 | 1.1 | 1.2 | 0.3 | 1.6 | 0.7 | 0.3 | 0.0 | 0.7 |
| Fe | 55.2 | 36.8 | 19.9 | 66.2 | 26.8 | 21.5 | 11.5 | 37.7 | 9.8 | 7.8 | 4.3 | 13.3 |

| | | | | | | | | | | | | |
|----|-----|-----|------|-----|-----|-----|-----|-----|-----|-----|-----|-----|
| Ni | 4.3 | 0.7 | 0.2 | 2.6 | 0.6 | 0.1 | 0.1 | 0.3 | 0.9 | 0.1 | 0.0 | 0.5 |
| Cu | 1.4 | 0.8 | 0.4 | 1.8 | 0.9 | 0.7 | 0.4 | 1.1 | 0.7 | 0.3 | 0.1 | 0.5 |
| Zn | 3.4 | 0.9 | 0.4 | 1.8 | 1.3 | 0.7 | 0.3 | 1.7 | 4.3 | 1.6 | 0.6 | 5.7 |
| Br | 1.1 | 0.4 | 0.1 | 1.3 | 0.4 | 0.2 | 0.1 | 0.5 | 1.9 | 1.1 | 0.5 | 2.4 |
| Sr | 0.2 | 0.2 | 0.1 | 0.3 | 0.1 | 0.1 | 0.0 | 0.2 | 0.1 | 0.0 | 0.0 | 0.1 |
| Zr | 0.0 | 0.0 | -0.1 | 0.1 | 0.1 | 0.0 | 0.0 | 0.1 | 0.0 | 0.0 | 0.0 | 0.0 |
| Mo | 1.9 | 0.1 | 0.1 | 0.7 | 0.2 | 0.1 | 0.0 | 0.2 | 0.1 | 0.1 | 0.0 | 0.1 |
| Sn | 0.3 | 0.1 | 0.0 | 0.2 | 0.2 | 0.1 | 0.1 | 0.2 | 0.2 | 0.1 | 0.1 | 0.3 |
| Sb | 0.2 | 0.1 | 0.0 | 0.2 | 0.1 | 0.1 | 0.0 | 0.1 | 0.2 | 0.1 | 0.0 | 0.2 |
| Ba | 1.0 | 0.4 | 0.2 | 0.8 | 0.5 | 0.4 | 0.2 | 0.7 | 0.3 | 0.2 | 0.1 | 0.4 |
| Pb | 0.3 | 0.1 | 0.0 | 0.3 | 0.3 | 0.1 | 0.1 | 0.5 | 1.6 | 0.5 | 0.2 | 1.8 |

1

2

Figure captions

Figure 1. Map of south eastern UK. Indicated are the sampling sites MR (kerbside site Marylebone Road), NK (urban background site North Kensington), DE (rural site Detling), and the elevated BT Tower site for meteorological measurements (adapted from Google Maps).

~~**Figure 2.** Total PM_{10} element mass concentrations measured by the RDI (sum of $PM_{10-2.5}$, $PM_{2.5-1.0}$ and $PM_{1.0-0.3}$ fractions) at MR and NK averaged to 24 hrs versus 24-hr PM_{10} filter measurements of elements for (a) elements that agree within $\pm 50\%$, (b) elements with poor correlations, (c) elements with good correlations but a factor 2 higher with RDI, (d) other elements. The one-to-one line is added in black. See Table S2 for fit coefficients and Pearson's R values. Note that many elements are scaled to improve visualization.~~

~~**Figure 2**~~**Figure 3.** Relative contribution for trace elements in $PM_{10-2.5}$, $PM_{2.5-1.0}$ and $PM_{1.0-0.3}$ to total PM_{10} mean concentration per element at MR (top), NK (middle) and DE (bottom). Absolute mean total PM_{10} element concentrations are shown above each bar.

~~**Figure 3**~~**Figure 4.** Mean, median and 25-75th percentile urban increment values for trace elements at NK relative to DE for $PM_{10-2.5}$ (top), $PM_{2.5-1.0}$ (middle) and $PM_{1.0-0.3}$ (bottom). Note that the median of Zr in $PM_{10-2.5}$ is below detection limit.

~~**Figure 4**~~**Figure 5.** Mean, median and 25-75th percentile trace element concentrations at MR split in four wind direction sectors (N, E, S, W) normalized to the global median concentration per element for $PM_{10-2.5}$ (top), $PM_{2.5-1.0}$ (middle) and $PM_{1.0-0.3}$ (bottom). See Sect. 4.2.2 for the definition of the wind direction sectors.

~~**Figure 5**~~**Figure 6.** Mean, median and 25-75th percentile kerb increment values for trace elements at MR relative to NK for $PM_{10-2.5}$ (top), $PM_{2.5-1.0}$ (middle) and $PM_{1.0-0.3}$ (bottom) split in SW and NE wind sectors. See Sect. 4.2.2 for the definition of the wind direction sectors.

~~**Figure 6**~~**Figure 7.** Diurnal cycles of 2 h median concentrations of Na, Si, S, Fe and Sb for $PM_{10-2.5}$ (left), $PM_{2.5-1.0}$ (middle) and $PM_{1.0-0.3}$ (right) at MR, NK, DE split in SW

1 and NE wind sectors. See Sect. 4.2.2 for the definition of the wind direction sectors.
2 Hour of day is start of 2 h sampling period, so 00:00 LT means sampling from 00:00
3 to 02:00 LT.

4
5 | **Figure 7.**~~Figure 8.~~ Weekly cycles of 2 h median concentrations of Na, Si, S, Fe and
6 Sb for $PM_{10-2.5}$ (left), $PM_{2.5-1.0}$ (middle) and $PM_{1.0-0.3}$ (right) at MR, NK, DE.

7
8 | **Figure 8**~~Figure 9.~~ (top) Diurnal (left) and weekly (right) cycles of traffic flow at MR,
9 (middle and bottom left) diurnal cycles of 2 h median NO_x and total PM_{10} mass
10 concentrations at MR, NK and DE split in SW and NE wind sectors, and (middle and
11 bottom right) weekly cycles of 2 h median NO_x and total PM_{10} mass concentrations at
12 MR, NK and DE. See Sect. 4.2.2 for the definition of the wind direction sectors. Time
13 stamp is start of 2 h averaging period, so 00:00 LT means averaging between 00:00
14 and 02:00 LT.

15
16 | **Figure 9**~~Figure 10.~~ (top panel) Time series of (top left axis) $PM_{1.0-0.3}$ S, K, Zn and Pb
17 concentrations at NK and (top right axis) wind direction from BT Tower, time series of
18 (bottom left axis) $PM_{10-2.5}$ Na, Si, S and Sb concentrations at NK and (bottom right
19 axis) total PM_{10} mass concentration at NK; (bottom panel) three NK footprints
20 simulated with the NAME model corresponding to the vertical lines (A, B, C) indicated
21 in the top panel. Trajectories are simulated for particles released from NK and
22 followed back at 0-100 m a.g.l. for the previous 24 h at: **(A)** 23 January 2012 09:00
23 LT, **(B)** 31 January 2012 21:00 LT, **(C)** 6 February 2012 18:00 LT; particle
24 concentrations increase from blue to red.

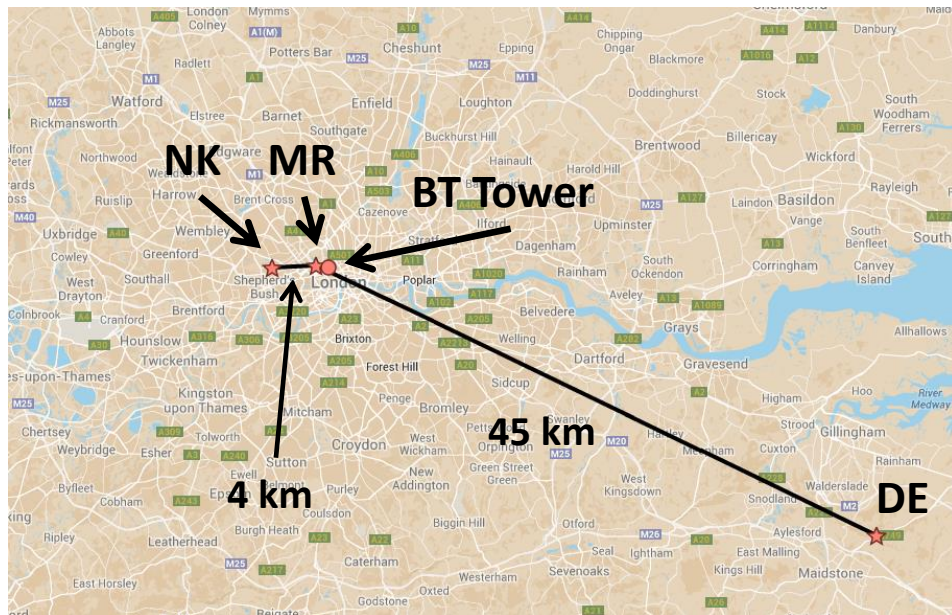


Figure 1. Map of south eastern UK. Indicated are the sampling sites MR (kerbside site Marylebone Road), NK (urban background site North Kensington), DE (rural site Detling), and the elevated BT Tower site for meteorological measurements (adapted from Google Maps).

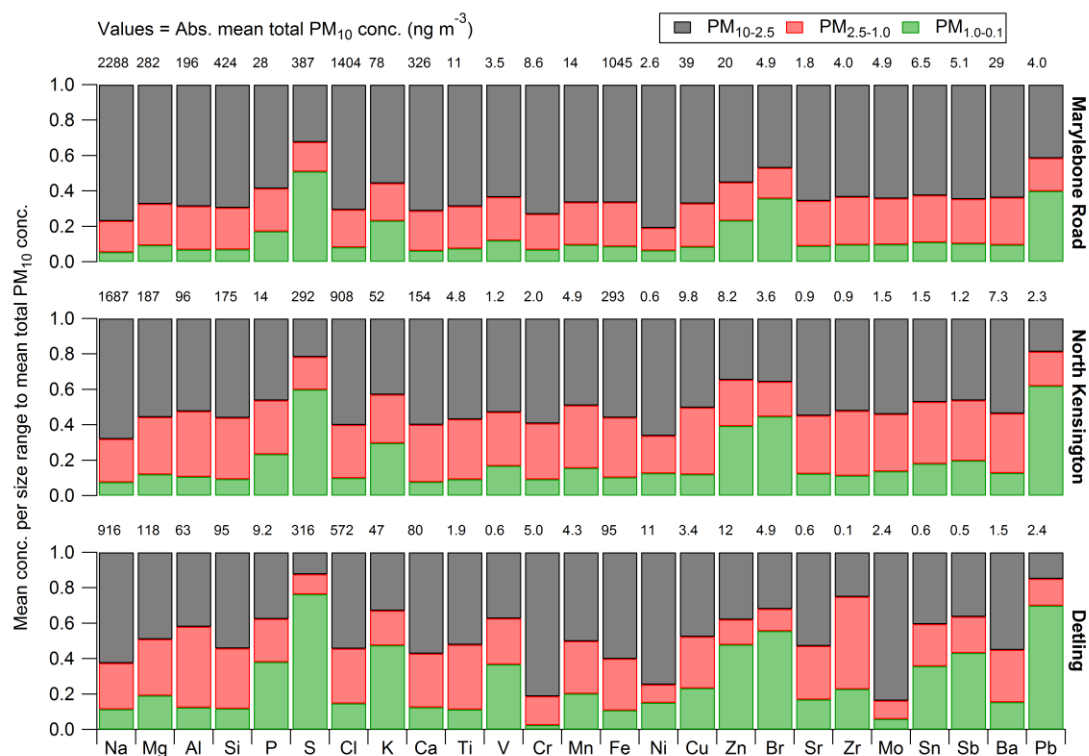


Figure 2 Figure 3. Relative contribution for trace elements in PM_{10-2.5}, PM_{2.5-1.0} and PM_{1.0-0.3} to total PM₁₀ mean concentration per element at MR (top), NK (middle) and DE (bottom). Absolute mean total PM₁₀ element concentrations are shown above each bar.

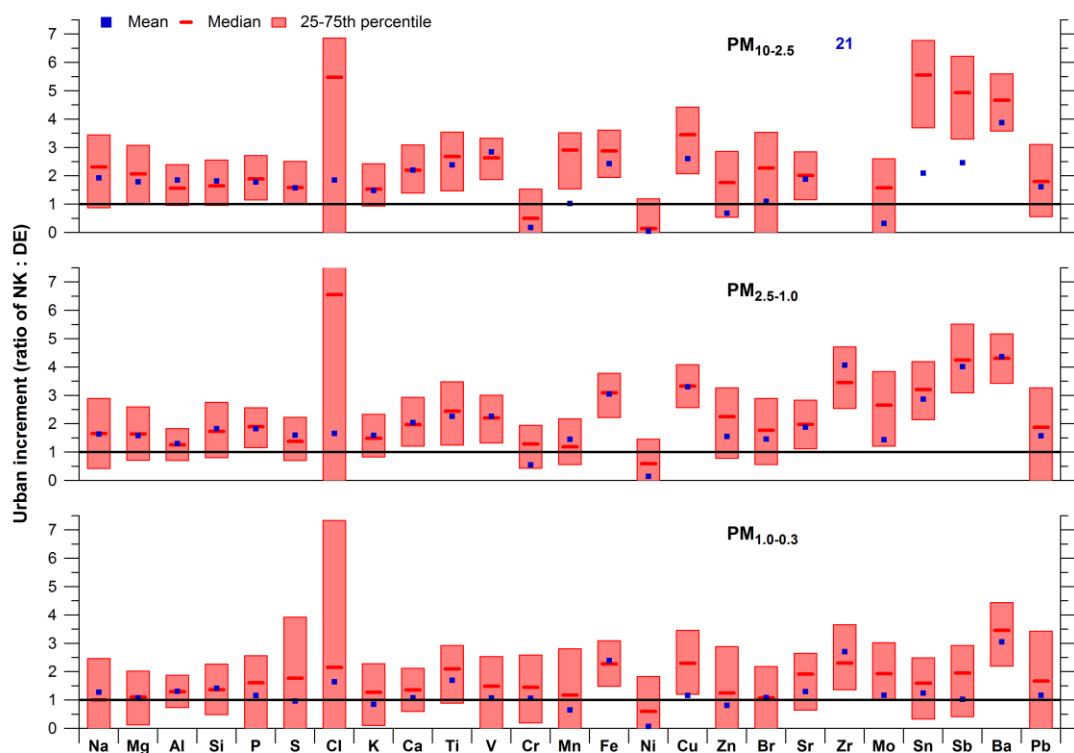


Figure 3 Mean, median and 25-75th percentile urban increment values for trace elements at NK relative to DE for PM_{10-2.5} (top), PM_{2.5-1.0} (middle) and PM_{1.0-0.3} (bottom). Note that the median of Zr in PM_{10-2.5} is below detection limit.

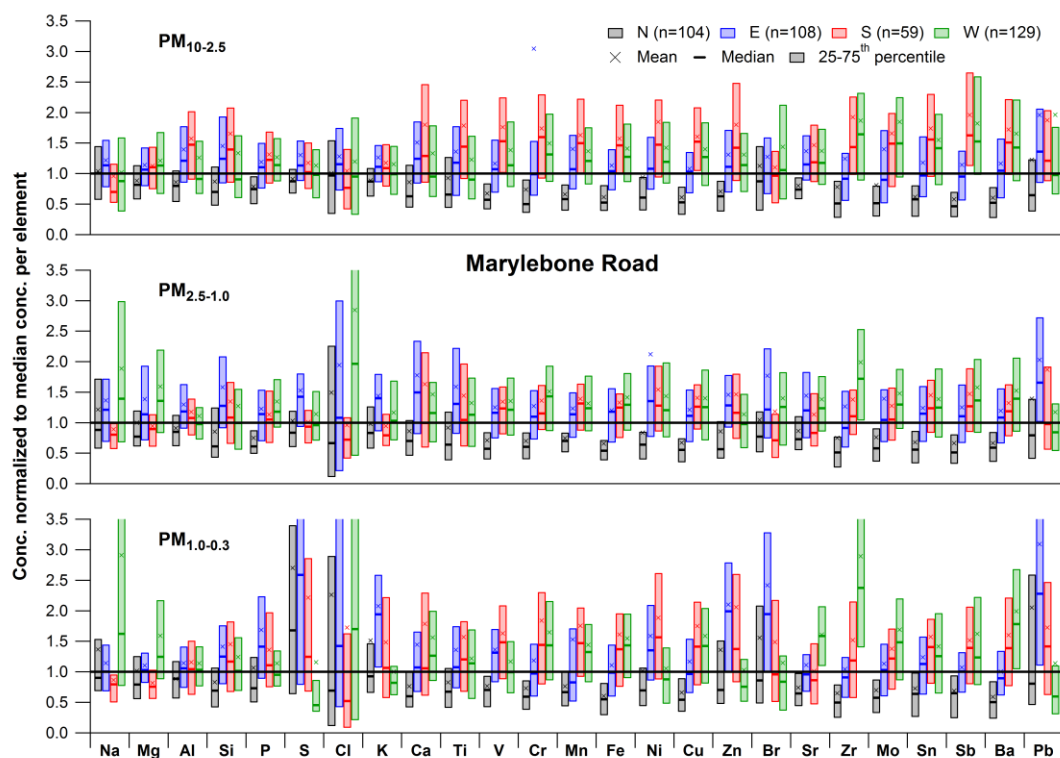


Figure 4Figure 5. Mean, median and 25-75th percentile trace element concentrations at MR split in four wind direction sectors (N, E, S, W) normalized to the global median concentration per element for $PM_{10-2.5}$ (top), $PM_{2.5-1.0}$ (middle) and $PM_{1.0-0.3}$ (bottom). See Sect. 4.2.2 for the definition of the wind direction sectors.

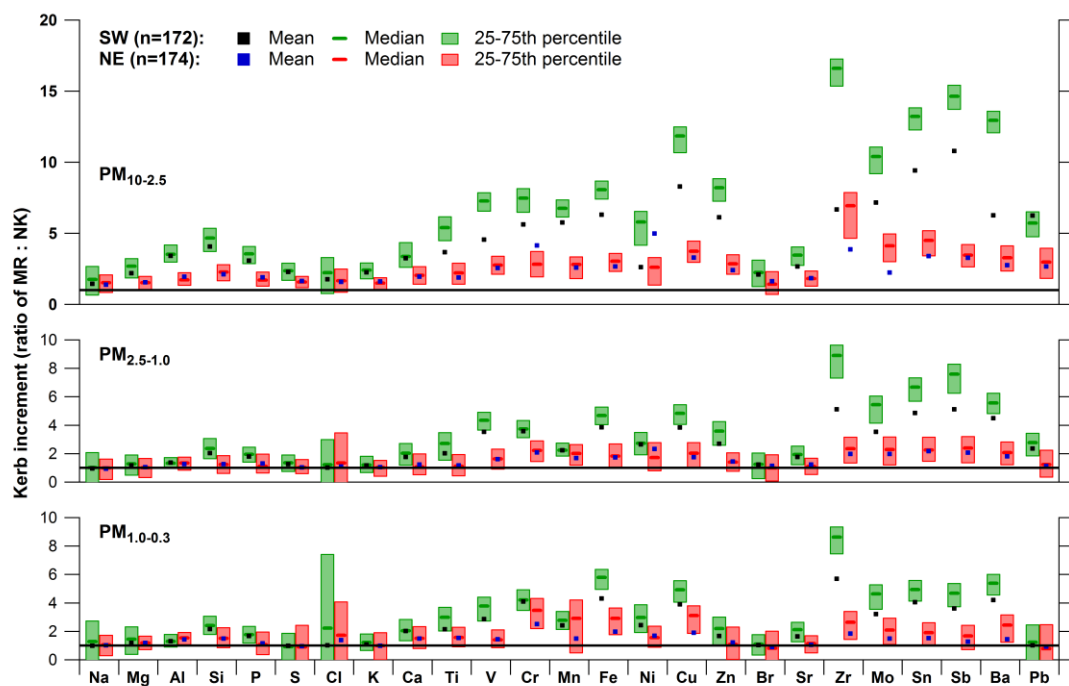


Figure 5 Figure 6. Mean, median and 25-75th percentile kerb increment values for trace elements at MR relative to NK for $PM_{10-2.5}$ (top), $PM_{2.5-1.0}$ (middle) and $PM_{1.0-0.3}$ (bottom) split in SW and NE wind sectors. See Sect. 4.2.2 for the definition of the wind direction sectors.

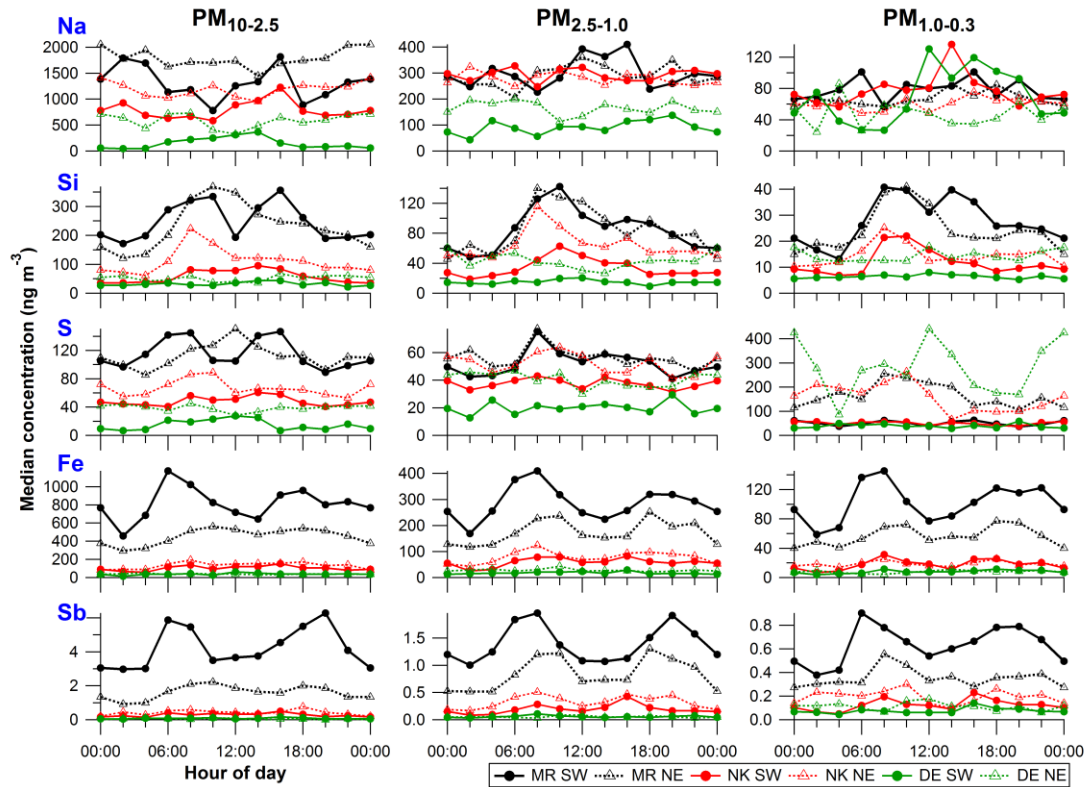


Figure 6 Figure 7. Diurnal cycles of 2 h median concentrations of Na, Si, S, Fe and Sb for $PM_{10-2.5}$ (left), $PM_{2.5-1.0}$ (middle) and $PM_{1.0-0.3}$ (right) at MR, NK, DE split in SW and NE wind sectors. See Sect. 4.2.2 for the definition of the wind direction sectors. Hour of day is start of 2 h sampling period, so 00:00 LT means sampling from 00:00 to 02:00 LT.

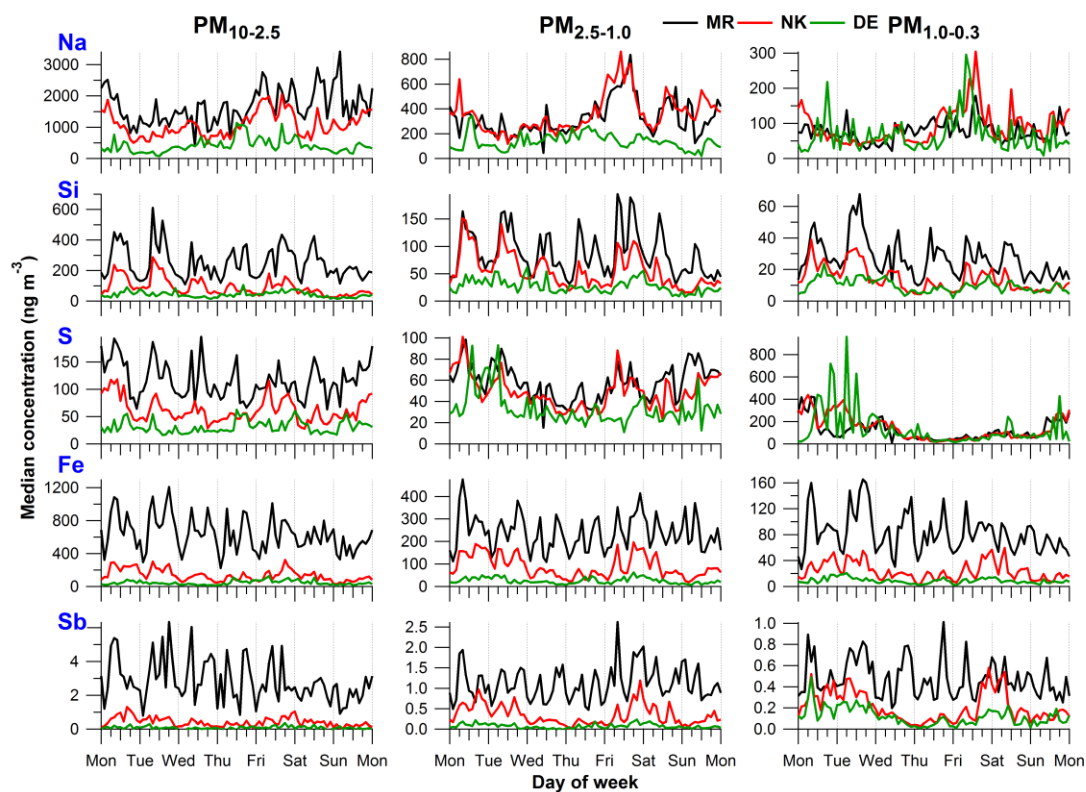


Figure 7. Figure 8. Weekly cycles of 2 h median concentrations of Na, Si, S, Fe and Sb for PM_{10-2.5} (left), PM_{2.5-1.0} (middle) and PM_{1.0-0.3} (right) at MR, NK, DE.

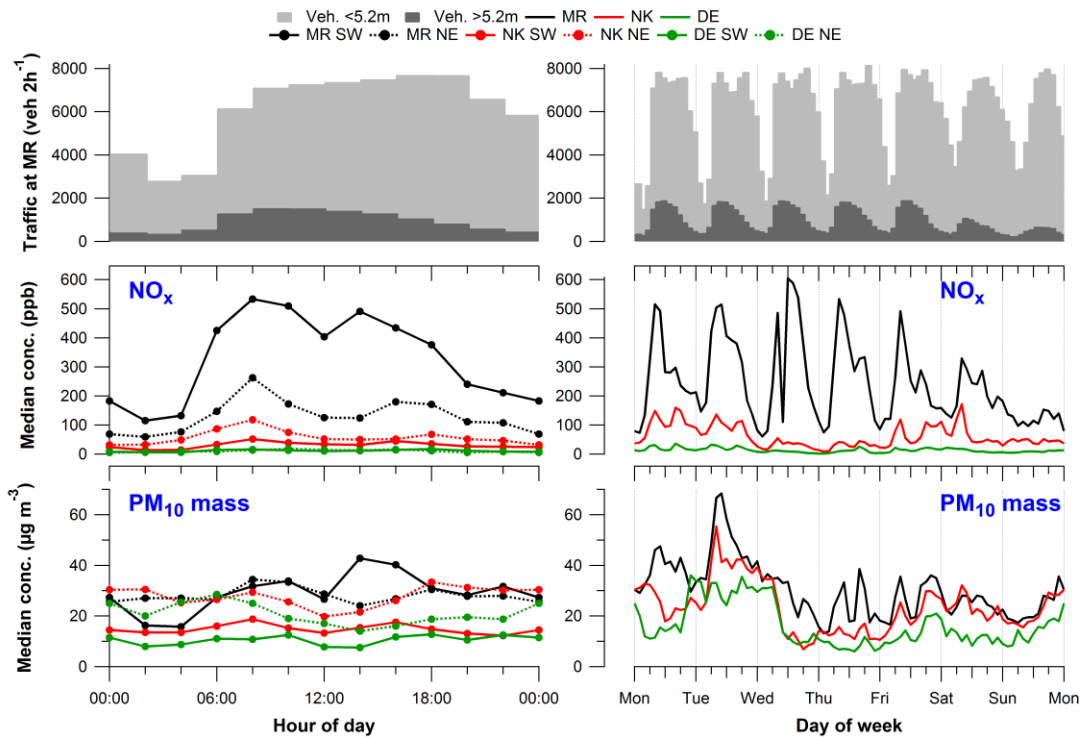


Figure 8 **Figure 9.** (top) Diurnal (left) and weekly (right) cycles of traffic flow at MR, (middle and bottom left) diurnal cycles of 2 h median NO_x and total PM₁₀ mass concentrations at MR, NK and DE split in SW and NE wind sectors, and (middle and bottom right) weekly cycles of 2 h median NO_x and total PM₁₀ mass concentrations at MR, NK and DE. See Sect. 4.2.2 for the definition of the wind direction sectors. Time stamp is start of 2 h averaging period, so 00:00 LT means averaging between 00:00 and 02:00 LT.

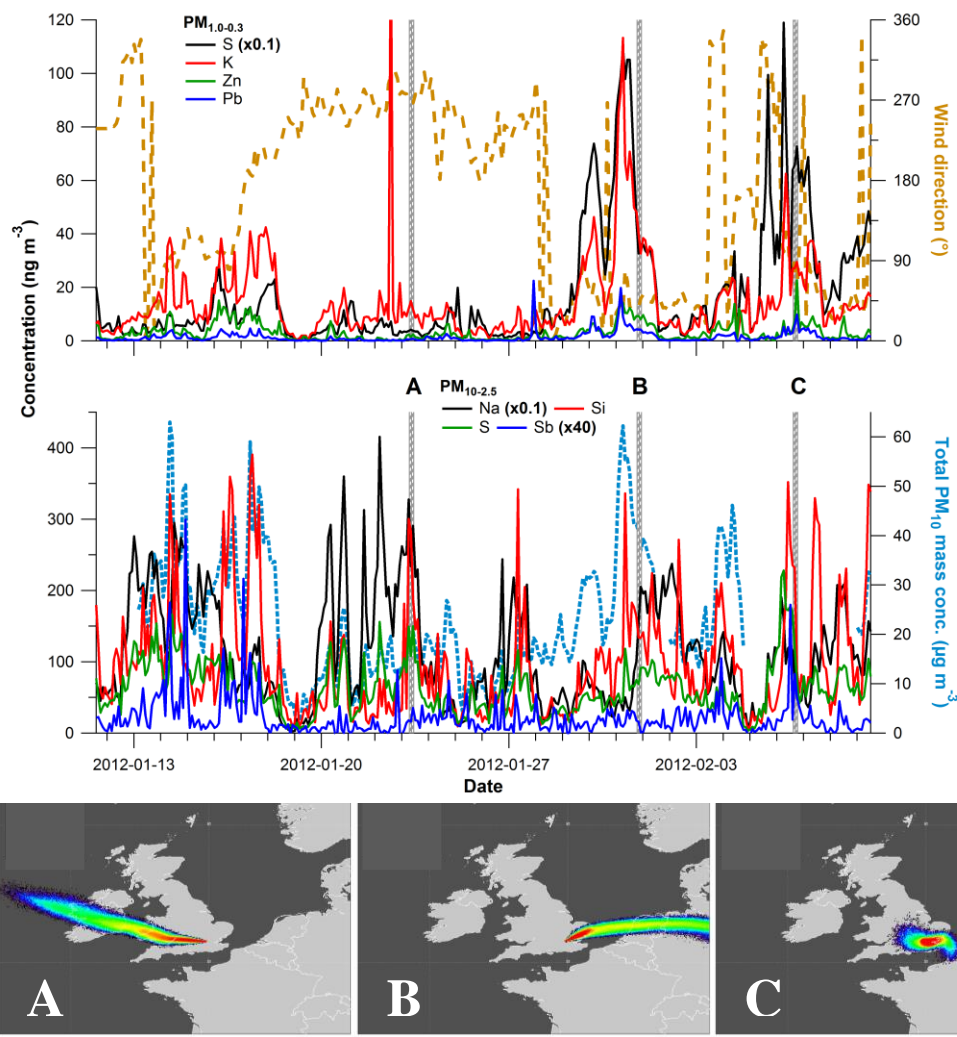


Figure 9 (top panel) Time series of (top left axis) $PM_{1.0-0.3}$ S, K, Zn and Pb concentrations at NK and (top right axis) wind direction from BT Tower, time series of (bottom left axis) $PM_{10-2.5}$ Na, Si, S and Sb concentrations at NK and (bottom right axis) total PM_{10} mass concentration at NK; (bottom panel) three NK footprints simulated with the NAME model corresponding to the vertical lines (A, B, C) indicated in the top panel. Trajectories are simulated for particles released from NK and followed back at 0-100 m a.g.l. for the previous 24 h at: **(A)** 23 January 2012 09:00 LT, **(B)** 31 January 2012 21:00 LT, **(C)** 6 February 2012 18:00 LT; particle concentrations increase from blue to red.

Supplement A: RDI backup filter and PM_{1.0} cut off analysis

RDI backup filter analysis

RDI backup filters (Balston 050-11-BQ 2 µm, microfiber, fluorocarbon resin binder) from the ClearfLo winter campaign were immersed in water and sonicated for about 1.5 h. One filter per measurement site was available. Total sulphate (SO₄²⁻) mass was obtained by analysing the solutions with ion chromatography and converted to concentrations by dividing by the total air volume that passed through the filter during the campaign.

Table S1 compares the S concentrations from the RDI PM_{1.0-0.3} stage with S (from SO₄²⁻) collected by the backup filter. The sum of both (Total S < 1 µm) is compared with S from AMS sulphate measurements. The ratio in the last column reveals mass-closure between the RDI and AMS within 2025 %.

Table S1. Comparison between S from RDI PM_{1.0-0.3} fractions and backup filters (S from SO₄²⁻) with S from the AMS (S from SO₄²⁻). Units in ng m⁻³. The ratio of S in the RDI to the AMS is given in the last column (ratio of RDI Total S < 1 µm to AMS S).

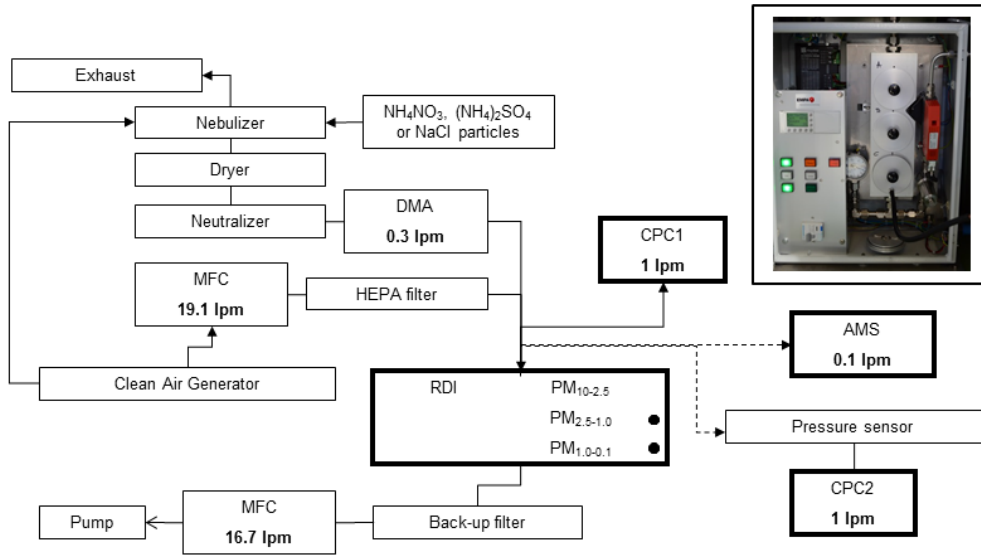
| Site | RDI | | | AMS | |
|------|-------------------------|--------------------|---------------|-----|-----------------|
| | PM _{1.0-0.3} S | S in backup filter | Total S <1 µm | S | Ratio RDI : AMS |
| MR | 195 | 398 | 593 | 476 | 1.25 |
| NK | 174 | 405 | 579 | 607 | 0.95 |
| DE | 224 | 359 | 583 | 715 | 0.82 |

RDI PM_{1.0} cut off analysis

As noted in the main text and in Supplement C, elements whose mass is dominated by the PM_{1.0} fraction are typically underestimated by RDI-SR-XRF relative to external measurements like the AMS and 24 h filter measurements. One explanation is that the collection efficiency of the RDI PM_{1.0} stage is smaller than expected, e.g. by a larger-than-expected size cut off. We therefore performed new laboratory measurements of the RDI size-dependent collection efficiency, and compare these to earlier characterisations by Bukowiecki et al. (2009) and Richard et al. (2010).

Figure S1 shows the setup used for the collection efficiency measurements. (NH₄)₂SO₄, NH₄NO₃ and NaCl particles were nebulized, dried and size-selected using a differential mobility analyser (DMA, TSI, Inc., Shoreview, MN, USA), and then sampled with the RDI. The DMA was operated with sample and sheath flow rates of 0.3 and 3.0 L min⁻¹, respectively. A condensation particle counter (CPC1, TSI, Inc., Shoreview, MN, USA) with a flow rate of 1.0 L min⁻¹ was continuously connected at the inlet stage of the RDI to measure the particles entering the RDI, and to correct for fluctuations in nebulizer performance. A second line led to an additional CPC (CPC2, 1 L min⁻¹) and an Aerodyne aerosol mass spectrometer (AMS, Aerodyne Research, Inc., Billerica, MA, USA) with a flow rate of 0.1 L min⁻¹. This line could be connected at the inlet, after the PM_{2.5-1.0} (B) stage or after the PM_{1.0-0.3} (C) stage. Measurements following the B and C stages were made by connecting the line to a small hole in the lid covering these stages, resulting in sampling of the air flow at a 90° angle (see picture in Fig. S1). The total flow through the system was controlled by a mass flow controller connected to a clean air generator pumping air into the nebulizer and RDI simultaneously. The RDI was operated using three wheels with freshly mounted 6 µm polypropylene foils coated with Apiezon to minimize particle bouncing effects, to simulate ambient field measurements. Tests ruled out differences in measurements

1 on the top or bottom side of the lid at the B and C stages. For the final results, all
 2 data was collected at the bottom side of the B and C stages.



3
 4 **Figure S1.** Setup of the collection efficiency measurements of the RDI $PM_{1.0}$ impactor stage.
 5 The line with the AMS and CPC2 was connected at the inlet, after the $PM_{2.5-1.0}$ or after the
 6 $PM_{1.0-0.3}$ stage. The picture of the RDI shows the connection at the bottom side of the lid of the
 7 $PM_{1.0-0.3}$ stage.

8
 9 As noted above, measurements were conducted at the RDI inlet, after the B stage
 10 impactor (nominal size cut = $1.0 \mu m$) and after the C stage impactor (nominal size cut
 11 = $0.1 \mu m$). RDI collection efficiency at each stage is defined as 1 minus transmission.
 12 To correct for fluctuations in nebulizer concentrations, all data for a given set of
 13 CPC2/AMS measurements were normalized to a constant inlet (CPC1)
 14 concentration. Transmission from the inlet across the B stage impactor was between
 15 90 and 100 % for all sizes (aerodynamic diameter $d < 950 \text{ nm}$), indicating negligible
 16 particle losses and/or unintended collection of small particles. C stage collection
 17 efficiency (CE_C) was therefore calculated using Eq. (S1):

$$18 \quad CE_C = 1 - \left(Conc_C * \frac{CPC1_{ref}}{CPC1_{measC}} \right) / \left(Conc_B * \frac{CPC1_{ref}}{CPC1_{measB}} \right) \quad (S1)$$

19 Concentrations were measured using both CPC2 and the AMS. For large particles,
 20 where the fraction of multiple charged particles passed by the DMA is negligible,
 21 these two methods yield similar results. For smaller particles, collection efficiency as
 22 calculated by the CPC2 is biased low due to the presence of multiple charged
 23 particles with larger diameters, as clearly evidenced from AMS size distributions. For
 24 simplicity, we therefore present only the AMS results here. RDI collection efficiencies
 25 are calculated by fitting a lognormal distribution to each mode and using the resulting
 26 mass concentrations in Eq. S1. This allows simultaneous calculation of RDI collection
 27 efficiencies for several sizes, providing an internal consistency and stability check for
 28 the measurements.

29 Figure S2 shows the collection efficiency of the $PM_{1.0-0.3}$ (C stage) nozzle for two
 30 RDIs (RDI1 and RDI2) as a function of d for NH_4NO_3 particles. D is calculated from
 31 AMS size measurements, assuming a density of 1.74 and a Jayne shape factor
 32 (DeCarlo et al., 2004) of 0.8. Cut points are estimated by a sigmoidal fit to the
 33 collection efficiency curves, and yield different cut points for the two RDIs. RDI1 has
 34 a cut point of $290 \pm 25 \text{ nm}$ and RDI2 a cut point of $410 \pm 15 \text{ nm}$. This discrepancy

was investigated using RDI2 equipped with the $PM_{1.0-0.3}$ nozzle of RDI1 (RDI2 (nozzle RDI1)), demonstrating that the difference between the two RDIs is governed by nozzle performance, because the cut point of this system is 300 ± 20 nm and therefore closer to the RDI1 performance. Similar cut points for the various systems were obtained using $(NH_4)_2SO_4$ and NaCl particles (not shown).

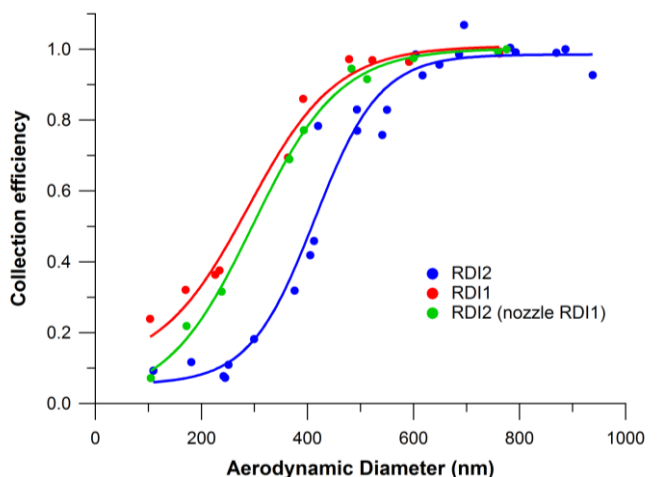


Figure S2. Collection efficiency of the RDI $PM_{1.0-0.3}$ impactor stage as a function of aerodynamic diameter.

Measurements of the nozzle sizes under a microscope reveal small differences between the RDIs. A $1.0 \mu m$ cut point at the B stage impactor is obtained with a nozzle size of 0.68×10 mm. The RDI1 and RDI2 B stage nozzles were 0.70×10 mm, and a third RDI that was used at Marylebone Road during ClearLo had a size of 0.71×10 mm. The C stage nozzle size should measure 0.30×10 mm for a cut point of $0.1 \mu m$. However, the nozzle sizes were $0.30-0.31 \times 10$, $0.30-0.32 \times 10$ and 0.32×10 for RDI1, RDI2 and the third RDI, respectively. We expect the deviations from these measurements from the machining of the nozzles, resulting in higher cut points than expected for the $PM_{1.0}$ stage, and possibly also for the $PM_{2.5-1.0}$ stage.

Conclusions

The $PM_{1.0-0.3}$ collection efficiency curves are different for the two RDIs. RDI2 has a larger small-end cut point of 410 ± 15 nm than RDI1 of 290 ± 25 nm. RDI2 with the $PM_{1.0-0.3}$ nozzle of RDI1 resulted in a similar cut point of RDI1 of 300 ± 20 nm. The slightly larger nozzles than theoretically calculated are the likely reason for the observed increase in the small-end cut point of the $PM_{1.0-0.3}$ nozzle and thus in reduced particle collection at the C stage.

Supplement B: Changes in SR-XRF analysis

The data described in the main text was obtained with RDI-SR-XRF analysis. The following significant changes were made in the SR-XRF analysis compared to the methodology described in Bukowiecki et al. (2005), Bukowiecki et al. (2008) and Richard et al. (2010):

1. At SLS, we replaced the silicon drift detector (Roentec Xflash 2001 type 1102, Bruker AXS) with an e2v SiriusSD detector (SiriusSD-30133LE-IS). This detector is equipped with a thin polymer window resulting in a wider energy range down to about 300 eV and a better energy resolution of 133 eV (Mn K α at 5.9 keV). In addition, the setup accepts a higher throughput resulting in negligible dead time effects. We also replaced the helium chamber with an in-house built vacuum chamber (sample exposure system for micro-X-ray fluorescence measurements, SESmiX) which reaches about 10⁻⁶ bar. This extended the measured range of elements down to Na and Mg.

2. Reference standards for calibration of element fluorescence counts to mass concentrations were produced on the same 6 μ m PP substrate as used for RDI sampling, in contrast to the previous standard where a much thicker 100 μ m PET foil (Folex, BG-32.5 RS plus) was used. Two standards suitable for measurements at both SLS and HASYLAB contained elements in equal concentrations, and have a similar mix of elements as the standard previously used. Two additional standards containing only specifically selected light elements were produced. One standard contained Na, Al, P and Ca; the other Mg, Si, S, K and Ca. The concentrations of these elements were increased by a factor 3.8 relative to the other two standards to improve signal-to-noise ratios in the SR-XRF calibration. Co was added to these additional standards, but in the same concentration as in the other two foils and was used as a quality check of the fabrication procedure of the four standards. The concentration difference of the light elements was taken into account before applying the relative calibration of the sample elements. The new reference standards allowed the use of identical geometry and irradiation time for RDI samples and reference standards, meaning that all SR-XRF measurements exhibit the same scattering and secondary fluorescence excitation. This reduced uncertainties in both the absolute and relative calibration of the samples.

3. Previously, spectra were fitted with the WinAxil software package (Canberra Inc; Van Espen et al., 1986). This rather old spectral fitting package allows little flexibility in spectrum continuum correction and peak fitting. PyMCA (Sole et al., 2007) on the other hand, is more flexible, but lacks the possibility to save uncertainty calculations in batch mode. In this study, spectra were fitted with an in-house developed software package called Spectral Analysis for Multiple Instruments – toolkit for XRF (SAMI-XRF) using the IGOR Pro software environment (Wavemetrics, Inc., Portland, OR, USA) to evaluate the data and create custom interfaces to accomplish specialized tasks. SAMI sequentially determines (1) energy calibration of the X-ray line as a function of detector channel; (2) spectrum continuum correction; (3) peak width calibration as a function of energy (assuming Gaussian peak shape and a general square root law of the full-width-half-maximum (FWHM) energy relation); and (4) peak fitting of the entire spectrum, at which stage only peak heights are fitted as a free parameter and all other parameters are fixed. Steps (1) and (3) are performed with user-selected reference peaks, and incorporates fitting of complex (multi-Gaussian) peak shapes caused by nearly complete overlapping K α_1 and K α_2 lines. Step (2) utilizes collected spectra of a blank foil as a reference for the continuum shape, and scales this reference to user-selected element-free regions of the processed spectra. Step (4) allows lines to be fitted freely or fixed to another line, e.g. to the strongest line in a shell. For example, the K α_2 and K β lines can be fixed to the

1 K α_1 line according to the relative intensities given by Bearden (1967). In this study, all
2 lines within an electron shell were fitted fixed to the strongest line in that shell.
3 Additionally, Ni, Cu and Zn L $\alpha_{1,2}$ lines were fixed to the K α_1 line to reduce the
4 influence of peak overlap with Na. The ratios of L $\alpha_{1,2}$ to K α_1 for Ni, Cu and Zn were
5 determined by fitting calibration standards having these elements but low Na. Final
6 fits were then obtained using the acquired relations, thereby reducing uncertainties in
7 the Na concentrations due to peak overlap and improving Na quantification.
8

Supplement C: Data intercomparison

A short description of the data intercomparison between RDI-SR-XRF data and independent filter data is given in Sect. 3 of the main text. Here the details of this comparison are given. We compare XRF data with filter data (24 h PM₁₀ trace element data analysed with ICP-MS; roughly 9 % uncertainty at a 95 % confidence interval and calibrated with NIST standards) for 18 elements collected at MR and NK (no filter data was available at DE). For this comparison, the three size ranges of the RDI were summed up to total PM₁₀ and averaged to the filter collection period. The intercomparison results are shown in Fig. S3, and are divided into four groups to facilitate discussion. Fit coefficients and Pearson's *R* values for the intercomparison are shown in Table S2, while XRF uncertainties and detection limits are given in Table S3. For all elements, except Mn, the sample inhomogeneity provides the largest source of uncertainty of maximal 20 %. RDI flow rate fluctuations are estimated at a maximum of 5 %. Absolute and relative calibration uncertainties are larger for lighter elements due to their low fluorescence yields, making them harder to detect. For Na-K these uncertainties are 13 %, for Ca-Pb only 2 %. The last source of uncertainty is the energy calibration of an X-ray line as function of detector channel and shows the effect of line overlap in the detection of a specific line. The uncertainties range between 1 and 22 % for most elements, but are around 60 % for Mn due to the overlap with Fe being present in much higher concentrations (on average a factor of 55). Overall, an estimate of the total uncertainties for the median of all data points lies between 21 and 27 % (46 % for Mn) for all elements in the three size fractions. All RDI data points lie well above their detection limits (last column Table S3).

Elements shown in Fig. 2a-Fig. S3a (Al, Ca, Ti, Mn, Fe, Cu, Zn, Sr, Sb, Ba) agree within approximately ± 50 % with good correlations (Pearson's *R* > 0.78). In Fig. S3b-dFigs. 2b-d, we show elements for which the intercomparison shows significant biases and/or no significant correlation between RDI and filters. Note that the elements exhibiting good agreement in Fig. 2a-Fig. S3a span orders of magnitude difference in concentration (and fluorescence counts), suggesting that there are no global or concentration-dependent biases in the RDI-SR-XRF data. For elements exhibiting lesser agreement (Fig. S3b-d), this leaves the element relative calibration (i.e. element fluorescence yield as a function of line energy), spectral peak fitting, and instrument size cut points as issues to address potential sources of error in the XRF analysis.

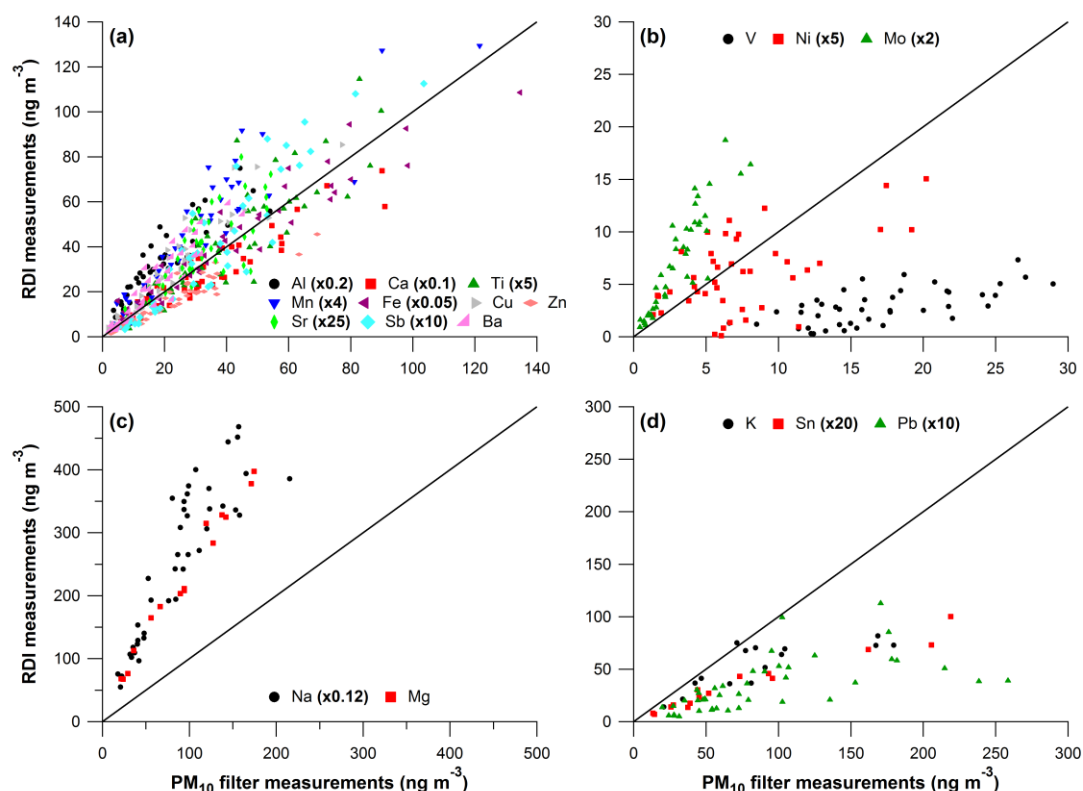


Figure S3. Total PM_{10} element mass concentrations measured by the RDI (sum of $PM_{10-2.5}$, $PM_{2.5-1.0}$ and $PM_{1.0-0.3}$ fractions) at MR and NK averaged to 24 h versus 24 h PM_{10} filter measurements of elements for (a) elements that agree within $\pm 50\%$, (b) elements with poor correlations, (c) elements with good correlations but a factor 2.5 higher with RDI, (d) other elements. The one-to-one line is added in black. See Table S2 for fit coefficients and Pearson's R values. Note that many elements are scaled to improve visualization.

Table S2. Fit coefficients and Pearson's R values for elements measured with the RDI ($PM_{10-2.5}$, $PM_{2.5-1.0}$ and $PM_{1.0-0.3}$ fractions summed to total PM_{10} and averaged to 24 h) relative to 24 h PM_{10} filter measurements. Data points were fitted with an orthogonal fit and forced zero intercept.

| Element | Fit coefficient | Pearson's R |
|---------|-----------------|---------------|
| Na | 2.82 | 0.89 |
| Mg | 2.34 | 0.99 |
| Al | 1.55 | 0.89 |
| K | 0.55 | 0.78 |
| Ca | 0.81 | 0.94 |
| Ti | 1.04 | 0.86 |
| V | 0.17 | 0.66 |
| Mn | 1.37 | 0.91 |
| Fe | 0.95 | 0.96 |
| Ni | 0.71 | 0.56 |
| Cu | 1.30 | 0.95 |
| Zn | 0.70 | 0.94 |
| Sr | 1.21 | 0.78 |
| Mo | 2.35 | 0.90 |
| Sn | 0.43 | 0.98 |
| Sb | 1.18 | 0.93 |
| Ba | 1.36 | 0.94 |
| Pb | 0.34 | 0.61 |

Table S3. Estimated total uncertainty (% of measured value) of the calculated element concentrations per size fraction, and detection limits for each element (ng m^{-3}).

| Element | PM _{10-2.5} (%) ^a | PM _{2.5-1.0} (%) ^a | PM _{1.0-0.3} (%) ^a | DL (ng m^{-3}) ^b |
|---------|--|---|---|---|
| Na | 25 | 25 | 25 | 2.552 |
| Mg | 24 | 24 | 24 | 0.962 |
| Al | 24 | 25 | 25 | 1.709 |
| Si | 24 | 24 | 24 | 0.420 |
| P | 25 | 25 | 25 | 0.118 |
| S | 24 | 24 | 24 | 0.503 |
| Cl | 24 | 24 | 24 | 0.158 |
| K | 24 | 24 | 24 | 0.031 |
| Ca | 21 | 21 | 21 | 0.267 |
| Ti | 24 | 26 | 27 | 0.024 |
| V | 30 | 30 | 24 | 0.008 |
| Cr | 27 | 27 | 26 | 0.015 |
| Mn | 83 | 69 | 46 | 0.042 |
| Fe | 21 | 21 | 21 | 0.033 |
| Ni | 22 | 22 | 21 | 0.005 |
| Cu | 21 | 21 | 21 | 0.028 |
| Zn | 21 | 21 | 21 | 0.058 |
| Br | 21 | 21 | 21 | 0.117 |
| Sr | 21 | 21 | 21 | 0.036 |
| Zr | 21 | 21 | 21 | 0.036 |
| Mo | 21 | 21 | 21 | 0.037 |
| Sn | 21 | 21 | 21 | 0.061 |
| Sb | 21 | 21 | 21 | 0.052 |
| Ba | 21 | 21 | 21 | 0.254 |
| Pb | 21 | 21 | 21 | 0.137 |

^a Combination of uncertainties regarding sample inhomogeneity (20 %), RDI flow rate (5 %), absolute and relative calibration (Na-K 13 %, Ca-Pb 2 %) and spectral analysis specific per element and size fraction (median uncertainties for all data points).

^b As 3x the standard deviation of the spectra signals used for continuum corrections.

^c Na uncertainties might be underestimated due to the overlap with the L lines of Ni, Cu and Zn. In the current analysis the ratio of the L α to K α lines are determined empirically, and quantification of the associated uncertainties is under investigation.

~~Figure 2b~~ Figure S3b shows good correlations for Mo (Pearson's $R = 0.90$), but the RDI measures a factor 2.4 higher concentrations than found on the filters, whereas V and Ni show no significant correlation between RDI and filters (Pearson's R 0.56-0.66). The most likely reason for the discrepancy between both methods is the ICP-MS extraction efficiency. This was 66 % for Ni, but unknown for V and Mo, leading to increased uncertainties of the filter data and potentially underestimated concentrations. As shown in the main text, the RDI time series of these elements (including both urban/kerb increments and diurnal/weekly cycles) are consistent with those of elements expected to be co-emitted by the same sources. -Visual inspection of the spectrum indicates that significant interferences between lines are unlikely, and this is confirmed by peak fitting sensitivity tests investigating the response of the calculated concentrations to uncertainties in line energy calibration (i.e. energy as a function of detector channel), ~~the continuum, and calculated peak width~~. We estimate a 3 % uncertainty in the measurement of Mo due to spectral analysis and an overall uncertainty of 21 %. ~~Strong correlations between filter and RDI time series also suggest that spectral fitting errors are not the cause of the discrepancy.~~ Mo falls in a well-constrained region of the calibration curve (although is not directly measured on calibration foils), so relative calibration errors would require a systematic bias across this entire region of the calibration curve. While there are not enough jointly measured elements within the intercomparison to evaluate this possibility, good

agreement between RDI and filter measurements is obtained through Sr ($K\alpha = 14.1$ keV) and at Sb ($K\alpha = 26.4$ keV) (Mo $K\alpha$ lines fall at 17.5 keV), suggesting such a bias is unlikely. ~~For ICP-OES the extraction efficiency was unknown for Mo, potentially indicating that the filter data might be underestimated. The other elements (V, Cr, Ni) in Figure 2b show no significant correlation between RDI and filters. Similar to the discussion of Mo, we do not expect significant spectral interferences for these elements. Spectral analysis uncertainties are somewhat higher for V and Ni and this is confirmed by the uncertainty analysis described above, which with about 19 % for V and 6 % for Ni (overall uncertainties of 28 and 22 %) yielded around 20 % uncertainty for V, Cr and Ni.~~ Unlike Mo, the relative calibration is well-constrained both in terms of elements directly measured on calibration foils and in terms of intercomparison with nearby elements in the XRF calibration curve, where V ~~and Cr falls~~ just above Ca and Ti and just below Mn and Fe, and Ni just above Mn and Fe and just below Cu and Zn. RDI and filter measurements are shown to be in good agreement for these six elements in ~~Figure 2a Fig. S3a.~~ ~~However, the ICP-OES had an extraction efficiency for Ni of 66%, whereas for V and Cr this was unknown, leading to increased uncertainties of these elements relative to others. Further, as shown in the following sections, the RDI time series of V, Cr and Ni (including both urban/kerb increments and diurnal/weekly cycles) are consistent with those of elements expected to be co-emitted by the same sources. We therefore assume the RDI V, Cr and Ni measurements to be valid, even though they are close to the minimum detection limits of SR-XRF.~~

~~Figure 2c Figure S3c~~ shows good correlations for Na and Mg (Pearson's $R_R > 0.89$), but the RDI concentrations are a factor 2.5 higher than the filters. The two measurement techniques each provide internally consistent results, with the Mg to Na ratio for the filter data at NK of 0.13 and the RDI data at NK and MR of 0.12, both of which ~~is~~are in very good agreement with the theoretical sea salt ratio of 0.12. The XRF relative calibration curve for Na and Mg is difficult to constrain due to the low response of these elements, but only led to an uncertainty of 13 % (for Na-K compared to 2 % for Ca-Pb) 10%. The extraction efficiency for Mg in ICP-~~OEMS~~ was 90 %, which does not explain the discrepancy between both methods, but was unknown for Na. ~~However~~Unfortunately, it remains unclear why the results of both methods differ for these two elements on an absolute scale. But since most analyses in the main text focus on relative changes/ratios per element across sites, the conclusions remain unaffected independent by the exact absolute concentrations.

The elements K, Sn and Pb in ~~Figure 2 Fig. S3d~~ show ~~reasonable to~~ good correlations between RDI and filter measurements (Pearson's $R_R > 0.78$) but the RDI data is less than half the filter data (filter measurements of K and Sn only at NK). Pb has a significant fraction of the mass in the fine fraction (see Fig. 2 in main text). Underestimation by the RDI is explained by an unexpectedly its high small-end cut point of 290-410 nm ~~(compared to 100 nm), as discussed below~~. K and Sn also have a significant fraction of their mass in the fine fraction, and might be affected by the cut off similarly to Pb.

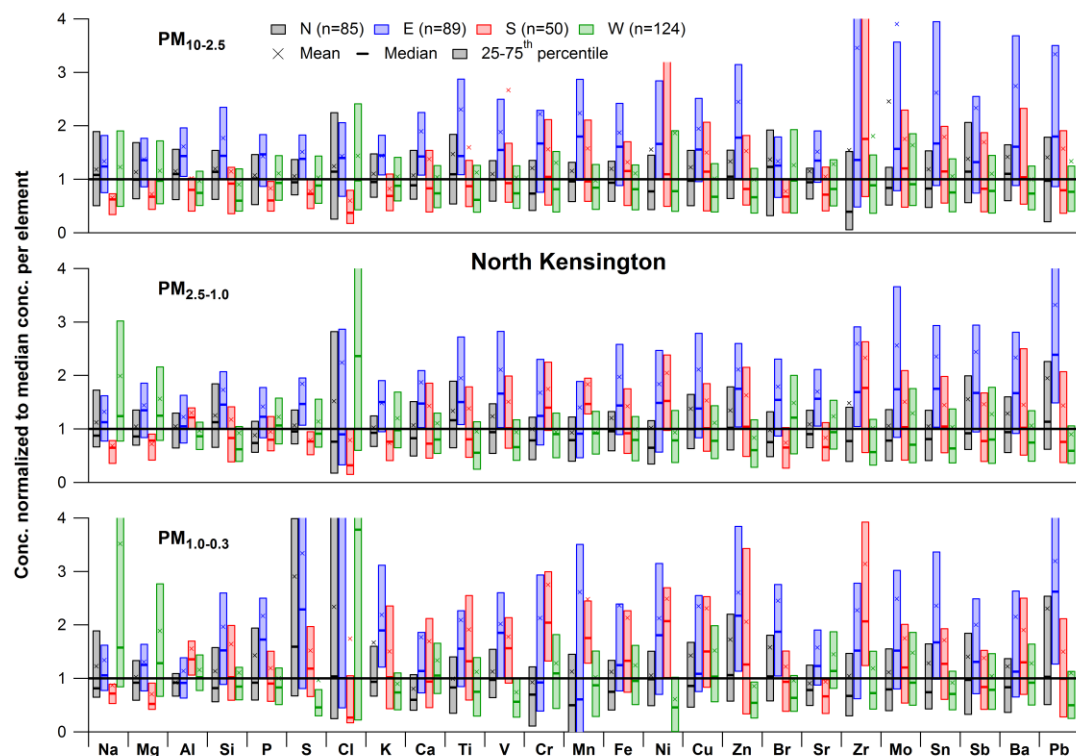
S is a useful element for evaluation of the small-end cut off, as it is dominant in the fine fraction and measurable by several techniques. Therefore, we compared S data obtained with the RDI to simultaneous S mass calculated from sulphate (SO_4) measured by an AMS at MR, NK, and DE. The results in Supplement A show that the S mass in the RDI is on average about three times lower than that measured by the AMS. This is consistent with the discrepancy difference between RDI and filter measurements for fine fraction dominated elements. The RDI backup filter, which collects particles too small to impact at the $\text{PM}_{1.0-0.3}$ stage, was analysed for SO_4^{2-} using ion chromatography (Supplement A). Adding the S from this analysis to the S collected at the RDI $\text{PM}_{1.0-0.3}$ stage yielded mass closure with the S from AMS

1 measurements within 25 % at all three sites. This suggests that elements with
2 considerable mass in the small end of the PM_{1.0} size range are not sampled by the
3 PM_{1.0-0.3} stage may be significantly underestimated. This affects S and Pb, and
4 potentially also K, Zn, Br and Sn. To further investigate this underestimation effect,
5 new RDI collection efficiency measurements for the PM_{1.0} deposition stage were
6 performed (Supplement A). The actual small-end cut off was determined to be 290-
7 410 nm, rather than the previously measured value of 100 nm (Bukowiecki et al.,
8 2009; Richard et al., 2010), and found to be very sensitive to the machining
9 tolerances of the PM_{1.0} nozzle.

10 Only a small fraction of the measured elements are affected by this cut off issue in
11 the sense that absolute values are smaller than with a PM_{1.0-0.1} stage. Further,
12 because the analyses presented in the following sections-main text depends on site-
13 to-site ratios (for the same element) and relative concentration changes, potential
14 biases are reduced by the similar (though not identical, see Fig. S2 in Supplement A)
15 cut offs of the different RDI units. The conclusions presented herein in the main text
16 are thus not significantly affected by this artefact.
17

1 Supplement **BD**: Additional tables and figures

2



3

4 **Figure S43.** Same as [Figure-Fig. 54 in main text](#), but for NK with mean, median and 25-75th
5 percentile trace element concentrations split in four wind direction sectors (N, E, S, W)
6 normalized to the global median concentration per element for $PM_{10-2.5}$ (top), $PM_{2.5-1.0}$ (middle)
7 and $PM_{1.0-0.3}$ (bottom). See [section-Sect. 4.2.2](#) for the definition of the wind direction sectors.

8

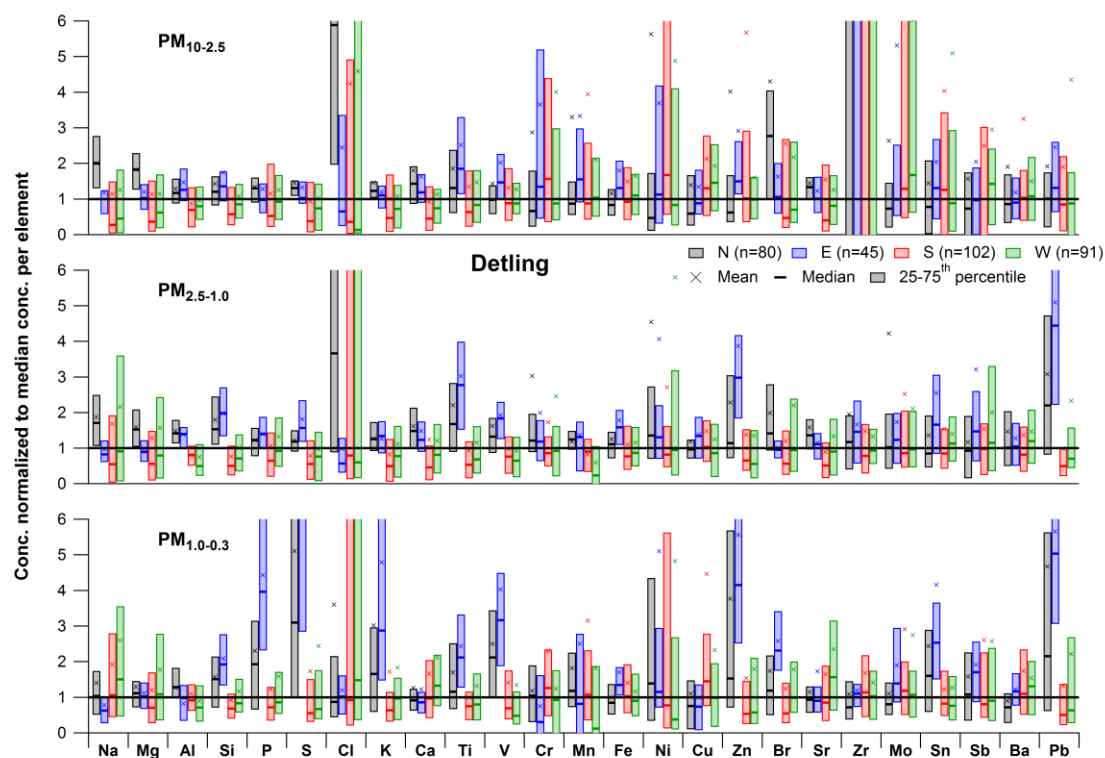


Figure S54. Same as Figure-Fig. 54, but for DE with mean, median and 25-75th percentile trace element concentrations split in four wind direction sectors (N, E, S, W) normalized to the global median concentration per element for $PM_{10-2.5}$ (top), $PM_{2.5-1.0}$ (middle) and $PM_{1.0-0.3}$ (bottom). See section-Sect. 4.2.2 for the definition of the wind direction sectors.

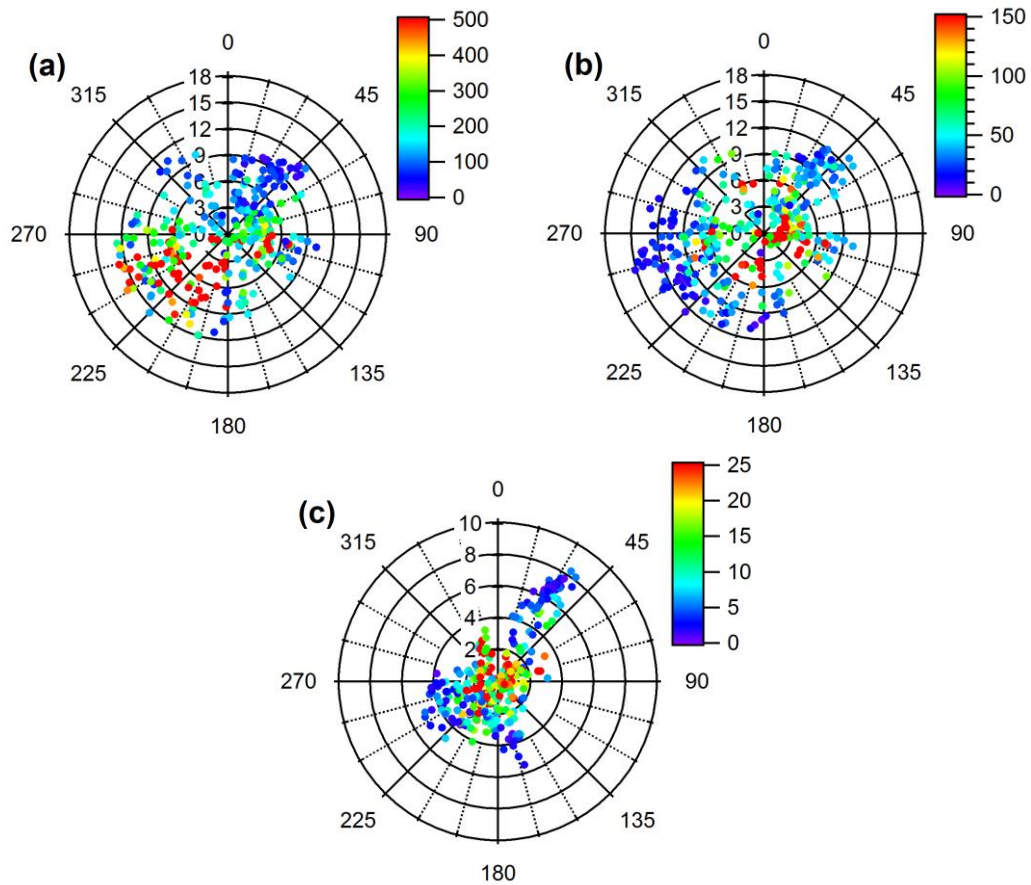


Figure S65. Wind roses as a function of wind direction (angle) and wind speed (diameter) at (a) BT Tower, color-coded by NO_x concentrations (ppb) at MR, (b) BT Tower, color-coded by NO_x concentrations (ppb) at NK, (c) DE, color-coded by NO_x concentrations (ppb) at DE for the RDI sampling periods (see Table 1 in main text).

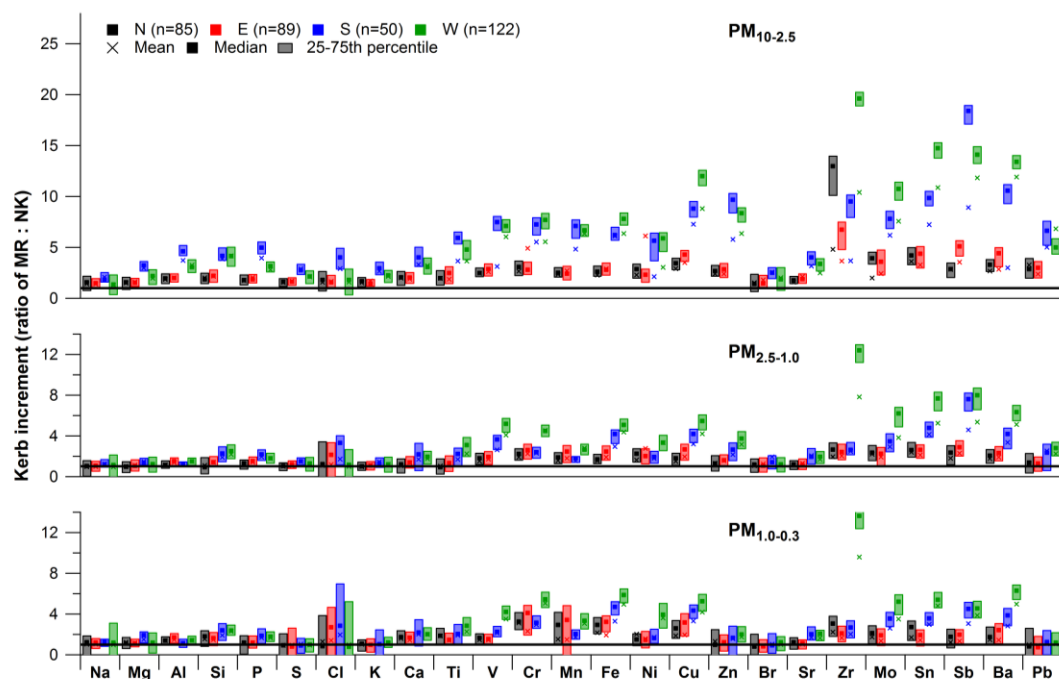


Figure S76. Same as [Figure-Fig. 65](#), but with mean, median and 25-75th percentile kerb increment values for trace elements at MR relative to NK for $PM_{10-2.5}$ (top), $PM_{2.5-1.0}$ (middle) and $PM_{1.0-0.3}$ (bottom) split in N, E, S and W wind sectors. See [section-Sect. 4.2.2](#) for the definition of the wind direction sectors.

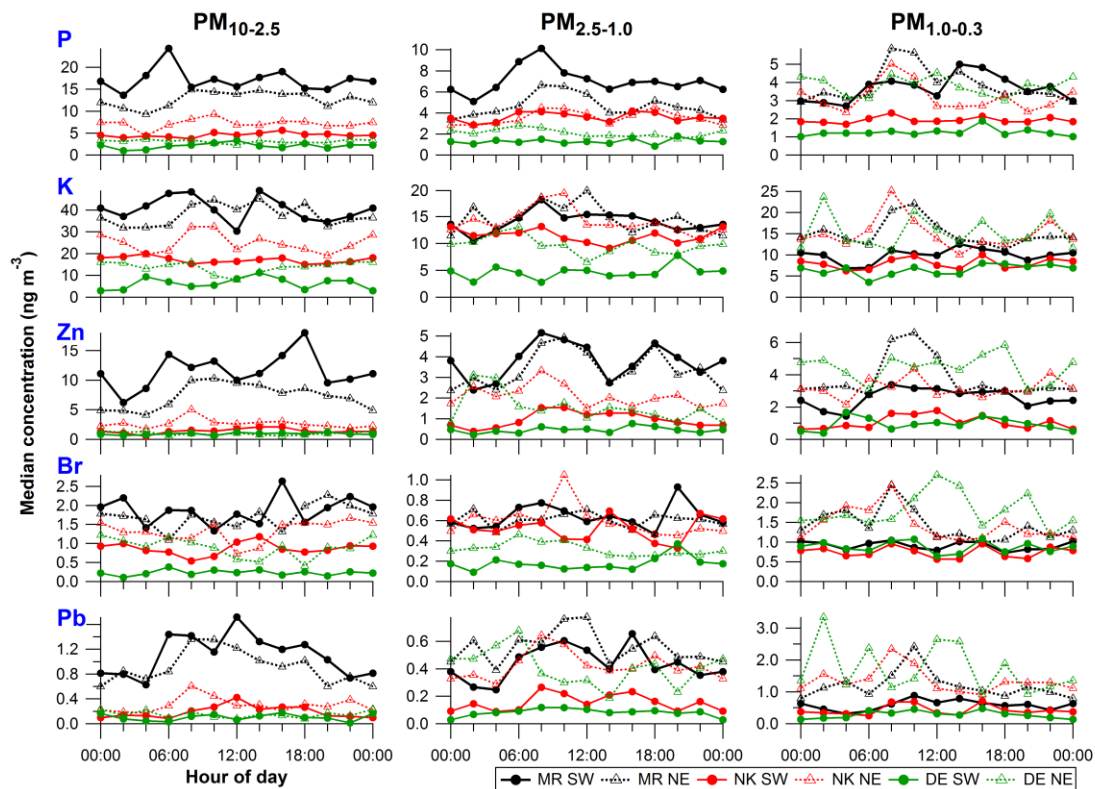


Figure S87. Same as [Figure Fig. 76](#), but for all other elements: P, K, Br, Zn, Pb (regional background); Mg (sea salt), Al, Ca, Ti, Sr (mineral dust); Cl (sea salt), V, Cr, Mn, Ni (traffic-related); Cu, Zr, Mo, Sn, Ba (brake wear). Diurnal cycles of 2-h median concentrations for PM_{10-2.5} (left), PM_{2.5-1.0} (middle) and PM_{1.0-0.3} (right) at MR, NK, DE split in SW and NE wind sectors. See [section Sect. 4.2.2](#) for the definition of the wind direction sectors. Hour of day is start of 2 h sampling period, so 00:00 LT means sampling from 00:00 to 02:00 LT.

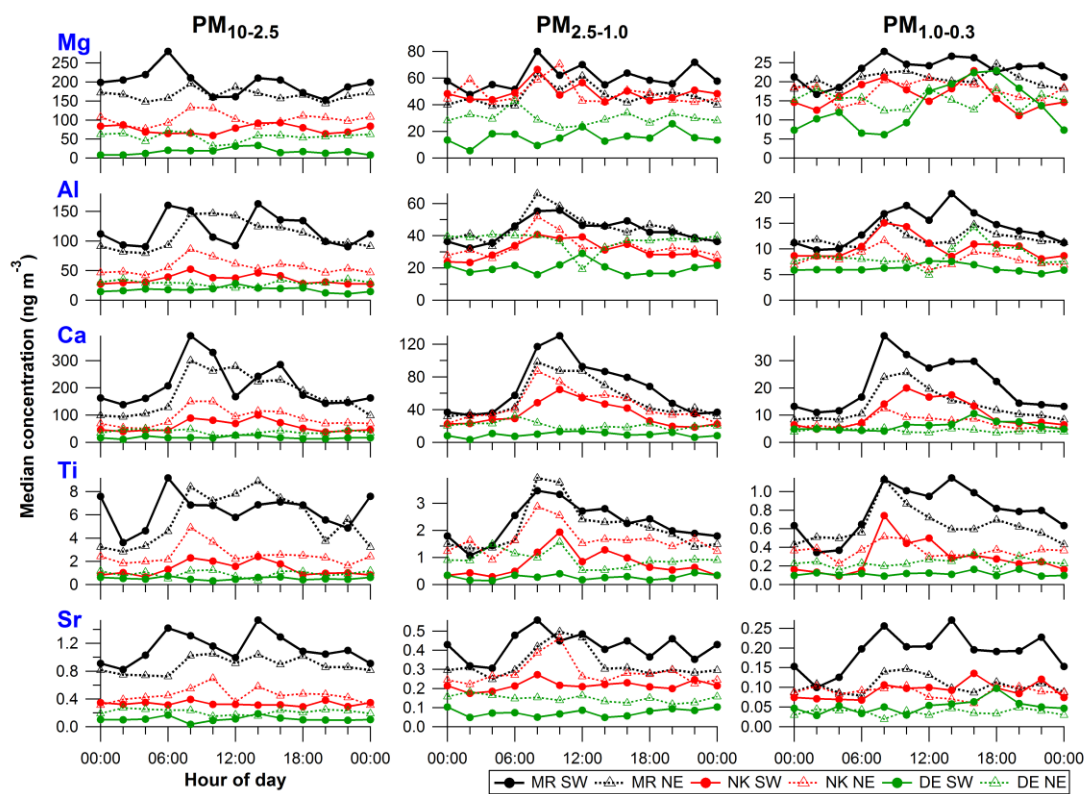


Figure S78. Continued.

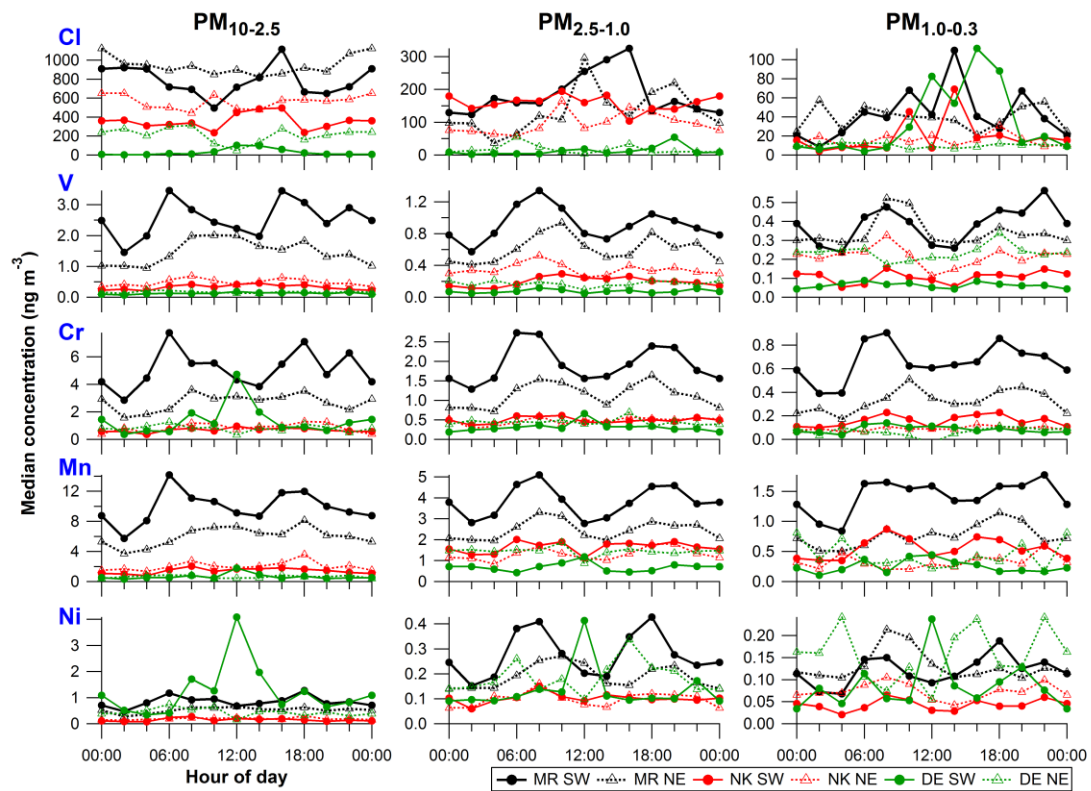


Figure S78. Continued.

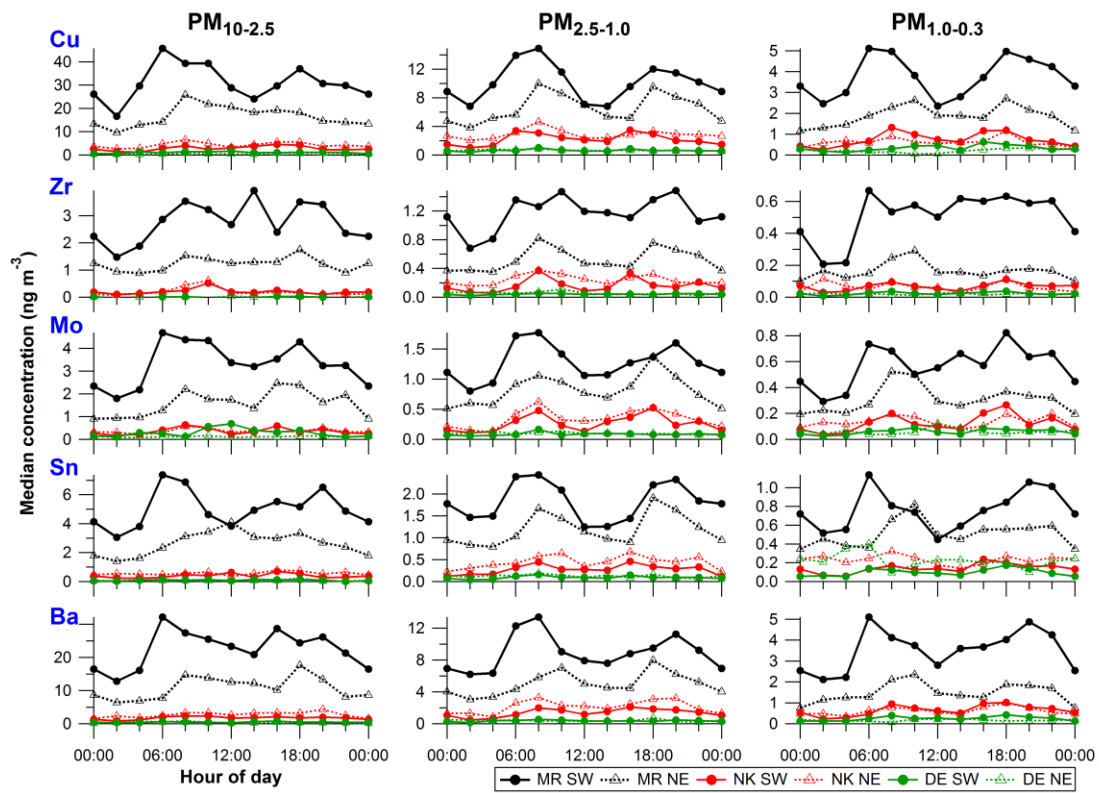


Figure S78. Continued.

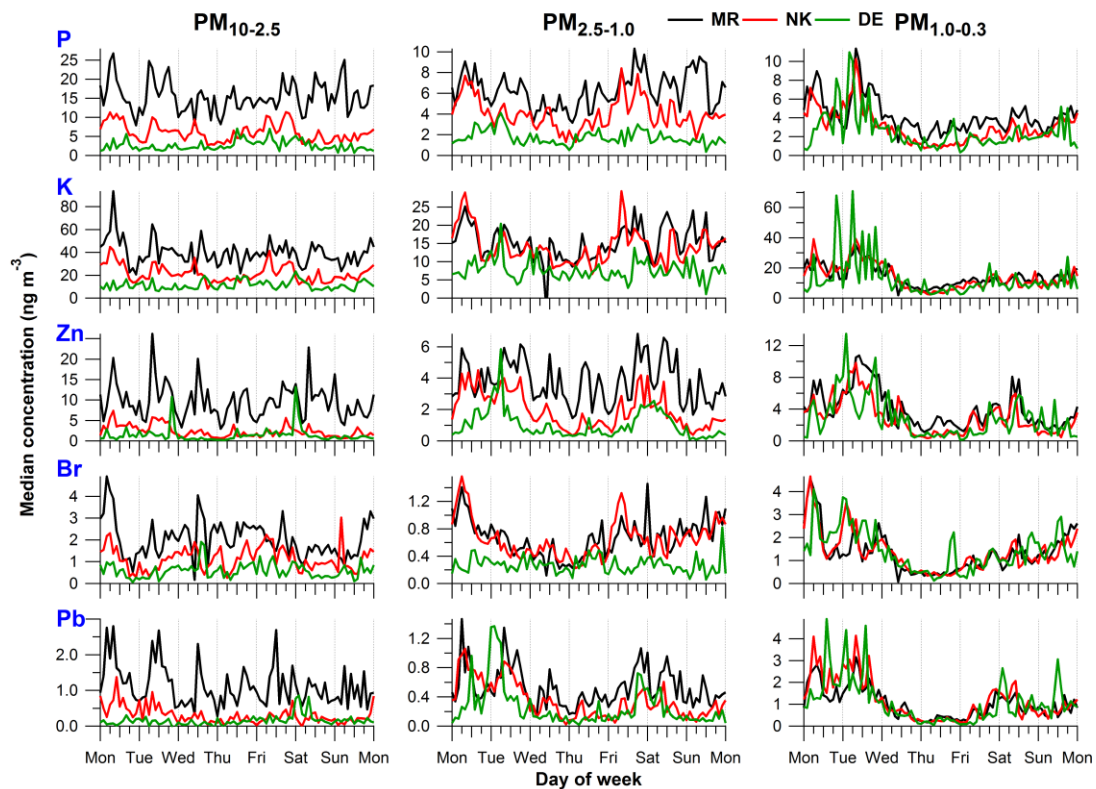


Figure S98. Same as [Figure-Fig. 87](#), but for all other elements: P, K, Br, Zn, Pb (regional background); Mg (sea salt), Al, Ca, Ti, Sr (mineral dust); Cl (sea salt), V, Cr, Mn, Ni (traffic-related); Cu, Zr, Mo, Sn, Ba (brake wear). Weekly cycles of 2-h median concentrations for PM_{10-2.5} (left), PM_{2.5-1.0} (middle) and PM_{1.0-0.3} (right) at MR, NK, DE.

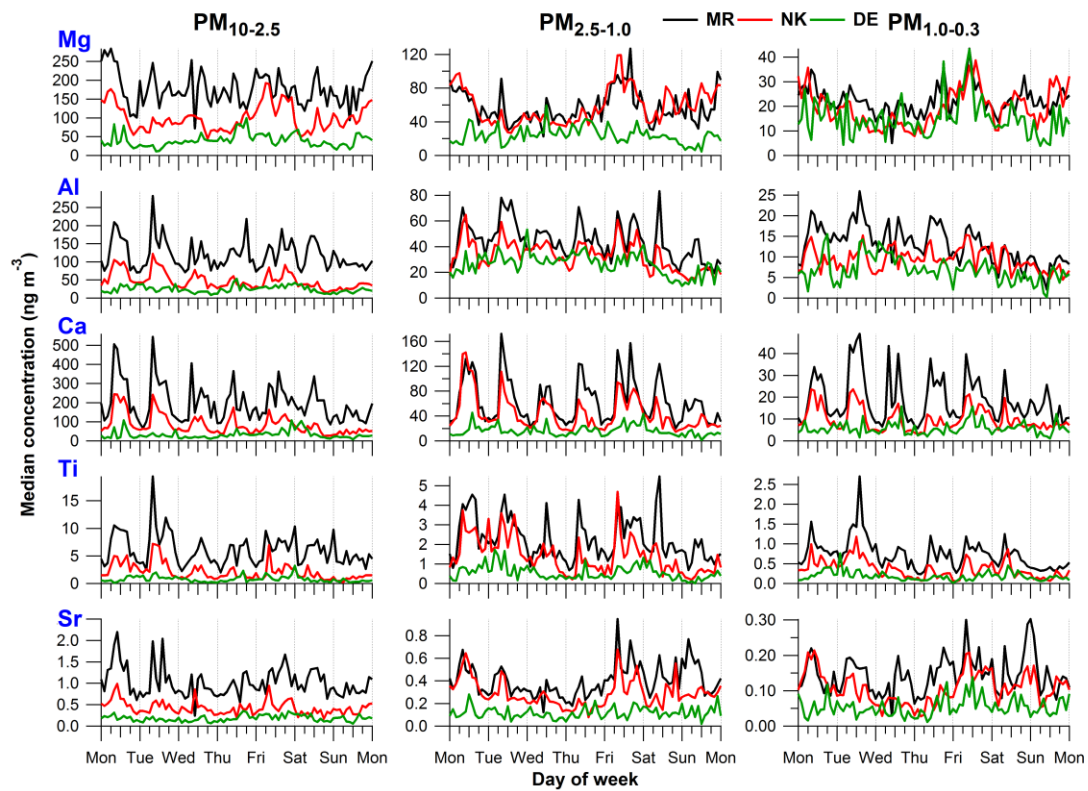


Figure S98. Continued.

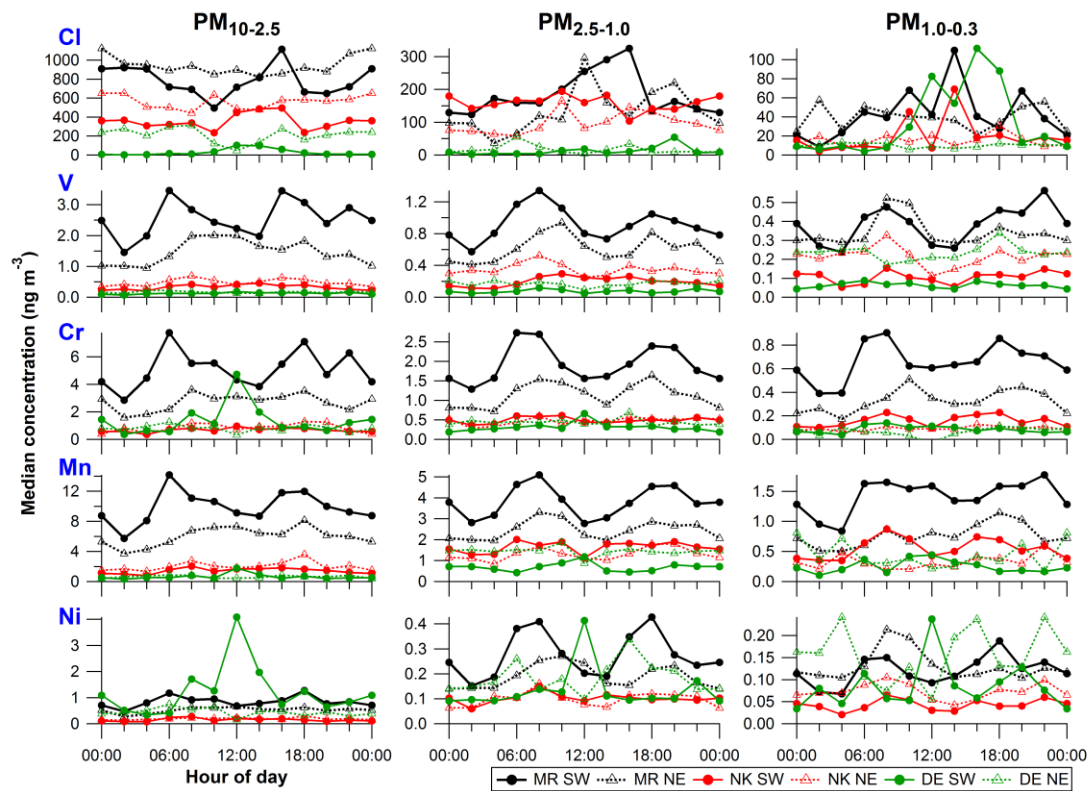


Figure S98. Continued.

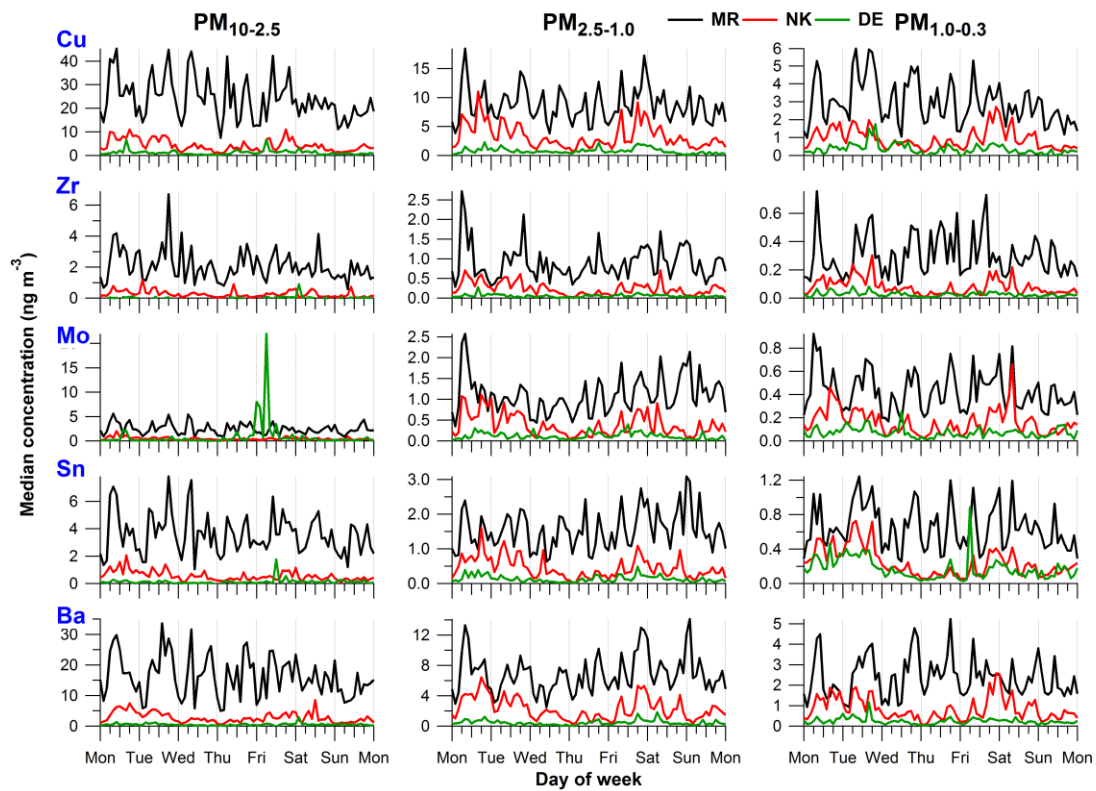


Figure S98. Continued.

References

- Bearden, J. A.: X-ray wavelengths, *Rev. Mod. Phys.*, 39, 78-124, doi:10.1103/revmodphys.39.78, 1967.
- Bukowiecki, N., Hill, M., Gehrig, R., Zwicky, C. N., Lienemann, P., Hegedus, F., Falkenberg, G., Weingartner, E., and Baltensperger, U.: Trace metals in ambient air: Hourly size-segregated mass concentrations determined by synchrotron-XRF, *Environ. Sci. Technol.*, 39, 5754-5762, 2005.
- Bukowiecki, N., Lienemann, P., Zwicky, C. N., Furger, M., Richard, A., Falkenberg, G., Rickers, K., Grolimund, D., Borca, C., Hill, M., Gehrig, R., and Baltensperger, U.: X-ray fluorescence spectrometry for high throughput analysis of atmospheric aerosol samples: The benefits of synchrotron X-rays, *Spectrosc. Acta Pt. B-Atom. Spectr.*, 63, 929-938, 2008.
- Bukowiecki, N., Richard, A., Furger, M., Weingartner, E., Aguirre, M., Huthwelker, T., Lienemann, P., Gehrig, R., and Baltensperger, U.: Deposition uniformity and particle size distribution of ambient aerosol collected with a rotating drum impactor, *Aerosol Sci. Technol.*, 43, 891-901, 2009.
- DeCarlo, P. F., Slowik, J. G., Worsnop, D. R., Davidovits, P., and Jimenez, J. L.: Particle morphology and density characterization by combined mobility and aerodynamic diameter measurements. Part 1: Theory, *Aerosol Sci. Technol.*, 38, 1185-1205, doi:10.1080/027868290903907, 2004.
- Richard, A., Bukowiecki, N., Lienemann, P., Furger, M., Fierz, M., Minguillon, M. C., Weideli, B., Figi, R., Flechsig, U., Appel, K., Prevot, A. S. H., and Baltensperger, U.: Quantitative sampling and analysis of trace elements in atmospheric aerosols: impactor characterization and synchrotron-XRF mass calibration, *Atmos. Meas. Tech.*, 3, 1473-1485, 2010.
- Sole, V. A., Papillon, E., Cotte, M., Walter, P., and Susini, J.: A multiplatform code for the analysis of energy-dispersive X-ray fluorescence spectra, *Spectrosc. Acta Pt. B-Atom. Spectr.*, 62, 63-68, 2007.
- Van Espen, P., Janssens, K., and Nobels, J.: AXIL-PC, software for the analysis of complex X-ray spectra, *Chemometrics Intell. Lab. Syst.*, 1, 109-114, 1986.